Advanced Control Design Tools for Autonomous Vehicles

by

Mohamed Ali Jemmali

Thesis submitted to the Faculty of Engineering in partial fulfillment

of the requirements for the degree of

Doctor of Philosophy

in

Electrical and Computer Engineering

School of Electrical Engineering and Computer Science

Faculty of Engineering

University of Ottawa

Ottawa, Ontario, Canada

© Mohamed Ali Jemmali, Ottawa, Canada, 2023

Abstract

This thesis deals with a new robust control design for autonomous vehicles. The goal is to perform lane keeping under various constraints, mainly actuator saturation of the steering system, lateral wind force, incident obstacles and unknown curvatures. To reach this goal, we propose an improved formulation of Parallel Distributed Compensation (PDC) law since it is a nonlinear system feedback state controller. A direct Lyapunov method to ensure the stability and the stabilization of the discrete-time Takagi-Sugeno (T-S) model representing the autonomous vehicle dynamics is suggested. We derived necessary and sufficient stability and stabilization conditions from the quadratic Lyapunov function. These conditions are expressed in terms of strict Linear Matrix Inequalities (LMIs) extracted from the linearization of the Bilinear Matrix Inequalities (BMIs). The vector state is measured entirely by the Luenberger multi-observers to be used in the feedback control. The results of Autonomous vehicle control are presented in this thesis to show the effectiveness of the proposed approach. Simulations are used to validate the theoretical results.

Acknowledgments

First and foremost, I am grateful to ALLAH for his unending support from the time I was born until now, in the future and in all time. I would like to thank my supervisor, Professor Hussein T. Mouftah, for his advice, patience, and concern. It would not have been feasible to do this work without his encouragement, support, and, most importantly, his candid remarks.

I would further like to thank Dr. Binod Vaidya for his assistance with the simulation part of my thesis.

I am grateful to my darling mother and wife, who made it all possible with their encouragement and support. My success is yours. My appreciation extends to my friends as well.

Table of Contents

Abstract ..... **ii**
Acknowledgments ..... **iii**
Table of Contents ..... **iv**
List of Figures ..... **vii**
List of Tables ..... **ix**
List of Acronyms and Symbols ..... **x**
Chapter 1 Introduction **1**
1.1 Background 1
1.2 Motivation 3
1.3 Objectives 10
1.4 Methodology 11
1.5 Thesis contributions 11
1.6 Thesis Outline 13
1.7 List of Publications 14
Chapter 2 Survey on autonomous vehicle lateral control **15**
2.1 State of the art 15
2.2 Fuzzy logic models overview 30
2.3 Lyapunov-Based Stability Analysis 34
2.4 Relaxations with Different Choices of Lyapunov Functions 35
2.5 Exploiting the Knowledge of the Membership Functions for Stability Relaxations 37
Chapter 3 Systems Control tools **39**
3.1 Introduction 39
3.2 Modeling process 39
3.2.1 Definition of a process 39
3.2.2 Definition of a model 39
3.3 Objectives of a modeling 40
3.4 Modeling methods 40
3.4.1 Model representation 40
3.4.2 Modeling in state space 42
3.5 LTI systems 42
3.6 Systems representation 43
3.7 The state form 43

3.8 State representation 44
3.9 State vector 44
3.10 Mathematical representation 44
3.10.1 Continuous case 45
3.10.2 Discrete-time case 46
3.11 Definition of identification 47
3.11.1 Perspectives on identification 47
3.11.2 Estimation of model parameters 47
3.11.3 Information 47
3.12 Building a T-S fuzzy model 48
3.12.1 By Identification 48
3.12.2 By Linearization 48
3.12.3 Polytopic transformation 49
Chapter 4 Identification and Takagi-Sugeno 51
4.1 Identification and Takagi Sugeno models 51
4.2 Related work 54
4.3 Iterative identification model 54
4.4 Subspace identification model 54
4.5 Contributions 55
4.6 Model description 56
4.6.1 Objective of N4SID method 56
4.6.2 Decomposition of deterministic-stochastic models 56
4.6.3 Assumption about the deterministic-stochastic model 57
4.6.4 N4SID algorithm 57
4.7 Takagi Sugeno control 59
4.7.1 Discrete-time Takagi-Sugeno system 59
4.7.2 Stabilization of a discrete-time multiple state feedback 60
4.7.3 Synthesis of multi-observers 62
4.8 Takagi- Sugeno stabilization 64
4.9 Conclusion 66
Chapter 5 The design of the new PDC controller based on identification models 67
5.1 Introduction 67
5.2 Numerical algorithm for subspace State Space identification 71
5.2.1 N4SID Algorithms 1 and 2 Steps 71
5.2.2 MOESP Algorithm and Steps 72
5.3 Discrete-time Takagi-Sugeno Systems control architecture and steps 72

5.3.1 Discrete-time Takagi-Sugeno System ... 73
5.3.2 Discrete-time Takagi-Sugeno Stabilization ... 74
5.4 Nonlinear Luenberger Observer Design ... 78
5.5 Results ... 80
5.6 Discussion ... 91
5.7 Conclusion ... 93
Chapter 6 The new PDC control applied to Autonomous vehicles control ... 94
6.1 Introduction ... 94
6.2 Vehicle modeling ... 97
6.2.1 Lateral dynamics model of the vehicle ... 98
6.2.2 Road-vehicle positioning ... 98
6.2.3 Steering system model ... 99
6.2.4 Vehicle control-based model ... 99
6.3 Control design for discrete-time T-S systems ... 100
6.3.1 Discrete-time Takagi-Sugeno system ... 100
6.3.2 Autonomous vehicles' stabilization ... 103
6.3.3 Developing of nonlinear Luenberger observer ... 107
6.4 Application of the lateral control for autonomous vehicles ... 109
6.5 Results ... 110
6.6 Conclusion ... 118
Chapter 7 Autonomous vehicle path following ... 120
7.1 Introduction ... 120
7.2 Lane keeping goals for autonomous vehicles ... 121
7.3 Road - vehicle modelling for path following ... 122
7.4 Simulation design ... 126
7.5 Simulation results ... 130
7.6 Conclusion ... 141
Chapter 8 Conclusions and Future Researches ... 142
8.1 Concluding remarks ... 142
8.2 Future Research Directions ... 142
References ... 144
Appendix A: Mathematical tools ... 167
Appendix B: Kalman states ... 169
Appendix C: Orthogonal projection ... 170

List of Figures

Figure1. 1 Autonomous vehicle sensors. 5

Figure 3. 1 Continuous state representation diagram 45
Figure 3. 2 Discrete State representation diagram 46

Figure 4. 1 Steps of the N4SID1 algorithm. 58
Figure 4. 2 Steps of the N4SID2 algorithm. 58

Figure 5. 1 MOESP algorithm steps. 72
Figure 5. 2 Real continuous system step response. 82
Figure 5. 3 Generation of two PRBS for identification of 2 input system. 83
Figure 5. 4 N4SID1 identification algorithm and real system step response. 83
Figure 5. 5 N4SID2 identification algorithm and real system step response. 83
Figure 5. 6 N4SID1 identification algorithm and real system frequency response. 84
Figure 5. 7 N4SID 2 identification algorithm and real system frequency response. 85
Figure 5. 8 MOESP identification algorithm and real system frequency response. 86
Figure 5. 9 Zoom on the samples [1,200] showing the N4SID1 and N4SID2 identification of the first output. 87
Figure 5. 10 Zoom on the samples [1,200] showing N4SID1 and N4SID2 identification of the second output. 87
Figure 5. 11 Y1 output of classic PDC control. 88
Figure 5. 12 Y1 output of improved PDC control. 88
Figure 5. 13 Y2 output of classic PDC control. 88
Figure 5. 14 Y2 output of improved PDC control. 89
Figure 5. 15 Y1 output using PDC control for T-S based on N4SID1. 89
Figure 5. 16 Y1 output improved PDC control for T-S based on N4SID1. 89
Figure 5. 17 Y2 output using PDC control for T-S based on N4SID1. 90
Figure 5. 18 Y2 output using improved PDC control for T-S based on N4SID1. 90
Figure 5. 19 Y1 output using PDC control for T-S based on N4SID2. 90
Figure 5. 20 Y1 output using improved PDC control for T-S based on N4SID2. 91
Figure 5. 21 Y2 output using PDC control for T-S based on N4SID2. 91
Figure 5. 22 Y2 output using improved PDC control for T-S based on N4SID2. 91

Figure 6. 1 Lateral vehicle dynamics modeling. 98
Figure 6. 2 Output1 of the lateral control using the classic PDC law. 112
Figure 6. 3 Output2 of the lateral control using the classic PDC law. 112
Figure 6. 4 Sideslip using the classic PDC law. 113

Figure 6. 5 Yaw rate using the classic PDC law. 113
Figure 6. 6 Lateral deviation error using the classic PDC law. 113
Figure 6. 7 Heading error using the classic PDC law. 114
Figure 6. 8 Steering angle using the classic PDC law. 114
Figure 6. 9 Steering rate using the classic PDC law. 114
Figure 6. 10 Output1 of the new PDC controller. 115
Figure 6. 11 Output2 of the new PDC controller. 115
Figure 6. 12 Sideslip of the new PDC controller. 116
Figure 6. 13 Yaw rate of the new PDC controller. 116
Figure 6. 14 Lateral deviation error of the new PDC controller. 116
Figure 6. 15 Heading error of the new PDC controller. 117
Figure 6. 16 Steering angle of the new PDC controller. 117
Figure 6. 17 Steering rate of the new PDC controller. 117

Figure 7. 1 Modelling of vehicle lateral dynamics. 123
Figure 7. 2 Simulation design. 126
Figure 7. 3 Autonomous vehicle path tracking1 at 10km/h. 130
Figure 7. 4 Autonomous vehicle path tracking1 at 40km/h. 131
Figure 7. 5 Autonomous vehicle path tracking1 at 60km/h. 131
Figure 7. 6 Autonomous vehicle path tracking1 at 100km/h. 132
Figure 7. 7 Autonomous vehicle path tracking2 at 10km/h. 133
Figure 7. 8 Autonomous vehicle path tracking2 at 30km/h. 133
Figure 7. 9 Autonomous vehicle path tracking2 at 55km/h. 134
Figure 7. 10 Autonomous vehicle path tracking3 at 10km/h. 135
Figure 7. 11 Autonomous vehicle path tracking3 at 36km/h. 135
Figure 7. 12 Autonomous vehicle path tracking3 at 55km/h. 136
Figure 7. 13 Autonomous vehicle path tracking4 at 10km/h. 137
Figure 7. 14 Autonomous vehicle path tracking4 at 28km/h. 137
Figure 7. 15 Autonomous vehicle path tracking4 at 36km/h. 138
Figure 7. 16 Autonomous vehicle path tracking4 at 45km/h. 138
Figure 7. 17 Autonomous vehicle path tracking5 at 10km/h. 139
Figure 7. 18 Autonomous vehicle path tracking4 at 25km/h. 140
Figure 7. 19 Autonomous vehicle path tracking4 at 30km/h. 140
Figure 7. 20 Autonomous vehicle path tracking4 at 40km/h. 141

List of Tables

Table 5. 1 Subspace algorithms convergence time. 82
Table 5. 2 Estimation error. 82

Table 6. 1 Definition of parameters 97
Table 6. 2 Comparison between states time convergence 118

Table 7. 1: Table Nomenclature 123

List of Acronyms and Symbols

ACC	Adaptive Cruise Control,
ACV	Autonomous and Connected Vehicle,
AV	Autonomous Vehicle,
BMI	Bilinear Matrix Inequality,
CG	Center of Gravity,
CNN	Convolutional Neural Network,
FLF	Fuzzy Lyapunov Function,
GPS	Global Positioning System,
KPMG	Klynveld Peat Marwick Goerdeler,
LIDAR	Light Detection and Ranging,
LILF	Linear Integral Lyapunov Function,
LKA	Lane Keeping Assist,
LMI	Linear Matrix Inequality,
LQR	Linear Quadratic,
LTE-V	Long Term Evolution- Vehicles
LTI	Linear Time Invariant,
MF	Membership Function,
MFL	Multidimensional Fuzzy Lyapunov function,
MIMO	Multiple Input Multiple Output,
MPC	Model Predictive Control,

MTL	Multi-Task Learning,
NCDB	National Collision Database,
NPR	National Public Radio,
N4SID	Numerical Algorithm for Subspace State Space System Identification,
PB	Piecewise Bilinear,
PDC	Parallel Distributed Compensation,
PI	Proportional-Integral,
PID	Proportional-Integral-Derivative,
PLF	Piecewise Lyapunov Function,
PMA	Piecewise Multiaffine,
QLF	Quadratic Lyapunov Function,
SAE	Society of Automotive Engineers,
SISO	Single Input Single Output,
T-S	Takagi-Sugeno,
UK	United Kingdom,
US	United State,
V-to-I	Vehicle to Infrastructure,
V-to-V	Vehicle to Vehicle,
Wi-Fi	Wireless-Fidelity,
WLAN	Wireless Local Area Network,
B_s	Steering system damping,

C_f	Front cornering stiffness,
C_r	Rear cornering stiffness,
E	Expected value,
$h_i(z)$	Normalized membership function,
I_n	Set of natural numbers ranging from 1 to n,
I_s	Steering system moment of inertia,
I_z	Vehicle yaw moment of inertia,
K_p	Manual steering column coefficient,
l_f	Distance from the CG to the front axle,
l_r	Distance from the CG to the rear axle,
l_s	Look-ahead distance,
l_w	Distance from the CG to the impact center of the wind force,
M	Mass of the vehicle,
R_s	Steering gear ratio,
$\mathbb{R}$	Set of real numbers,
$\mathbb{R}^{n\times n}$	Set of matrices with dimension (n×n) with n elements,
$\mathbb{R}^p$	Euclidian real space of dimension P,
$\mathbb{R}^{p\times q}$	Set of matrices with dimension (p×q) with real elements,
σ_t	Tire length contact,

Chapter 1

Introduction

1.1 Background

Nowadays, vehicles have become an integral part of our daily lives. Most people worldwide need vehicles to move around, such as cars, buses, bicycles, taxis, etc. In addition, those who are physically challenged use special vehicles. Due to the constant use of vehicles globally, so many people die every day because of vehicle collision, therefore, vehicle accidents have always been a leading cause of death. Even though, cars have gotten safer and have developed safety features, but still, the unsafe driver behavior is extremely the main cause of fatality crashes. NPR in 2017 and the National Highway Traffic Safety Administration in 2020, which are among the first agencies that conduct research on roadway and driver safety, report in a study looking at critical reasons of car accidents that 94% of deadly car accidents are caused by drivers. Vehicles, environmental factors, and other unknown reasons are responsible for 2% of accidents each. Many researches declare that the main origin of these accidents comes back to inattention, drowsiness and illness [1], [2].

The National Collision Database (NCDB) of Transport Canada contains data on all reported motor vehicle collisions in Canada provided by the provinces and territories each year. The federal, provincial and territorial governments of Canada work to improve road safety to reduce the number of fatalities and serious injuries; hence, they have the safest roads in the world. The year 2016 saw a decrease in the number of serious injuries, but showed a slight increase in fatalities and total injuries. In 2016, the number of serious injuries was 10,322, down by 4.0% from 10,748 in 2015. Similarly, in 2016, the number of motor vehicle fatalities was 1,898, up by 2.0% from 1,860 in 2015. The number of fatalities per 100,000 populations was 5.2 in 2016, unchanged from the rate seen the two previous years. Similarly, the number of fatalities per billion vehicle kilometers travelled was 5.1 in 2016, also unchanged from the previous year. Nevertheless, statistics urges us to work hard in trying to stop this flood of blood and human losses.

Therefore, in recent years, the field of intelligent vehicles, including the aspect of autonomous vehicles, has attracted great attention and has taken a great place among the researches fields. Indeed, due to its humanitarian services as a great solution to reduce accidents and large human losses, many others aspects are covered by the AV's features as we mentioned below:

1) Helping to save lives and prevent injuries.

2) Helps drivers avoid drifting into adjacent lanes.

3) Helps from making unsafe lanes changes.

4) Warns drivers of other vehicles behind them when they are backing up.

5) Brakes automatically if a vehicle ahead of them stops or slows suddenly.

6) 60% drop in harmful emissions: Fewer accidents mean less traffics congestion, which means a drop emission, Ohio University's states that harmful emissions will be reduced by 60% after the advent of AV.

7) Eliminate stop-and-go wares by 100%: According to the University of Illinois at Urbana-Champaign, this, in turn, will not only save people time but decrease the time their cars are on the roads and therefore, reduce emissions.

8) 10 % improvement in fuel economy: Rand's Autonomous Vehicle Technology guide states that self-driving cars will provide a reduction in fuel economy by between 4% and 10%. This is supported by the Ohio University study, which puts a figure of 3.1 billion gallons of fuel as the amount wasted by US drivers each year.

9) 40% reduction in travel time: UK Citizens travel time could be reduce by 40 % according to KPMG's connected and Autonomous vehicles.

10) Consumer saving: In the UK, according to KPMG, the savings to be had to on reduce insurance coasts, reduced running coasts and parking mean the UK consumer market would save 5bpounds a year.

11) Environmental gains: have the potential to reduce fuel use and carbon emissions.

12) Better health: Less traffic will improve people's health, since traffic jams have been shown to cause a rise in blood pressure, depression and anxiety, as well as decrease in cardiovascular fitness and quality sleep.

For these facts, autonomous vehicles have attracted growing attention from both academic and industrial settings, with the aim of improving safety, comfort, and efficiency [3], [4]. The trends of modern vehicles are embedded steering assistance systems which can assist the driver in various driving situations by enhancing their sensing ability [1], [5]. It has been

shown that these systems contribute to reduce significantly the driver workload and also road accidents by warning in case of human errors [4]. The introduction of a steering assistance system into the vehicle implies fateful impacts on the driving process [5]. Intelligent vehicles has the advantage of perception and understanding of the different and sudden situations of the surroundings in which it can fully control the driving if necessary [6]. Most of research focus on improving the automatic control of the steering system called lateral control. Many lateral controllers have been presented for the path following control problem in the literature [7], [8], and [9]. The authors in [10] have developed an automatic-steering control architecture based on a combination of fuzzy logic and PID control. Several researches were interested on steering system control especially on fuzzy control systems [7], [8], [9], [10]. These authors achieved very interesting results regarding the lateral control based on fuzzy logic control.

1.2 Motivation

Vehicles were created more than a century ago to facilitate better transportation of both people and commodities. Although the goal has remained the same throughout the previous century, modern automobiles are nearly indistinguishable from the early 19th-century cars due to improvements in safety, comfort, and efficiency. In the previous century, autonomous automobiles were a thing of the imagination, giving rise to classic movie characters like Herbie in 1968 and Johnny Cab in 1990. Statically 94% of accidents in the United States are caused by human decisions [11]. What if this was reduced? Although the topic of autonomous vehicles is not new, it is gaining importance on a global scale. For instance, the government of the United Kingdom hopes to have "self-driving automobiles on UK roads by 2021". The car industry and society face a number of obstacles prior to this, including: What does it imply for companies? In a collision, who is at fault? Do people actually feel safer? Should we just do it because we can, though? The opportunities and problems that society and technology will confront as a result of the usage of autonomous cars on public roads will be the main topics of this section on motivation. The Society of Automotive Engineers (SAE) degrees of automation [11] will be used for the motivational component as follows:

- Level 0: no automation; the driver performs all tasks

• Level 1: driver assistance; the vehicle is controlled by the driver, but driver assist features may be present, the majority of cars on the road today have some driver assist features, such as cruise control, blind spot detection or park assist.

• Level 2: partial automation; the vehicle has combined automated functions, but the driver must always remain engaged and monitor the environment, Tesla autopilot provides this level of automation.

• Level 3: conditional automation; driver must always be ready to take control of the vehicle but is not required to monitor the environment, the next Audi A8 claims to deliver autonomous driving at level 3 although in some countries, such as the UK, it is illegal to utilise this functionality.

• Level 4: high automation; the vehicle can perform all driving functions under specific conditions. The driver has the option to control the vehicle, this is considered by many as autonomous driving.

• Level 5: fully autonomous; the vehicle can perform all functions in all conditions and the driver may have the option to control the vehicle, but no driver is required at this level, there may be no need for a steering wheel.

The definition of a vehicle in this motivation section is "a machine used for carrying people or products on land. The present technological difficulties include: For a car to be autonomous, the automobile needs sensors to gather data about the road and a central processing unit to analyse all the information and make the necessary judgments. LIDARs, radars, cameras, GPS, and ultrasonic sensors are required; they will be used to recognise the environment around the vehicle and calculate the distance between it and adjacent objects so that the central processing unit can assess them and react appropriately [12]. (See Figure1.1).

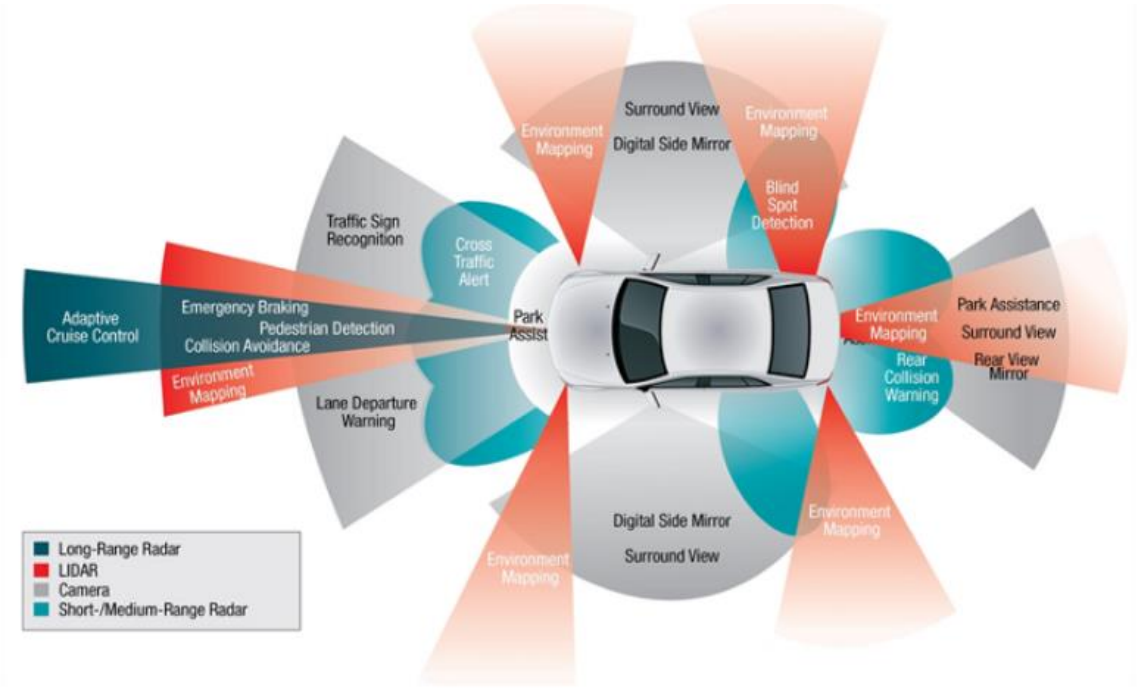

Figure1. 1 Autonomous vehicle sensors [227].

Although many level 1 cars already have GPS systems and cameras for park assist, there are many issues with consistently identifying objects at levels 2 and above. For instance, rain, snow, road construction, intricate city driving, and other obstacles can prevent the vehicle from taking the proper driving action.

The software and algorithms present the next significant challenge; it will be very difficult to write a programme that can recognise every scenario; the vehicle may need to be able to learn to react to situations for which it has not been specifically programmed, or in other words, to be artificially intelligent. The cars must be able to interact with one another (vehicle to vehicle (V-to-V) communication) either directly through temporary connections between vehicles in close proximity or over a network in order to function effectively. This implies that while travelling, cars would continuously broadcast information on their direction and speed. For instance, a car entering a traffic jam would decelerate and send signals. All following cars would pick up on these signals and either slow down or warn the driver to do so. It is anticipated that the technology would lessen collisions in scenarios without human drivers. In order to be aware of speed restrictions, traffic updates, and route optimization, vehicles will also need to connect with the infrastructure (V-to-I communication); many of these functions are currently available.

A number of level 1 vehicles on the market now can read road signs, have satellite navigation systems connected to networks that track traffic, and can change their course when a desired route is congested. For these features to become more dependable and able to handle greater data volumes, further investment will likely be required. Governments will have to make a major investment in this. "Smart highways," which utilise technology to actively regulate the flow of traffic, are being updated in several areas of the UK. Developing the environment for autonomous cars may start with this. Installing 5G will be the next stage in enabling both V-to-V and V-to-I connectivity. As part of the government's goal to deploy "self-driving cars on UK roads by 2021," Highways England is looking at methods to improve Wi-Fi [13] and 5G connection. Audi is comparing WLAN 802.11p and LTE-V (long term evolution- vehicles) communication technology for real-time V-to-V communication in a variety of settings on the A9 autobahn in Germany, which enables the industry to specify the specifications for the standardisation of future 5G communication [12]. Autonomous cars could gather a lot of data as a possible side consequence of this. As a result, there is an ethical component to data, its ownership, and usage. The data may be utilised to build personalised services and goods, but it may also be used to track our travels and lifestyle. The possibility of hacking is another drawback of this programme. There might be problems like kidnapping or accident-causing on purpose. This is a new dilemma for the car industry, despite the fact that these are concerns that are being argued throughout the world, with firms such as Apple and Google at the forefront of the argument, both of which are entering the field of autonomous vehicles. To avoid these issues, the automotive sector will need to spend considerably in cybersecurity. We also discuss the economic and corporate implications: According to a research conducted by Morgan Stanley Research in 2013 [14], autonomous vehicles might save the United States $1.3 trillion in fuel consumption, greater productivity of the vehicle's passengers, and a reduction in accidents and their associated expenses. The ability to save time is a significant advantage of autonomous driving. Drivers in the United States spent an average of 50.6 minutes per day driving in 2016. People would no longer need to drive with a level 5 autonomous car, allowing them to sleep, read, or acquire a new skill.

Figure 1.1 depicts the most common Sensors in Autonomous Vehicles: Autonomous cars might provide mobility to individuals who are unable to drive, boosting freedom for the aged, crippled, and young, and creating additional social and economic possibilities. Car manufacturers or third parties are likely to supply automobiles for single journeys or periods of time, similar to the service provided by Drivenow [15] or taxis; this might lead to a decrease in

car ownership. As a result, less space will be required for automobile parking, which will be especially beneficial in large cities, freeing up room for playgrounds, parks, and sports fields. As automobile manufacturers' old business models shift, there will be less focus on hardware and more reliance on software. Traditional automobile manufacturers are no longer the only players; businesses such as Google, Apple, and others are also joining the industry with electric cars, the second revolution in personal transportation. Car makers must be prepared to adapt and build a new business model; while the additional data and processing power within the car will allow the vehicle to become an entertainment centre, the vehicle's ultimate function will remain the same: to transport people and their things. As with any new technology, autonomous driving may result in employment losses, with truck and taxi drivers being the most likely. Using data from 2010 to 2014, the Merged American Community Survey indicated that more than four million jobs may be lost. However, many new opportunities may be generated in many industries including as software development and engineering, as well as cybersecurity and data management; autonomous cars will generate vast amounts of data that must be controlled and secured. Other industries that may gain include entertainment and marketing; driving time could be substituted with entertainment offerings.

Another major concern is the legal and political challenges: The introduction of self-driving cars raises several legal issues, including who is accountable in the event of an accident. The driver has no control in level 5 cars, and many individuals believe that the makers, designers, and software developers may face culpability [16]. There will also be a universe where level 5 automation interacts with levels 1–4, another possible flashpoint when apportioning responsibility following an accident. If the self-learning autonomous vehicle is used, it may be hard to tell whether the vehicle's behaviours are the result of what it autonomously learnt or its original programming. This begs the question of whether you can blame the manufacturer if the car learned to do it. Many nations have taken measures to legalise autonomous car testing on public roads. In 2017, Germany enacted legislation enabling firms to test self-driving vehicles on public roads as long as a qualified driver is present to take control if required [17]. California and China have followed suit, with China issuing national rules on road tests and allowing autonomous cars on the road network if the vehicle passes a technical examination and is equipped with sensors and cameras to monitor the driving position. These rules have allowed California firms such as Cruise and Apple to perform testing that provide data for the continued development of V-to-V and V-to-I communication. If governments do not enact different regulations, then vehicle manufacturers will relocate to other countries where

these laws exist. In the United Kingdom, for example, Regulation 104 of the Road Vehicles Regulations 1986 states that "no person shall drive, or cause or permit any other person to drive, a motor vehicle on a road if he is in such a position that he cannot have proper control of the vehicle or have a full view of the road and traffic ahead." [18] Fully autonomous driving (level 5) will necessitate changes to both national and international legislation. The 1968 Vienna agreement states that a human driver must always maintain control of the vehicle and be accountable for its behaviour in traffic [18], therefore this will need to be altered in nations that signed it in order to allow level 5 cars on the roads. Ethics and public perception: One of the most difficult challenges for autonomous vehicles is public perception; if autonomous vehicles are labelled disruptive, as genetic engineering was for years before proper debates were possible, autonomous vehicles will not progress, demonstrating that public opinion resistance can bring technology to a halt... To avoid this, business and government must openly and honestly confront the concerns facing autonomous cars. People are aware of the potential hazards, but they are less focus on the potential advantages. For example, in 2016 [19], a Tesla on autopilot transported a man 20 miles to hospital, saving his life; an example of autonomous driving providing mobility to those who cannot drive. The concerns with cybersecurity may influence people's perceptions, making some reluctant to accept the new technology; it is possible that there will be a divide between those ready to use the technology and those who reject. Ethics will be a significant subject in the development of self-driving cars; the trolley experiment, which is based on a theatrical thought experiment [20], is one example of this. Should an automobile veer towards a pair or a huge gathering of onlookers? In 2016, the Massachusetts Institute of Technology conducted a moral machine study, which discovered that half of people would prefer their driverless car to hit pedestrians rather than passengers, and that the majority of people would prefer to save the lives of humans over animals and to save the lives of many rather than a few. If level 5 automation is implemented and widely used, these types of difficulties might arise at any time, requiring pre-programmed algorithms to make decisions. Ethics may need to be coded ahead of time, and moral judgements must be made by individuals. This might also lead to legal concerns since it raises the question of whether the person who coded the ethics should be held accountable. Unless the software teaches itself ethics, the question of liability falls back on the manufacturer. Some of these issues have previously been handled; for example, Germany established the first ethical standards that specify that "in the case of an unavoidable accident scenario, any differentiation based on personal attributes (age, gender, physical or mental constitution) is completely banned."

Offsetting victims against one another is also banned." This is a solid start and permits German automakers to continue forward with their plans; nevertheless, further rules are needed. It will be necessary to compromise both national and international issues.

The most terrifying part of driving a car is changing lanes. When you try to change lanes, several thoughts cross your head. When should I leave? Must I wait? Can I change lanes or will I cut off another vehicle? Will that automobile let me into that lane, and so on. You could begin the lane change without realising there is a car just ahead of you, strike that car, and cause further damage. Due of this reality, many businesses including Waymo, Uber, and notably Tesla built an autopilot to address this issue. Can I trust this autopilot? How can I get off the highway? How successfully does it identify vehicles in blind areas and neighbouring lanes? When a car is turning on a curve, will auto lane change function?

The automobile only does a single lane change, moving across the new lane with the necessary acceleration before turning off the turn signal indicator on its own. If you wish to switch to the next lane again, it won't make several lane changes at once. You must signal once again.

The automatic lane change feature in far earlier versions would shift to the next lane and then wait for some time before accelerating up, which was really unnatural. One of the issues with the most recent update the GPS is not particularly precise, and the car tends to slow down when changing lanes has been slightly addressed. In most situations, such as on a motorway, the car's speed reduction in the new lane is quite risky. Accidents can be readily caused by it. Because the GPS is not very precise, the auto lane change computer believes it is close to an exit lane or an off-ramp when it is actually not. If you are changing lanes and there is an obstacle nearby, such as a car or large truck on your right or left side, and the lane is dashed rather than solid, you will notice that it is detected on the ultrasonic sensors and the car will not change lanes until the lane to its left or right and ahead of it is clear. We must be cautious if a car is approaching from behind us at a high pace, especially on the highway. If we try to change lanes and the autopilot is unable to identify the car, it will begin making the turn. In that moment, you must not allow it to do so. As a result, it is critical to keep an eye on your blind areas. Do not rely on the controller to make all of your decisions for you. The blind spot monitoring system does feature ultrasonic sensors that detect automobiles in your blind zone, but their range is just approximately 24 feet or 8 metres. So if there is a closed automobile, it will identify it, but if there is a car coming at you from behind, the ultrasonic sensors do not have the range to detect this type of behaviour. As a result, you must double-check that the path is clear. Until

now, the automated lane change feature has been unable to take a highway exit if you signal. Because there is no dashed line in the departure lane, the automobile just ignores it.

For the Waymo cars (Google cars) the change lanes still unsafe, the turning as well not safe. The Tesla vision system is clearly able to tell the difference between a dash or dotted line that we can change lane into, versus a solid lane blind which is a restricted access lane, when we try to change lane into solid line the car simply will not do it.

To do this, you need really the best road for this kind of manoeuvre. The autopilot controls the longitudinal and the lateral control. We mention also that two fatalities happened in March 2018 with Uber level 3 and level 4 in Tempe, Arizona hitting a pedestrian and leading to a fatality. We mention as well with Tesla level 2 the third fatality that Tesla autopilot led to and the last one in 2018 in Mountain view, California, when Tesla slammed into a divider killing his driver. But still we have mention that Tesla is three times safer than manual driven vehicles.

In this thesis, we focus on the lateral control of the autonomous vehicles. In the literature review on have a lot of techniques such as: PID controller, Fuzzy controller, H_∞/H_2 controllers, Linear Quadratic (LQR) method, Sliding Mode technique for the lateral control, Back Stepping, Model Predictive Control (MPC) for trajectory tracking of autonomous cars and so on. In the coming section we discuss and present a state of the art of the lateral control for autonomous vehicles.

1.3 Objectives

This thesis devoted on the development of a new control law for autonomous vehicles. I called the new controller that I enhanced and designed in this PhD thesis, the improved PDC controller. The control goal is to perform lane keeping under multiple constraints such as:

1) Actuator saturation of the steering system.
2) Road with unknown curvature.
3) Uncertain lateral wind force.

In this thesis, we suggest new steering control architecture to keep a vehicle between the lane boundaries in the centerline of the lane to prevent unwanted lane departure.

1.4 Methodology

The methodology presented in this thesis to achieve the main goals is the following:

1) Presenting the dynamics of the autonomous vehicle into T-S fuzzy system.
2) Choosing the Quadratic Lyapunov function to come up with the stability and stabilization sufficient conditions for the discrete-time Takagi-Sugeno system.
3) Build a Luenberger multi-observer in order to construct the entire state for the control aim of the autonomous vehicle.
4) .Solving Linear Matrix Inequalities (LMIs) presented as the optimization method to come up with the optimized gains first for the Luenberger multiobserver to ensure that the dynamic of the estimation error of the state vector converges to zero, which means that, the estimated state converges to the real state and then, coming up with the optimized gains that ensure the stabilization of the autonomous vehicle.
5) By solving the Luenberger Multiobserver LMIs we get the full state vector information since the dynamics of the estimation state error converges to zero using the optimized gains. So, since we have the entire state, we applied both the classic and the improved Parallel Distributed Compensation (PDC) law to the closed loop autonomous vehicle system presented by the discrete-time T-S system. The goal is to prove that the improved PDC control provides better results than the classic one in term of stabilization time, relaxation and minimizing the heading error state, note that the heading error state is a key state in autonomous vehicle lane keeping since this states provides the error between the actual autonomous vehicle heading and the desired heading.
6) Simulating the lane keeping scenarios to prove the robustness of the controller that I improved called the improved PDC controller.

1.5 Thesis contributions

The main contributions are the improvement of the PDC control law, and applying this improved PDC controller to the Takagi-Sugeno fuzzy system that presenting the dynamics of the autonomous vehicle, to perform the lane keeping under various constraints for autonomous vehicle.

1) Actuator saturation of the steering system.
2) Road with unknown curvature.
3) Uncertain lateral wind force.

The Parallel Distributed Compensation (PDC) controller is a control scheme commonly employed when the system being controlled has uncertain or varying parameters. In this PhD thesis we used both The Takagi Sugeno based model and the PDC control to deal with the time-varying feature of the vehicle speed. Our model explicitly takes into consideration the variations of the longitudinal vehicle speed as a parameter. In this case, the longitudinal speed is treated as uncertain and varying parameter that can affect the system dynamics and control behavior. The idea is to design a new steering controller to keep the autonomous vehicle in the centerline of the lane.

The state vector of the autonomous vehicle contains six states defined as follow:

1) The sideslip angel at the center of gravity or/ lateral velocity. (The lateral velocity or the sideslip angle (there is a direct relation between these 2 variables) are crucial for vehicle stability, thus playing a key role in lateral control. However, in practice these variables can be only measured with very expensive sensors. Then, we should design an observer to estimate them. In the contribution on lateral control, we also used state feedback control to avoid using such expensive sensors for control implementation. $\vartheta_y = \vartheta_x \beta$. Where ϑ_y is the lateral velocity ϑ_x is the vehicle speed and β is the sideslip angle.
2) The yaw rate or /yaw velocity.
3) The heading error between the tangent to the road and the vehicle orientation.
4) The lateral deviation error from the centerline of the lane projected forwards a look ahead distance.
5) The steering angle.
6) The steering rate.

   We approved the efficiency of our controller as follow:

   1) The state [0, 0, 0, 0, 0, 0] will represent the centerline of the desired lane, we disturbed the system by starting out of the origin which represents the centerline of the lane, if the internal variables of the state vector converge to zero our controller works well and ensure the global asymptotic stabilization of the autonomous vehicle. We compared our new controller with the classic PDC

controller to approve that the improved PDC controller is robust. The comparison is in term of convergence speed, relaxation and in term of ensuring a smallest heading error degree since the heading error informs us about the orientation of autonomous vehicles on the road.

2) We applied a later wind force to the autonomous vehicle and we disturb the state vector by starting with internal variables different than zero. If the lateral wind force applied to the autonomous vehicle does not affect the slip angel and the lateral velocity, precisely, if the later velocity is too small that means the improved PDC controller is robust.
3) Due to the high expense of vehicle sensors, measurements of particular vehicle states, such as lateral speed and/or sideslip angle, are not accessible on series-production cars, we designed an observer to estimate the six internal variables.

Another significant addition is the use of deterministic-stochastic subspace identification to estimate autonomous vehicle parameters in real time.

1.6 Thesis Outline

The remainder of this thesis is organized as follow. Chapter 2, represents a survey of the state of the art regarding autonomous vehicle keeping lane controllers. Chapter 3 provides an overview on the systems control tools. Chapter 4 discusses the relationship between the system identification and the system control. Chapter 5 covers the design of the new PDC controller based on identification models. Chapter 6 explains the new PDC control law applied to autonomous vehicles control. Chapter 7, presents the path following of the autonomous vehicle. Finally, chapter 8 draws the conclusions, and future researches.

1.7 List of Publications

- Journal Papers

1. Jemmali, M.A.; Mouftah, H.T. Discrete-Time Takagi-Sugeno Stabilization Approach Applied in Autonomous Vehicles. *J. Sens. Actuator Netw.* 11, 12, **2022**, https://doi.org/10.3390/jsan11010012

2. Jemmali, M.A.; Mouftah, H.T. Improved Control Design for Autonomous Vehicles. International Journal of Information Technology, Control and Automation, , vol. 12, **2022,** DOI: 10.5121/ijitca.2022.12301

3. Jemmali, M.A.; Mouftah, H.T. Intelligent Lateral Control for Autonomous Vehicles. *Journal of Intelligent Transportation Systems, Technology, Planning, and operations,* **2023** (Submitted).

4. Jemmali, M.A.; Mouftah, H.T. Advanced Robust Control for Discrete-Time Takagi-Sugeno Identification Model. . *International Federation of Automatic Control-PapersOnLine* , **2023** (Submitted).

- Conference Papers

1. M. A. Jemmali and H. T. Mouftah, "Takagi-Sugeno fuzzy control for Multi-input Multi-output systems based on subspace state space identification," 2020 20th International Conference on Sciences and Techniques of Automatic Control and Computer Engineering (STA), Monastir, Tunisia, **2020**, pp. 18-23, doi: 10.1109/STA50679.2020.9329299.

2. M. A. Jemmali and H. T. Mouftah, " Autonomous Vehicles Lateral Control Under Various Scenarios", 9th International Conference on Artificial Intelligence and Applications, Vancouver, Canada, **2022.**

Chapter 2

Survey on autonomous vehicle lateral control

As we mentioned before, the main goal of the control design for automated or autonomous vehicles is an increased safety by reduced accidents. Moreover, traffic utilization and energy efficiency are considered as additional control objectives.

2.1 State of the art

Robust Model Predictive Control (MPC) combines robust control theory and MPC to effectively deal with path tracking control system uncertainty. Tan [21] investigated a robust control strategy based on H MPC for system uncertainties during the control period. Sun et al. [22] proposed a Tube-based MPC path tracking strategy to account for random disturbances such as road adhesion coefficient and lateral wind. Traditional robust MPC control algorithms, on the other hand, are typically inefficient and conservative. Linear parameter varying (LPV) can approximate a nonlinear system as a superposition of multiple linear systems, making it ideal for designing vehicle path tracking controllers in high-velocity environments. Matteo et al.

Path tracking control system performance is poor due to uncertainty in vehicle model parameters, modelling errors, and external disturbances, particularly under high velocity and large curvature extreme conditions. [23] addresses this issue by presenting a novel gain-scheduled robust control strategy based on a linear parameter varying system with model predictive control (MPC) and H∞. To begin, a novel linear parameter varying system model for path tracking control of an autonomous vehicle is developed by the authors, taking into account the time-varying characteristics of vehicle velocity and tyre cornering stiffness. Then, using a gain-scheduled approach, a path tracking robust controller is designed, and the linear matrix inequality (LMI) is used to solve the optimization problem.

Compared with MPC method, the proposed algorithm can systematically deal with model parameters uncertainties, modeling error and external disturbance. It can improve the real-time performance and tracking accuracy.

However, this method cannot handle a nonlinear driving situation since it is a linear case study.

On the other hand, based on a scenario adaptive MPC on longitudinal motion and a weight adaptive MPC on lateral motion, the authors proposed a novel combined motion planning and control scheme for autonomous vehicles [24]. The scenario adaptive MPC is proposed to automatically determine the local motion of the vehicle (driving along the global path, car-following, lane-change) to ensure road safety and meet the desired velocity requirements. The weight adaptive MPC is intended to track the global path and perform the lane-change or lane-change cancellation manoeuvre in response to the scenario adaptive MPC's command. However, the proposed algorithm is not adapted for several driving styles, for example, the desired velocity is set manually; however, it can be designed as an adaptive parameter to various conditions and personalised driving styles with varying preferences in safety, comfort, and efficiency. To achieve this goal, some artificial intelligence (AI) technologies such as deep learning and reinforcement learning should be integrated into the proposed algorithm. Also, there is a lack on varying longitudinal velocities. It is supposed to be constant in this work.

This paper [25] describes the design and experimental validation of grid-based and Linear Fractional Transformation (LFT) approaches for autonomous vehicle lateral control. These new methodological approaches are compared to the traditional polytopic approach from theoretical design to real-world implementation on a real-world automated Renault ZOE vehicle. By adjusting the look-ahead distance, it is possible to address both lane change and lane tracking issues with a single LPV controller. Each LPV controller is built around the LPV/H concept. Computational costs, vehicle performance (e.g., lateral tracking error or control effort optimization), and on-board integration complexity are all factors in performance comparison.

This research offered a theoretical and experimental evaluation of LPV techniques for lateral control of autonomous vehicles. Among the others, the gridded-based model has the simplest structure and the least conservatism in optimisation. The weighting factors employed in control design might physically convert the real actuator constraints to a filter added to the optimisation issue. The practical constraints of each strategy were highlighted by looking at

simulation results from several important circumstances. The findings obtained in practical implementation then revealed intriguing results regarding the minimising of lateral error, which supports the use of LPV/robust techniques on autonomous cars. In reality, such techniques aid in the management of parameter-variant systems as well as the handling of external disturbances (wind speed, poor road conditions/slopes). However, An LPV actuator model must be improved to increase performance, it cannot handle some nonlinear lane keeping scenarios. This paper, focused on only linear driving situations which is not really realistic. Furthermore, a nonlinear bicycle model should be welcome to be utilised as a control plant, and the developed controller should be evaluated in more complicated environments with higher lateral accelerations (friction decrease, gust wind).

Other authors [26], focused on Linear Quadratic Regulator (LQR) controller based on the optimal front-tire lateral force. This LQR controller is presented to track the path properly after assessing the path tracking model. The LQR controller consists of a feedforward controller and a feedback controller that may not only minimise lateral distance error but also assure vehicle steerability and lateral stability by integrating multi-parameter joint estimation. Furthermore, the longitudinal dynamics control includes PI control based on speed feedback and drive/brake force compensation based on fuzzy system. The suggested estimation and control algorithms are deployed on a test road by an autonomous vehicle platform. However, this technique still in linear case, which mean in very specific driving situation. The kinematics technique based on longitudinal acceleration and the optimum robust control method can be investigated to improve the robustness of the parameter estimator and lateral dynamics controller.

[27], this article describes imitation learning for a flapping-wing aerial vehicle inspired by Monarch butterflies, in which a set of ideal trajectories computed offline is treated as an expert demonstration to be copied. A novel restricted imitation learning method is suggested to achieve exponential convergence and ultimate boundedness without the need for extra trajectory optimization, significantly enhancing computing efficiency. This has been used effectively to the nonlinear dynamics of a flapping wing aerial vehicle. However, because it is difficult to anticipate the whole condition of a flapping wing aerial aircraft in practice, the authors considered only one particular situation and, one potential future route is to use visual information directly in sensorimotor control.

The parallelized implementation of unsupervised machine learning algorithms to observe and direct the travel of a self-driving car from its starting place to the target destination was

provided in this paper[28], the authors used five different control approaches, including closed-loop PID feedback-based motion control and unsupervised machine learning-based motion control.

The hierarchical application of unsupervised machine learning control methods enabled a faster reaction for regulating the autonomous vehicle's lateral, longitudinal, and rotational movements. Furthermore, it was discovered that the best machine learning approach should be applied for improved vehicle angular velocity stability. This was accomplished by parallelizing the machine learning methods. Overall, successful deployment of unsupervised machine learning algorithms might help to reduce traffic congestion and collisions in the future autonomous vehicle integrated transportation system. However, the authors don't stud compare the algorithms given in this article to other types of learning methods and share the results.

The Deep Monte Carlo Tree Search (DeepMCTS) is proposed in this letter to improve the control performance of feedback steering controllers. Tracking accuracy and stability may be greatly increased due to the accuracy of the learning-based model in modelling nonlinear vehicle dynamics and the look ahead search capacity of MCTS.

The proposed solution in this article [29] avoids the large computational overhead by planning steering movements using efficient tree search rather than online numerical optimization like MPC (Model Predictive Control). In typical case studies, simulation findings justify the strengthening of feedback controllers.

However, this work needs to integrate heuristic rules or NN-based (Neural Network) estimations like AlphaGo [30] to address more complicated circumstances and significantly enhance the DeepMCTS's time efficiency. Furthermore, leveraging continually updated driving data to retrain the learning-based model is an essential direction. When used in real-world autonomous cars, the suggested technique may have the following two drawbacks. First, in emergency situations where vehicle speed fluctuates with severe acceleration or deceleration, control performance may suffer dramatically. To solve this issue, coordinated longitudinal and lateral control might be explored. Second, in the case of a large viable steering action space, the DeepMCTS may struggle to find an adequate trade-off between control precision and calculation time. Combining the DeepMCTS with particular policy and value networks, like AlphaGo [30], might be a feasible approach for efficiently reducing the tree search space.

The suggested technique [31] may significantly improve tracking performance and reduce the impact of uncertainties in a variety of driving scenarios for 4WIDAV. As a result, the suggested control strategy can serve as a theoretical foundation for the advancement of route following. However, experiments could be conducted in the future under more rigorous and complicated settings to validate the performance of the suggested technique. In addition, various vehicle conditions with limited access, such as adhesion coefficient should be considered.

In this paper [32], the optimization was carried out with the help of a Genetic Algorithm (GA), and the resulting trajectory was injected into a Potential Field (PF) to be reactive to unanticipated occurrences using a point mass model. The previously established GA-PF planification technique is included into a new comprehensive global planning and tracking system and used to a validation nonlinear vehicle model in this paper. A GA-PF planning approach is placed in a global planning and control system including a vehicle model in this article. The key contributions are in the control structure itself, which employs a Genetic Algorithm and the Potential Field technique, as well as the several synthesised regulators utilised for trajectory tracking. Both longitudinal and lateral tracking are taken into account, and the trajectory Cartesian coordinates are intelligently translated into control variables by bicycle model inversion via flatness principles. The longitudinal tracking approach considers variations in vehicle model parameters as well as variations in road parameters like as adherence and slope. The lateral tracking method is a nonlinear method that was inspired by kite-surf trajectory tracking research. A feedforward control is used to sustain the feedback control by inverting the trajectory reference Cartesian coordinates into control variables. The tracking is efficient since the ideal reference is followed accurately and the errors are extremely minimal. However, the oscillations caused by the potential field approach may render the trajectory suboptimal, and they should be investigated further to reduce them.

Traditional Frenet-based planners implicitly assume that the vehicle should trace the reference line, proceed in the same direction, and constantly monitor the reference line. However, when the curvature is large and the vehicle is far from the reference line, the assumptions may not always hold true. The authors [33] conducted an in-depth investigation of the required and sufficient conditions for producing continuous and accurate heading pathways in Frenet frames in this work. They suggested an efficient Frenet-based Path Generation Method

(PGM) that ensures proper heading but not continuity. Experiments show that the PGM is successful in generating plausible pathways.

An early publication on control issues on automated highway systems has been published in [34]. Much research has been conducted and many vehicles have been equipped with automated driver assistance functions since that time. Adaptive cruise control (ACC), which controls the longitudinal vehicle speed with respect to a target vehicle or a desired velocity, is widely used in common cars. Lane keeping assist (LKA) and lane departure warning are available lateral assistance functions. The assistance is achieved by active steering and braking. The dynamics of a highly automated vehicle is divided into main behaviors. The Lateral behavior which can be presented as:

1) The kinematics bicycle model (Geometric description of motion).
2) The dynamic (are about the laws of the causes of motions forces /moments in Newton's laws. bicycle model [5], [4], [35].

The longitudinal modelling which can be represented by a simple first order system. The simple kinematics bicycle model assumes left and right wheels being collapsed into one and single wheel at the center of the front and rear axle. In this case the wheels are assumed to not consider the lateral sideslip and in additional only the front wheel is steerable. Most of paper focused on the dynamic bicycle model.

In recent years, the intelligent vehicles technology appears, trying to solve the fatal vehicles collision problem. Attention and gradual development have taken place especially in the field of autonomous vehicles heretofore. Indeed, due to its humanitarian services, autonomous vehicles have attracted great attention from both academic and industrial settings, in order to achieve the main goal, which is the safety, comfort, and efficiency [3], [4]. The trend of modern vehicles is embedded steering assistance systems, which can support the driver in divers driving situations by enhancing their sensing ability [36] [1]. These systems have been shown a significant contribution in reducing the driver workload and road accidents by warning signals in case of human errors [4]. The implementation of the steering assistance system into the vehicle can be crucial due to its fateful role on the real time driving action [1]. Intelligent vehicles have the advantage of perception and understanding of the different and sudden situations of the surroundings, and they can fully control the driving if necessary [5]. Our research will focuses on improving the automatic steering control system, called lateral control.

Many steering controllers have been developed to solve the path tracking issues [6] [7] [37]. The authors of [37] combined the fuzzy logic and the PID control to suggest new lateral control system architecture. The authors of [38] [39] have developed a steering system controller based on sliding mode, while the paper [40] has proposed an analytical solution with no computation burdens to the vehicle lateral control problem based on Model Predictive Control. In [41] the authors present a tracking control method for the lateral motion of an autonomous land vehicle. This method is based on active disturbance rejection control.

In [41] the authors focused on stabilizing lateral dynamics with considerations of parameters uncertainties and control saturation through robust yaw control, this paper presents a robust yaw-moment controller design for improving vehicle handling and stability with consideration of parameters uncertainties and control saturation. The parameter uncertainties dealt with are the changes of vehicle mass and moment of inertia about the yaw axis and the variations of cornering stiffness's. The control saturation considered is due to the physical limitations of actuators and tires. The control objective is to stabilize the closed loop system with optimal performance on sideslip angle and yaw rate subject to parameter uncertainties. In [42] this article presents a non-model-based controller for vehicle dynamics systems to improve lateral stability, where output tracking control and adaptive dynamic programing approaches are employed to track the desired yaw rate and, at the same time, mitigate the sideslip angle, roll angle, and roll rate of the vehicle. In [42] the proposed control strategies, which distribute tire forces by learning, uses the information of states, input, and reference signal instead of the knowledge of the vehicle system. The four longitudinal forces of tires and the front wheel steering angle were used as the inputs to generate the yaw moment to control the lateral motion of the vehicle. [43] This paper investigates the vision-based autonomous driving with deep learning and reinforcement learning methods. Different from the end-to-end learning method, this method breaks the vision-based lateral control system down into a perception module and a control module. The perception module which is based on a multi-task learning neural network first takes a driver-view image as its input and predicts the track features. The control module which is based on reinforcement learning then makes a control decision based on these features. In order to improve the data efficiency, The end-to-end control system directly maps the observation to the desired Thus the end-to-end control methods usually need a large dataset or data augmentation process to enhance the coverage of the observation space. Otherwise, the learner will learn a poor policy. In contrast to the end-to-end control methods, the perception and control separation methods disassemble the control pipeline into a perception module and

a control module. The perception module takes the image as its input and extracts the features that are used to locate the vehicle on the track. The control module is responsible for making an optimal decision to follow the desired trajectory. Since the perception and control separation methods provide the flexibility that one can employ the state-of-the-art algorithm for perception and control. The main task for the perception module is to extract useful features from the image and locate the vehicle in the track. The previous works perceive the underlying features which include lane boundaries, distance to lane boundaries, vehicle poses, and road curvature, etc. from the image. By obtaining the distance to the lane boundaries and the heading angle difference with the lane heading direction, the vehicle can be located in the track coordinate. In fact, these features show strong visual correlation. For example, the lane boundaries can present the bending degree of the track, and the curvature estimation describes the bending degree with precise value, i.e. curvature. Thus, these two perception tasks are correlated and show some common features. However, the authors solved the perception tasks separately. To utilize the general features and improve the learning performance, they formulated the perception problem in the framework of the multi-task learning (MTL) convolutional neural network (CNN).

In [44] the authors investigated the combined active front wheel steering/direct yaw moment control for the improvement of a vehicle lateral stability and vehicle handling performance. A more particular assumption is this work is that the longitudinal velocity is not constant but varying within a range. Both the nonlinear tire model and the variation of the longitudinal velocity are considered in vehicle system modeling to track the system reference, a generalized proportional-integral (PI) control law is proposed. This technique was applied for electrical vehicle. The [40] paper presents the asymptotic stabilization problem for a class of nonlinear under-actuated systems. Its solution, together with the back stepping and the forward control design methods, is exploited in the control of the nonlinear lateral dynamics of a vehicle. This technique proved that with the established controller the vehicle is able to track any feasible reference at a constant speed and the lateral deviation converges to zero.

Several studies have focused on steering system control, especially fuzzy control systems [6] [7] [37]. These authors achieved very interesting results regarding lateral control based on Takagi–Sugeno models. They used a non-quadratic Lyapunov function complicated in terms of implementation because of quadratic Lyapunov function conservatism. They also used assumptions and approximations to compute the state vector containing six state variables. In our work perspectives, we present simple, new and effective solutions. Quadratic Lyapunov

function, which is simple in implementation, and novel PDC control law were used to minimize conservatism. The state vector in our work is not approximated. It is entirely computed using multiple Luenberger observers, proposed by [45]. The main features of T-S fuzzy system compared to other techniques are:

1) The possibility to sweep in large vehicle speed variation range. This feature helps improving the closed loop performance of the autonomous vehicle under different driving situation.
2) In this thesis, we developed a new controller not only for one or two states as the all other technics did, we controlled a six states which are: The sideslip angel at the center of gravity /or the lateral velocity, the yaw rate (yaw velocity), the heading error between the tangent to the road and the vehicle orientation, the lateral deviation error from the centerline of the lane projected forwards a look ahead distance, the steering angle and the steering rate and the most important and fantastic thing, that we measured all the intern variables based on system observability called observers. We call this result a robust result in automatic control.
3) We tested the robustness of our controller by adding three constraints which are not considered in the most of previous cited papers. The T-S able to handle a various system constraints which are:
    - The lateral wind applied to the autonomous vehicle.
    - The unknown curvature.
    - The steering saturation (actuator saturation).
4) T-S model-based control developed in Lyapunov framework offers a systematic model for the nonlinear complex systems.
5) The T-S used as a universal approximator for any smooth nonlinear system T-S (1985)
6) The T-S control ensures the stabilization of nonlinear systems.

This is why I used the Takagi-Sugeno fuzzy logic control to achieve my goal.

The most crucial performance of an autonomous vehicle is its high-speed safety. In this regard, yaw stability control (YSC) is an important technique for improving vehicle safety. However, high-speed cars are easily out of control in the nonlinear zone, resulting in catastrophic accidents. To accomplish YSC in the nonlinear domain, this paper offers a model predictive control (MPC) approach based on the Takagi-Sugeno (T-S) fuzzy model. To characterise the vehicle dynamic characteristics in the nonlinear zone, a T-S fuzzy model of the vehicle is

created based on a two-degree of freedom model. The robust MPC is then built, and its solution is supplied in the form of linear matrix inequalities (LMIs). Then, to prevent wheel lock in the YSC process, a sliding mode controller (SMC) is proposed [46].

The yaw stability control (YSC) technology is an effective safety technique to increase vehicle steering sensitivity or minimise lateral instability [47], [48], which has been the focus of vehicle dynamics and autonomous driving research for decades. YSC controls the yaw in autonomous cars, vehicle rate and sideslip angle for improved path tracking performance.

The T-S fuzzy MPC analyses the vehicle's nonlinearity using the T-S fuzzy model, making the technique workable even when the vehicle drives in nonlinear zones. Furthermore, the suggested issue is converted to LMIs form with an appropriate computing burden in the vehicle controller. However, first, The LPV cannot drive in nonlinear regions. Secondly, further research is needed to investigate the effect of alternative fuzzy tyre models on control performance, to devise a method when a realistic solution of LMIs is not available, and to investigate the performance of the T-S fuzzy MPC on vehicle nonlinear region.

Vehicle uncertainty and time-varying characteristics may impair autonomous vehicle stability control efficacy. As a result, the author of [49] offer a unique robust linear matrix inequality (LMI)-based H-infinite feedback algorithm for vehicle dynamics stability management, which controls the vehicle steering system and braking system via direct yaw moment control (DYC) and active front steering control (AFS). However, only a few important tests are carried out due to the limitations of our test conditions. Different test kinds and experimental tests with varying parametric variations must still be investigated to validate and enhance the suggested controller. Furthermore, the current control technique has only been confirmed through hardware-in-the-loop (HIL) platform testing, and its real-world applicability is an issue that must be addressed.

Another study [50] is about a new control mechanism for autonomous ground vehicles' route tracking. To cope with the time-varying characteristic of the vehicle speed and the highly unpredictable behaviours of the tire-road forces involved in the nonlinear vehicle dynamics, we use a fuzzy model-based control framework. A novel fuzzy static output feedback (SOF) system is presented to minimise the need of costly vehicle sensors for feedback control while prioritising the simplest control structure for real-time implementation.

Path tracking control systems are broadly categorised into three types [51]: model-free control, vehicle geometric-kinematic-based control, and dynamic model-based feedback control. To begin, model-free controllers such as PID control [52] or fuzzy logic control [53], [54] create steering actions only based on tracking failures. Without the need for vehicle information, these control approaches often need a time-consuming tuning operation to attain satisfactory route tracking performance [55]. Second, the geometric-kinematic-based route tracking controllers are created with the use of a vehicle kinematics model [56] and/or geometric relations [36]. Despite their simplicity, these control methods are only appropriate for driving scenarios when the vehicle dynamics can be ignored. Third, the dynamic model-based control design is based on vehicle parameter and dynamics information. We concentrate on these model-based feedback control techniques because they may be utilised to address the limitations outlined above, as evidenced by recent comparative studies [57], [55], and [58]. However, the authors need to extend the proposed fuzzy SOF scheme to deal with coupled longitudinal-lateral control issues. Experimental validations with real autonomous vehicles under extensive driving conditions should be also be considered.

Model predictive control (MPC) approach has been widely used to the motion planning [59], [60], [61], route tracking [62], and obstacle avoidance [63], [64] of autonomous vehicles due to its intuitive premise and benefits in dealing with system restrictions. However, the MPC approach necessitates the solution of an online optimization problem at each control step, which results in a prohibitively high computing load for real-time implementation, particularly for nonlinear MPC systems.

The preview tracking control has been developed [51] to avoid this key practical difficulty while taking forward prediction ability into consideration. However, dealing with model uncertainty and system limits remains a challenge for this control strategy.

To address vehicle tracking control difficulties, Takagi-Sugeno (T-S) fuzzy techniques have been developed [65], [66], and [67]. In contrast to model-free fuzzy control [53], [68], [69], T-S fuzzy control techniques [70] may achieve rigorous stability analyses and performance demonstrations. However, fuzzy model-based output feedback control for uncertain systems continues to be difficult [65], [71]. Despite tremendous progress in autonomous vehicle route tracking, the three control issues listed below still need significant research efforts.

First, the employment of full state feedback designs, in which control efficacy is dependent on data collection rate, is a significant limitation [72], [73]. The majority of path tracking research assumes that all vehicle states can be monitored for real-time control implementation [36]. However, in practise, this assumption is rarely correct. For example, low-cost sensors cannot consistently determine the sideslip angle and/or lateral speed, which are critical for vehicle control [74]-[75]. As a result, several strategies for designing observers for the estimate of unmeasured vehicle variables have been proposed, see [72], [76]-[77], and references thereto. Then, for path tracking of autonomous vehicles, an observer-based control strategy may be constructed [65], [66], and [75].

Regrettably, the design of an effective observer-based controller for vehicle route tracking under modelling uncertainties and system restrictions is still a work in progress [73]. The second problem is the control design's reliance on vehicle modelling. It is difficult, if not impossible, to fully describe the vehicle's nonlinear dynamics [55]. On the other side, a precise vehicle model may (unnecessarily) complicate control design. Although various semi-empirical models exist to properly characterise tire-road friction, such as the Pacejka magic formula, the LuGre model, and the Burckhardt model [78], they are scarcely exploitable for control purposes due to their significant nonlinearities. As a result, designing a model-based controller that is resistant to unmodeled vehicle dynamics, time-varying parameters, and external disturbances is critical [79]. The third issue is to include system restrictions, such as steering actuator physical limits and vehicle state constraints, in the control design approach to increase driving safety and comfort [80], [9]. This critical issue has received little attention in the current literature on route tracking control [9], [73], particularly with regard to output feedback control systems.

This work [52] offers a novel fuzzy static output feedback (SOF) controller to handle the three aforementioned vehicle route following difficulties at the same time. To deal with the nonlinear uncertain vehicle dynamics, fuzzy model-based control is used, as in [65].

In this paper [81], the authors examine the simultaneous estimate problem of lateral speed, steering input, and effective engine torque, all of which play critical roles in autonomous ground vehicle handling, stability control, and fault detection. A new nonlinear observer design approach is suggested to ensure asymptotic estimation performance due to the associated longitudinal-lateral coupling dynamics and the existence of unknown inputs (UIs). To that purpose, we employ a Takagi-Sugeno (TS) fuzzy representation with nonlinear consequences

to precisely characterise the nonlinear vehicle dynamics within a restricted set of vehicle states. This TS fuzzy modelling not only allows for huge reductions in real-time computing work to estimate the vehicle variables, but it also provides an effective technique to deal with unmeasured nonlinearities. Furthermore, UI decoupling may be accomplished using a generalised Luenberger observer structure without the need for prior UI knowledge. The UI observer design is framed as an optimization problem under linear matrix inequalities, which can be successfully addressed with typical numerical solvers using Lyapunov stability assumptions. The suggested TS fuzzy UI observer's efficacy real-time hardware-in-the-loop experiments are used to show the design.

Real-Time (RT) knowledge of vehicle dynamics and driver-related variables is required for autonomous ground vehicle active safety control [82], car problem detection and diagnostics [9], [83], and driver vehicle monitoring systems [84], [85]. Unfortunately, due to economic and/or technical constraints, onboard vehicle sensors are not always accessible [83], [84]. In instance, in some cases, physical sensors cannot directly monitor the human driver characteristics [85]. As a result, building estimating methods to rebuild vehicle dynamics from online input from low-cost sensors is gaining popularity across the world [85]-[86]. The lateral speed or sideslip angle is an important indicator for vehicle handling and lateral stability.
However, commercial physical sensors for measuring lateral speed are too costly and cannot be utilised in practise [87]. Hence, a large number of research work has been delegated to the lateral speed estimate [83], [87], and [88]. [89] proposes an industrially applicable kinematic-based solution. This technique, which does not need tire-road friction characteristics or other dynamical vehicle features, might result in the drift phenomenon caused by bias errors [83]. Kalman filtering methods have been frequently used for predicting sideslip angle, particularly in the setting of nonlinear estimates [90], [91]. Despite their efficacy, these approaches need fine-tuning and previous knowledge of the sounds emitted by automobiles in order to attain a reasonable estimate performance.

Robust observers based on dynamical vehicle properties have been proposed to alleviate these shortcomings [92], [93]. However, in the presence of nonlinear dynamics and/or unexpected disturbances, which is inherent in critical driving scenarios, the design of robust observers becomes difficult [89]. Fusion-data-based strategies have been shown to be an efficient methodology for estimating the vehicle sideslip angle by using the essential features of many low-cost sensors [94], [95]. However, such strategies raise sensor prices and

complicate estimate algorithms [89]. It is critical to note that most model-based estimate approaches overlook longitudinal-lateral coupling [90].

The fundamental issue is the difficulties involved in designing the proper nonlinear observer [72]. Because the steering angle directly impacts the vehicle direction, this variable is a critical input for intelligent vehicle path tracking control, path planning, active safety control, and detection of driver failure [4], [96]. Absolute rotary encoders, which are relatively costly and delicate in most passenger automobiles, can exactly measure the steering angle [72]. Low-cost sensors may produce inaccurate measurement findings or deliver incorrect steering indications. As a result, estimating the steering angle has received more scientific interest. Based on data from the global positioning system and the microelectronic system, In [97], an unscented Kalman filter is presented to predict the steering angle of agricultural tractors. [98] proposes a linear extended observer for steering angle estimation, which is subsequently used to recreate the road curvature signal for vehicle lateral control. Effective engine torque is also important in a variety of automobile applications, such as brake torque control, speed control, and adaptive cruise control [99]. However, for commercial vehicles, it is difficult to properly assess this vehicle variable due to both cost and technological reasons [100]. The effective engine torque is thus often provided in the form of look-up tables (LUTs) as a function of in-cylinder air flow rate, engine speed, injected fuel, and other parameters defined and calibrated by steady-state engine testing [100], [101].

Various model-based techniques for estimating effective engine torque have been developed to decrease the expenses of development, testing, maintenance, and robustness associated with LUTs-based estimations. In [102], a high-order sliding mode observer is presented to estimate engine friction torque and load torque. [103] devised a technique for calculating engine combustion torque based on the concepts of Kalman filtering. To estimate RT engine torque, a two-step observer design with distinct intake air measurement sensors and RT engine speed has been suggested [104]. Using observed engine speed, load torque, and air mass flow rate, Na et al. [105] developed an unknown input (UI) observer for online estimate of unknown effective engine torque. Despite substantial breakthroughs in vehicle estimating approaches, simultaneous estimation of the sideslip angle, steering angle, and effective engine torque has yet to be accomplished. The value of such an estimation solution is multifaceted. To begin, the estimated sideslip angle may be employed for vehicle active safety management [4], [82], whereas the estimated steering angle and effective engine torque can be used for fault

diagnostics of intelligent automotive systems [9]. Second, the suggested estimating approach is inexpensive since it simply requires online data from low-cost sensors.

These difficulties inspire the novel observer design technique presented in this paper. The suggested UI observer design is based on a combined longitudinal-lateral vehicle model, which includes steering angle and effective engine torque as UIs. There are two design challenges: 1) coping with unmeasured nonlinearities in vehicle dynamics; and 2) ensuring asymptotic convergence of both the car state and the UIs. Takagi-Sugeno (TS) fuzzy model-based approaches [106], [70] have been attempted to create nonlinear UI observers [72], [107] to solve comparable issues.

However, previous results often lead to over conservative conclusions or sophisticated observer design frameworks based on the Lipschitz feature of membership functions (MFs) [108]. It should also be noted that, due to technical difficulties associated with dealing with unmeasured MFs, fuzzy UI observer design and fuzzy fault detection/diagnosis have primarily focused on systems with measurable nonlinearities [107], which is not the case with the considered nonlinear vehicle dynamics. To estimate the vehicle state, lateral speed, and effective engine torque of autonomous ground vehicles, a novel nonlinear UI observer design technique has been developed. To deal with the unmeasured nonlinearities of the coupled longitudinal-lateral vehicle dynamics, TS fuzzy modelling with nonlinear consequences is used for observer design. The suggested modified Luenberger observer structure enables effective UI decoupling, ensuring asymptotic convergence of both vehicle state and UI estimate errors. Lyapunov arguments are used to construct LMI-based observer design conditions. The novel fuzzy UI observer's practical performance is RT evaluated using a high-fidelity AMESim car model.

Hardware-in-the-loop (HiL) tests indicate that the proposed nonlinear UI observer can predict both vehicle status variables and UIs accurately.

However, this work [81] should concentrates on extending the suggested estimate approach to deal with limit driving circumstances, such as by including a nonlinear tyre model or parametric uncertainty of the cornering stiffness parameters into the observer design. Another intriguing research subject is utilising the suggested UI observer structure for an effective fault-tolerant control strategy of autonomous cars.

On the other hand, In this thesis, we start the with the identification of multi-inputs, multi-outputs (MIMO) systems [109], and then in [110] we come up with a new control law, This new control was applied to autonomous vehicle control that we shall go into further depth in the next thesis report chapters. In [101] the authors developed a lateral dynamic of an unmanned

vehicle by using a system identification method and designed a lateral controller. The system input is the steering wheel angle of the vehicle with constant longitudinal speed, and the output is the yaw of the vehicle. With the identification method using subspace method, to achieve a control objective, the authors designed a robust lateral controller using the model equation. In [112] the use of model-based controller or fault diagnosis systems in automotive control requires reliable dynamics models. The reliability consists in accurate prediction of the vehicle's behavior, in order to evaluate current driving situations. Model parameters have to be precisely identified. This depends on the model's capability to reproduce the complex dynamics of the real system, by remaining a simple as possible, for online computation.

In this thesis, a practical approach of modelling vehicle dynamics is presented. Conventional simplifications are removed by coupling lateral and roll motion. Besides, nonlinear tire characteristic is presented. The accuracy and performance of the identified model is demonstrated by tests on real automotive systems. In the case of T-S fuzzy model we are allowed to construct the constrained model by using system identification. N4SID algorithm and multiple model approach integration, in one algorithm to control a nonlinear multivariable system, should be reflected in an increase of the robustness. The algorithm identifies MIMO systems that are modelled by a state space representation. The algorithm reliably considers the parameters of a deterministic-stochastic, dynamic and linear time invariant multivariable system. It is known that this estimate gives accurate parameters of the process.

N4SID is a convergent algorithm and is simple to implement. Our algorithm will be used with a nonlinear system in a local area, around an operating point. The Multiple model approach will interpolate this local area to cover all nonlinear area. The combined result will would yield an improved nonlinear control. This work will be the first that combines these two robust methods to get an efficacy and new technique of nonlinear stabilization.

2.2 Fuzzy logic models overview

Fuzzy logic control continues to be one of the most effective methods for managing complex systems, and research into fuzzy control systems is continually expanding and improving. This development resulted from the demand for findings that were more accurate and comfortable. Fuzzy logic control consists of two different kinds of modelling:

The model-free control strategy is built on expert experience and knowledge. This type of modelling is known as Mamdani fuzzy logic. As a result of the lack of a systematic framework for studying these types of systems, we have seen an increase in interest in fuzzy model-based systems.

Model-based control strategy: Takagi-Sugeno fuzzy systems and singleton-type fuzzy systems are shown (further called piecewise multiaffine systems). The key characteristics of the three types of fuzzy systems discussed above are presented here. We highlight the historical reasoning for each type of fuzzy system and its current research mainstreams using these qualities. Nonetheless, the emphasis is on fuzzy model-based techniques created using the Lyapunov stability theorem and linear matrix inequality (LMI) formulations, which are most of the time generated from bilinear matrices.

Mamdani and Assilian successfully used fuzzy logic control to a laboratory steam engine [113], which had a significant influence on fuzzy control research. Since the original study was published in 1975, several fuzzy control methods have been presented. According to the subsequent sections of IF-THEN rules, there are three sorts of fuzzy systems, as classified by Sugeno in [114]. First, we introduce Mamdani-type fuzzy systems [113], which are characterised by IF-THEN rules that are linked to linguistic variables as follows:

$$Rule\ i: if\ x_1\ is\ F_1^i\ , x_2\ is\ F_2^i, \dots\dots, x_m\ is\ F_m^i \tag{2.1}$$

$$THEN\ y\ is\ H^i\ , i = 1,2, \dots, n$$

where H_i and F_i^j , $i = 1,2, \dots, m$ are fuzzy sets, $\boldsymbol{n}$ is the number of fuzzy rules.

Second, the widely used Takagi-Sugeno (T-S) fuzzy systems [115] with functional consequences:

$$Rule\ i: if\ x_1\ is\ F_1^i\ , x_2\ is\ F_2^i, \dots\dots, x_m\ is\ F_m^i \tag{2.2}$$

$$THEN\ y\ is\ G^i = (x_1, x_2, \dots, x_m), i = 1,2, \dots, n.$$

Where $G^i(.)$ is a linear function:

$$G^i = (x_1, x_2, \dots, x_m) = b^i + a_1^i x_1 + a_2^i x_2 + \cdots + a_m^i x_m.$$

where the coefficients b^i, a_j^i , with j = 1, . . . , m, are constants.

Third, singleton-type fuzzy systems [114] are with fuzzy rules of the following form:

$$Rule\ i: if\ x_1\ is\ F_1^i\ , x_2\ is\ F_2^i, \dots \dots , x_m\ is\ F_m^i \tag{2.3}$$

$$THEN\ y\ is\ b^i, i = 1,2, \dots , n.$$

where b^i is a real number and, a singleton. In [126] the input-output relation with regard to an affine-in-control system is shown to be a multiaffine function, resulting in a singleton-type fuzzy system or piecewise multiaffine (PMA) system. This sort of fuzzy system is also known as a PB system (piecewise bilinear) since the output of a two-dimensional example, multiplication of two variables, may be represented as $b^i = ax_1 + bx_2 + cx_1x_2 + d$, for scalars a, b, c, and d, see [114], [117]. When fuzzy variables are completely utilised in both the antecedents and the consequents, Mamdani-type fuzzy systems are linguistically comprehensible.

Nonetheless, T-S fuzzy systems, on the other hand, are based solely on functional membership functions (MFs), which are utilized without labels. We don't have linguistic variables in the T-S system. PB or PMA systems are simpler subsets of the two preceding varieties of fuzzy systems. PMA systems are Mamdani fuzzy systems with singleton consequents, and they may be generated from T-S fuzzy systems by removing the constant terms from the consequents. T-S fuzzy systems are simply concerned with fuzzy set in their premises, but Mamdani fuzzy systems are profoundly concerned with both fuzzy set and logic. Because neither language variables nor MFs are required, PB systems operate independently of fuzzy sets and logic. In the case of PMA systems, these functions in the premises have a triangular form and solely serve as interpolation parameters, which are not always regarded as membership functions in the typical "fuzzy" meaning. . However, Mamdani-derived PMA systems may retain their position as fuzzy control, and linguistic labels may be provided to singletons if necessary. It is worth noting that all three forms of fuzzy systems are known to be capable of generic approximation for any nonlinear function [118]. T-S fuzzy modelling.

On the other hand, can significantly minimise the amount of fuzzy rules, especially for high-dimensional complex systems [114]. During the first 10 years following Mamdani's successful use of fuzzy logic control, researchers faced several challenges from traditional control theorists, as recounted in [114], [119], and [120]. The fundamental reason for this is because no stability study for fuzzy control was available at the time [121]. T-S fuzzy systems

were initially created in 1985 in response to these complaints. Because T-S fuzzy systems are related with linear models in their consequences, model-based stability analysis and control design for fuzzy systems may be accomplished using traditional Lyapunov-based methodologies, as demonstrated initially in [122]. T-S fuzzy modelling may be used to precisely describe a nonlinear system in a compact set of the state space, with nonlinearities incorporated in membership functions [106].

As a result, using T-S fuzzy model-based methodologies, it is often difficult to perform a non-conservative stability analysis of a given nonlinear system. T-S fuzzy systems, more specifically, belong to a type of polytopic uncertain systems, the uncertainties of which are induced by the nonlinearity of the MFs. As a result, the T-S fuzzy model-based stability analysis is always conservative [123]. PMA models were subsequently introduced to address this shortcoming of T-S fuzzy models. As seen in [114] PMA models are totally parametric and quite comparable to linear systems, while being approximate representations of nonlinear systems in nature. Because of this benefit, PMA systems can potentially have required and adequate stability criteria, much like linear systems [124].This cannot be true for other kinds of fuzzy systems. Because T-S fuzzy systems and PMA systems both contain linear systems as a special case, any theoretical framework built for these two types of fuzzy systems is likely to be broader than its linear version.

The goal of this section of the thesis is to present a succinct review of fuzzy control research since Mamdani's group's pioneering work at Queen Mary College. There is no attempt here to evaluate the literature in its entirety, which includes many good volumes [106], [125], [126] and hundreds of technical papers, for example [114], [119], [121], [127] and references therein. Instead, following the growth of fuzzy control systems is limited to a chosen and representative list of certain breakthrough discoveries. Our major goal is to present a historical reasoning and current research status for each form of fuzzy system without unnecessary mathematical complexity. The emphasis is on fuzzy model-based stability analysis rather than model-free fuzzy stability analysis. To keep things simple, only techniques based on Lyapunov stability theory for continuous-time dynamical systems will be addressed. However, theoretical results on stability analysis and control design with or without various performance specifications, such as H∞ and H2 with respect to external disturbances, robustness with respect to time delay or modelling uncertainty, and so on, as well as their discrete-time counterparts, have been widely reported in the fuzzy control literature [106], [128].

2.3 Lyapunov-Based Stability Analysis

Consider the open loop T-S fuzzy system as follow:

$$\dot{x}(t) = \sum_{i=1}^{r} h_i(z) A_i x(t) \tag{2.4}$$

The initial stability analysis findings were proposed in [129] for the T-S fuzzy system (2.4), and in [122] for its discrete-time equivalent. Consider the quadratic Lyapunov function:

$$\mathrm{V(x)} = x^T \mathrm{Px}, \mathrm{P} > 0. \tag{2.5}$$

The outcome listed below is simple to get.

Theorem 2.1: [129] The equilibrium of the T-S fuzzy system (2.4) is globally asymptotically stable if there exists a common positive and symmetric definite matrix P such that:

$$A_i^T P + P A_i < 0, i \in \varphi_r. \tag{2.6}$$

The three points that follow demand special consideration.

Remark 2.1: Conditions (2.6) are expressed in terms of linear matrix inequalities (LMIs).The stability analysis can be easily verified with available numerical solvers [130].

Remark 2.2: A common Lyapunov matrix variable P has to exist for all local linear subsystems.

Remark 2.3: The uncertainty of the system (2.4) is presented on MFs nonlinearities. Then, the stability analysis is embedded in the conventional robust control theory.

Regarding the first observation, it is certainly true that the prospect of reformulating the stability analysis of T-S fuzzy systems as a convex optimization problem has stimulated the rising interest in this category of fuzzy systems [125]. This makes it possible to develop systematic and efficient frameworks for the stability analysis and control design of broad nonlinear systems; see [106] and [131] for full reviews of important discoveries from the 1990s and the early 2010s. [132] has a relatively current overview of this area of study. The two further comments focus on the T-S fuzzy control theory's conservativeness problem [126].

The majority of the research effort is currently focused on this topic. The next sections address two strategies for reducing the conservatism of T-S fuzzy model-based approaches. The first is based on the selection of several families of Lyapunov function candidates, which are

then mixed with slack variables introduced by robust control methods such as the Finsler lemma, Sprocedure, and so on [130]. The second mainstream entails figuring out how to make better use of the information on the MFs for stability analysis.

2.4 Relaxations with Different Choices of Lyapunov Functions

The application of the quadratic Lyapunov function to deal with stability and stabilisation yields surprising conservative results in most circumstances, as shown in [133], [129]. To address this limitation, more general classes of Lyapunov functions have been proposed in the T-S fuzzy literature, such as fuzzy Lyapunov functions (FLFs) depending on the MFs [134], [135], [136], piecewise Lyapunov functions (PLFs) [133], [131], [137], line integral Lyapunov functions (LILFs) [135], [138], [139], polynomial Lyapunov functions depending on the MFs with arbitrary, multidimensional fuzzy Lyapunov functions [140], [141], and so on. When utilising FLFs for the stability analysis of the continuous-time T-S fuzzy system (2.4), the stability criteria are dependent on the time-derivatives of the MFs.

When utilising FLFs to analyse the stability of the continuous-time T-S fuzzy system (2.4), the stability criteria are dependent on the time-derivatives of the MFs, and hence the derivatives of the system state. This demands more theoretical breakthroughs, significantly more numerical complexity, and a significantly greater effort to get convex formulations than a quadratic Lyapunov-based framework.

To circumvent this challenge, many approaches for considering the upper boundaries of the MFs' time derivatives have been offered. This, however, frequently results in a local analysis setting [140]-[142]. Another option is to employ PLFs or LILFs to avoid the existence of MF time derivatives in the stability requirements. However, in these circumstances, some particular structures that inject some conservatism should be placed on the Lyapunov matrices. Furthermore, PLFs are only appropriate for T-S fuzzy systems with triangular or trapezoidal MFs that induce certain state-space partitions [143], [144]. Furthermore, LILFs-based techniques often need the premise variables to be the system state, i.e., x. Nonetheless, this assumption has lately been eliminated in [139]. The use of Polynomial Lyapunov Functions for the stability study of T-S fuzzy systems has already been thoroughly described in [128]. As a result, only the two additional situations, FLFs and LILFs, are discussed briefly.

Consider a simple example of FLFs depending explicitly on MFs as follows [134]:

$$V(x) = x^T(\sum_{i=1}^{r} h_i(z)P_i)x,\ P_i > 0. \tag{2.7}$$

Whose time derivative is given by:

$$\dot{V}(x) = \begin{bmatrix} x \\ \dot{x} \end{bmatrix}^T \begin{bmatrix} \sum_{i=1}^{r} \dot{h}_i(z)P_i & * \\ \sum_{i=1}^{r} h_i(z)P_i & 0 \end{bmatrix} \begin{bmatrix} x \\ \dot{x} \end{bmatrix} \tag{2.8}$$

Remark 2.4: When the positive definite and symmetric matrices are enforced as $P_1 = \cdots = P_r = P$, the QLF (2.9) is recovered quite well (2.12). As a result, QLFs are simply a subset of FLFs. Also note that the variables $\dot{h}_i(z),\ i \in \Omega_r$ occur directly in the expression of V˙ (x). This decision complicates the stability analysis significantly. It should be noted that the fuzzy Lyapunov function (2.12) is part of a broader class of Lyapunov function possibilities. In comparison to the quadratic one, we conclude that there is no assurance that FLFs-based conclusions are less conservative than those generated from QLFs, as demonstrated by [145].

This is owing to the inclusion of previously discovered time-derivatives of the MFs in theoretical advancements utilising FLFs [136]. As a result, the stability conservatism is directly related to how such unpredictable temporal derivatives are handled. To prevent complexity, one might use notions linked to MF characteristics to deal with their temporal derivatives. For example, the convex sum condition (2.7) states that $\sum_{i=1}^{r} \dot{h}_i(z)X = 0$ for every matrix X. This implies that: $\sum_{i=1}^{r} \dot{h}_i(z)P_i = \sum_{i=1}^{r} \dot{h}_i(z)(P_i + X)$ Assume there are upper constraints on the MFs' time derivatives such that $|\dot{h_i(z)}| \leq \theta_i$, for some positive scalars θ_i , $i \epsilon \varphi_i$.Then comes the following:

$$x^T(\sum_{i=1}^{r} \dot{h}_i(z)(P_i + X)x \leq x^T P_\theta x\ . \tag{2.9}$$

Where $P_\theta = \sum_{i=1}^{r} \theta_i(P_i + X)$. Using a null-term approach or Finsler lemma [144], inequality (15) can be exploited for stability analysis as summarized in the following theorem.

Theorem 2.2: [135] Given a T-S fuzzy system (2.4) and upper bounds on the time-derivatives of the MFs as $|\dot{h}_i(z)| \leq \rho_i\ , i \in \Omega_r$. If there exist positive definite matrices $P_i \in R^{nxn}$, with $\boldsymbol{i} \in \Omega_r$, and matrices $X \in R^{nxn}$, $M \in R^{nxn}$, $N \in R^{nxn}$, satisfying the following linear matrix inequalities:

$$P_i + X > 0\ , i \in \Omega_r$$

$$\begin{bmatrix} P_\theta - MA_i - A_i^T M^T & * \\ P_i + M^T - NA_i & N + N^T \end{bmatrix} < 0, i \in \Omega_r \tag{2.10}$$

With P_θ is given by (2.10). Then, the fuzzy system (2.4) is asymptotically stable.

Remark 2.5: Unlike Theorem 2, Theorem 2.5 only allows for local stability analysis of the system (2.8), since the system state must meet $\left|\dot{h}_i(z)\right| \leq \rho_i$, $i \in \Omega_r$. As a result, the primary purpose is to increase the domain of attraction encompassed within the state area indicated by the preceding assumption [140]. Different and many local stability requirements have been presented in the FLFs literature [142] employing various sorts of features of fuzzy MFs and relaxing methods from robust control theory. It is worth noting that, unlike the continuous-time example, the stability analysis for discrete-time T-S fuzzy systems does not encounter any difficulties when dealing with the time-derivatives of MFs when utilising FLFs [128], [146].

Remark 2.6: In Theorem 1, the matrices X, M, and N are treated as slack variables for relaxation reasons. It is simple to demonstrate that the result of Theorem 2 includes the result of Theorem 1 by enforcing $X = 0, P_i = P > 0, i \in \Omega_r$, and $= -\mathrm{P}$. This theory shows that FLFs offer less conservative stability analyses as compared to quadratic Lyapunov functions.

2.5 Exploiting the Knowledge of the Membership Functions for Stability Relaxations

The continuous time Takagi-Sugeno model is given as follow:

$$\dot{x}(t) = \sum_{i=1}^{n} h_i(z)\big(A_i x(t) + B_i u(t)\big). \tag{2.11}$$

Where the normalized Membership Function $h_i(z)$ is defined as:

$$h_i(Z) = \frac{w_i(z(t))}{\sum_{i=1}^{n} w_i(z(t))} \; ; \; w_i\big(z(t)\big) = \prod_{j=1}^{q} \mu_{ji}(z(j)). \tag{2.12}$$

The grades of membership of the premise variables in the respective fuzzy sets $\mathrm{M}_\mathrm{j}^\mathrm{i}$ are given as $\mu_{ji}\big(z(j)\big)$. Note that the normalized MFs satisfy the following convex sum property:

$$\begin{matrix} \sum_{i=1}^{n} h_i\left(z(t)\right) = 1, \\ h_i(z(t)) \geq 0. \end{matrix} \tag{2.13}$$

T-S MFs are used to "blend" the local linear submodels (2.11), which describe the system's nonlinearity (2.13). Nonetheless, these MFs have been extensively viewed as system uncertainty, with most previous research based on quadratic, fuzzy, and polynomial Lyapunov functions [124] relying only on their convex sum feature (2.13). The conservativeness issue always exists when the form of the MFs and its intrinsic time changing feature are not explicitly taken into consideration in the stability analysis, as detailed in [137], [147]-[148]. Several ways of explicitly include the form of the MFs in the stability analysis have been presented. These techniques may be classified into two types [149].

To begin, there are membership-function-approximation techniques that use MF information via alternative comparable functions such as staircase MFs [150], piecewise linear MFs [151]. Second, there are membership bound-dependent techniques that use MF bound information for stability analysis [152]. In addition, the MFs image space and order relations among the MFs have been used, as shown in [149], [153], and [154]. It should be noted that membership-function approximation and image-space techniques produce a greater number of convex stability constraints. Slack variables are typically added into the stability requirements of membership-bound-dependent techniques for relaxing reasons.

The next theorem illustrates the approach in [152] of leveraging the MFs shape information to further lower the stability conservatism of Theorem 1 by introducing a new relaxation variable. [137] has more comments and analyses on membership-function-dependent stability.

Efforts have also been made to lessen the stability conservatism generated by the sufficiency of fuzzy summations, i.e., the methods by which MFs are dropped out to get a finite set of LMI criteria. Although several solutions to this source of conservatism have been presented [155], [152], the most renowned technique is based on Pólya's theorem. The authors of [156] used Pólya's theorem to develop asymptotically necessary and sufficient LMI-based requirements for the stability and performance of T-S fuzzy systems based on testing the positiveness of multidimensional matrices. It should be noted that when the homogeneous degree of a multiple summation fuzzy Lyapunov function grows, the conservatism of the stability criteria reduces as additional degrees of freedom are introduced.

Chapter 3

Systems Control tools

3.1 Introduction

Before we start the control theory we present in this chapter the main definitions that help to understand the rest of the this thesis chapters

3.2 Modeling process

In this section, we define the meaning of modeling and process.

3.2.1 Definition of a process

A process is a system that is subjected to one or more input signals and that delivers one or more output signals. We distinguish the input signals on which it is possible to act, these are the control signals. On the other hand, disturbance signals are signals faced by the process. The output signals are a function of the internal process state and the input signals. They are measured using sensors.

3.2.2 Definition of a model

A model is a mathematical representation of a process. It describes the behavior of the process in the considered operating domain. We are talking about the domain of validity of the model. This representation can be in the form of:

• Scalar representation which is a representation in the form of differential, recurrent (with differences) or algebraic equations.

• Frequency representation (transfer function).

• Matrix representation (state representation).

3.3 Objectives of a modeling

The objectives of modeling a process can be:

• Simulate the process in order to predict its behavior.

• Perform the synthesis of a control law in order to regulate or subjugate the process.

3.4 Modeling methods

A distinction is made between the knowledge model and the representation model. The knowledge model is developed by applying the general laws of physics, chemistry, biology, etc. The different phenomena that characterize the evolution of the process are described by mathematical relationships. The knowledge model is often nonlinear and involves process parameters. The representation model is a mathematical relationship obtained experimentally between the input signals and the output signals of the process. In order to control a process, the automation specialist seeks to obtain the simplest representation model that best describes the behavior of the process. When the process is nonlinear, we obtain a valid local model around the operating point considered. The parameters of the model are determined from the measurements of the applied input signals and the measurements of the obtained output signals. Since no knowledge of the laws reacting to the process is required, it is called a "black box" model. Certain authors [157], [158] prefer to use “gray box” models which are obtained on the one hand from known laws on the process and on the other hand from experimental measurements, for example the parameters of the process involved in the physics equations, chemistry, biology, etc. can be estimated experimentally.

3.4.1 Model representation

It is necessary to specify the input signals applied to the process and the output signals measured using sensors. If the process has a single input signal and a single output signal (SISO), it is monovariable system. Otherwise, it is multivariable system (MIMO). In the SISO case it can be represented simply by a transfer function, but in the MIMO case, simplicity is lost because the initial conditions are not easily taken into account, so the representation is matrix. We have to choose between a static model and a dynamic model. The model must be

dynamic if we want to take into account the time constants of the process. The static model is represented by algebraic equations while a dynamic model is represented by differential equations or difference equations. Experimental tests make it possible to know whether the process is linear or nonlinear in the operating domain considered, a linear process verifies the properties of superposition and homogeneity [159] [160]:

Let $y_1(t)$ and $y_2(t)$ be the outputs obtained by applying the inputs $u_1(t)$, $u_2(t)$.

Superposition property: The system output is equal to $y_1(t)+y_2(t)$ when we apply the input $u_1(t)+u_2(t)$.

Homogeneity property: The process response to the input $\alpha u_1(t)$ is equal to $\alpha y_1(t)$.

A process is said to be invariant if it respects the principle of time invariance:

Principle of temporal invariance: Let y (t) be the output obtained when we apply the input $u(t)$. If the input is translated by τ, u (t-τ) the output is also, y (t-τ).

The representation of an invariant linear dynamic system can be in the form of:

• Differential equations or linear difference equations with constant coefficients between the input signals and the output signals

• Frequency curve.

• Linear state curve with constant matrices.

We can classify the models according to the evolution of the parameters, we then distinguish the deterministic model such as we know the behavior of the advance system and does not involve any random variable. And the stochastic model such that there are random variables in the system, and we do not know its behavior in advance e.g. noise. When trying to achieve a dynamic model, a "noise" type disturbance exists. This noise is modeled by a sequence of random variables. A noise can affect a process in different ways. There are two distinct families of noise:

• Output noise which is additive noise that affects the measurement of the process output.

• The state noise vector which is an additive noise that affects the state of the process.

As, in general, we do not know with precision the nature of the noise, which affects the process, we must make assumptions about it: we deduce from these the structure of the model-hypothesis and the algorithm used for the adjustment of parameters. An incorrect assumption can significantly degrade the performance of the model. These problems have been very widely studied in the case of linear modeling [161].

3.4.2 Modeling in state space

The description of processes by state models was, and still is, an approach widely used in several disciplines, such as Automation. Several results relating to the analysis of the processes described by state models have been developed, and this in various fields (modeling, estimation, filtering, control, etc.) The first most interesting works in Automation are due to Kalman (1960); most often used continuous state models. Since the extraordinary development of IT resources, especially in recent years, and the remarkable development of digital computers (large memory capacity, speed of calculation, etc.), continuous state models are used less and less, leaving place for discrete state models. Thus, we are then only interested in processes that can be described by discrete state models. We can distinguish two categories of state models.

• State model in canonical form

The process can be described by a state model in the canonical form of controllability or observability. The canonical form of controllability is interesting for the study of process controllability and for the development of a feedback control. Whereas the canonical form of observability simplifies the study of process observability and the determination of an observer.

• Report model in general form

The process is described by a state model where the matrices involved in this model have any shapes.

3.5 LTI systems

An LTI system is a linear time invariant system, we saw the definition above. On the other hand, the algorithms that have been developed within the framework of this thesis only

concern discrete time LTI systems. There is, however, no theoretical obstacle to their transposition to continuous systems.

3.6 Systems representation

The systems represented by linear models can be in different forms [162]:

The input-output differential form: The mathematical description of a system operation consists in writing the set of algebraic and differential relations which connect the m input variables represented by a vector denoted *u (t),* the l output variables represented by a vector noted *y (t)* and the internal variables of the system.

Using the fluency graph method, it is possible to eliminate the mathematical relations involving internal variables and thus obtain algebraic or differential relations.

These relations can be put in the following form:

$$L(s)y(t) = M(s)u(t)$$

The input-output transfer matrix: The input-output transfer matrix, denoted *F(s)* where s represents the derivation operator $\left(\mathrm{s} \doteq \frac{\mathrm{d}}{\mathrm{dt}}\right)$, describes the evolution of the output *y(t)* as a function of the input *u(t)* where $y(t) = F(s)u(t)$.

3.7 The state form

The approach that we used in this thesis is the modeling of the system by equations of state. When designing the control law, it is necessary to use either the matrix or the input-output transfer function, or the state form [162]. The transfer function is the easiest to use and represent a system if the initial conditions are taken into account which is not the case for multivariable systems. Hence the use of state representation.

3.8 State representation

State representation was introduced in 1960 for linear invariant systems. The state representation is a matrix representation that can be linear or nonlinear continuous time or discrete time. It allows the monitoring of the temporal evolution of inputs-outputs plus the monitoring of the evolution of the dynamics of a system thanks to a state vector X which contains all the internal variables of the system. The state representation is made up of the state equation and the output or measurement equation. In the continuous case it is determined by first order differential equations while it is represented by difference or recurrent equations in the discrete-time case. It also helps determine the future state by knowing the state at the initial instant. State representation enables the use of linear algebra computational techniques and powerful tools for state feedback control synthesis. The state representation also highlights the problems linked to the simplification of a pole by a zero of the transfer function [163].

3.9 State vector

The mathematical model defining any physical system, must make it possible to represent the evolution of the outputs for given inputs, thus translating the principle of causality and the physical laws of the process [164]. The quantities characterizing the state of the system evolve from an instant t_0 called the initial instant. From a deterministic point of view, the knowledge of these quantities at a time t_0 and the knowledge of the inputs values for all $t > t_0$ makes it possible to determine in a unique way the value of the outputs for all $t > t_0$ [165] That is to say, the internal initial state must be known to ensure the subsequent uniqueness of the behavior of the process over time. We can say that the initial state vector behaves like the minimum past memory of a system that must be known in order to predict its evolution.

3.10 Mathematical representation

In this section, we present the mathematical linear models that can present continuous and discrete-time systems.

3.10.1 Continuous case

Continuous-time dynamic systems are described by a system of equations of the form [152]:

$$\begin{cases} \dot{x}(t) = f(x(t), u(t), t) \\ y(t) = g(x(t), u(t), t) \end{cases} \tag{3.1}$$

The vector $u(t) \in \mathbb{R}^m$ denotes the input (or the command) of the system, and $y(t) \in \mathbb{R}^p$ is the output and the vector $x(t) \in \mathbb{R}^n$, solution of the first equation (ordinary differential equation, known as the evolution equation), is called the state vector of the system. The state of a model represents the set of variables necessary to know the behavior of the output of a system according to the inputs to which it is subjected. Modeling a system using these equations of state consists in building a model involving only differential equations of order 1. The structure of the representation of state is common to all linear systems. A continuous linear invariant system is described by the following state representation [162]:

$$\begin{cases} \dot{x}(t) = Ax(t) + Bu(t) \\ y(t) = Cx(t) + Du(t) \end{cases} \tag{3.2}$$

$A \in \mathbb{R}^{n \times n}$ is called the system state matrix, $B \in \mathbb{R}^{n \times m}$ is the control matrix, $C \in \mathbb{R}^{p \times n}$ ius the observation matrix and $D \in \mathbb{R}^{p \times m}$ represents the direct transmission matrix.

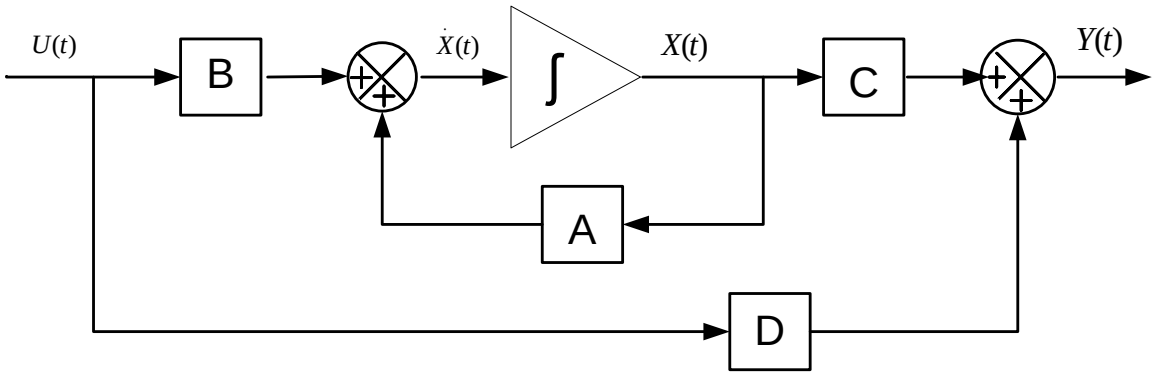

Figure 3. 1 Continuous state representation diagram

The state representation of a system is not unique, because you can change the state vector. Indeed, it suffices to consider the new vector $z = P\,x$ where P is an invertible matrix, so that the state representation becomes:

$$\begin{cases} \dot{z}(t) = Mz(t) + Nu(t) \\ y(t) = Qz(t) + Ru(t) \end{cases} \quad (3.3)$$

Where $M = PAP^{-1}$, $N = PB$, $Q = C\,P^{-1}$ *and* $R = D$.

3.10.2 Discrete-time case

In the discrete-time case, the state representation of a system is generally given in the following form [164]:

$$\begin{cases} \mathrm{x(k+1) = f(x(k), u(k), k)} \\ \mathrm{y(k) = h(x(k))} \end{cases}$$

Where the first vector equation is first order, at time k

x (k): is the state vector of the studied system.

u (k): the input or command of the system.

y (k): is the output of the system.

If the system is linear invariant, the representation of the system is of the form:

$$\begin{cases} x(k+1) = Ax(k) + Bu(k) \\ y(k) = Cx(k) + Du(k) \end{cases} \quad (3.4)$$

Where the matrices *A, B, C and D* are with constant coefficients. Like the continuous case, a state representation of a discrete-time system is not unique. It suffices to perform a change of the state vector *z (k) = Px (k)* where *P* is an invertible matrix, to obtain a new state representation.

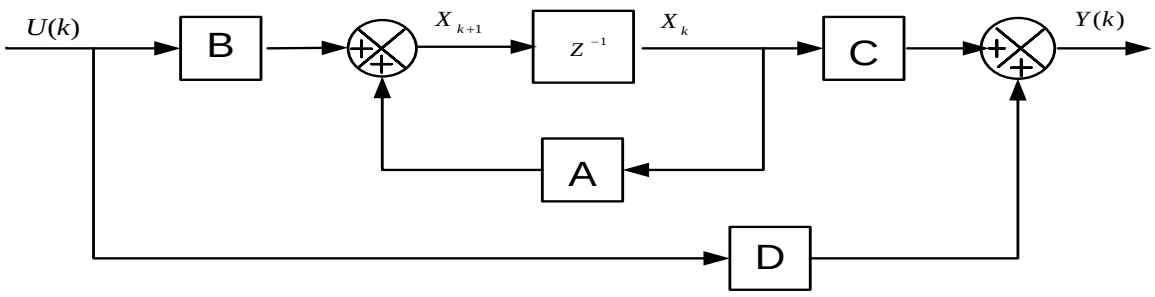

Figure 3. 2 Discrete State representation diagram

3.11 Definition of identification

Definition in the sense of Zadeh (1962): "The identification of a process is defined as the determination, based on knowledge of the inputs and outputs of the process, of a model belonging to a specified class, equivalent to the process". The purpose of identifying a system is to determine its mathematical model from measurements and experimental observations. The identification is used for black box models (non-physical model) and gray box models (semi-physical) for which the general laws of physics, chemistry, biology, etc. cannot be applied. The objective is then to determine a model of the system as close as possible to the behavior of the real physical system by using identification techniques.

3.11.1 Perspectives on identification

System identification is the art and science of building mathematical models of dynamical systems from observation of input-output data. It can be seen as the interface between the real world of applications and the mathematical world of control theory and model abstraction. The identification of a system is a very big subject, with different techniques, which will depend on the nature of the models to be identified: linear, non-linear, hybrid, non-parametric, etc [167].

3.11.2 Estimation of model parameters

It consists in determining the values of the parameters of the model chosen on the basis of the input / output observations of the model such that the output of the model is closest to the real system.

3.11.3 Information

This concerns both the information provided by the observed data and prior information on the object to be modeled as the class of the model [167].

3.12 Building a T-S fuzzy model

T-S models represent nonlinear systems as an interpolation between local linear models. Each local model is a dynamic LTI system valid around an operating point. Three separate methods can be used to obtain a TS model: By identification, by linearization around the different operating points (in this case they are local models affine due to the presence of the linearization constant) or by convex polytopic transformation. In the first situation, from data on inputs and outputs, we can identify the parameters of the local model corresponding to the different operating points. In the second and third situation, we assume that we have a non-linear mathematical model.

3.12.1 By Identification

Black box type models are identified from input and output data around different operating points. Regardless of the type of model chosen, this identification requires the search for an optimal structure, the estimation of the parameters and the validation of the final model [168]. Work on the stability analysis of T-S MIMO fuzzy models often adopts the state representation (rather than an input-output model). In the same way, the synthesis of control laws of the processes modeled thanks to the T-S method use the representation of state in order to extend to the nonlinear case the techniques controlled by state feedback. The construction of a so-called multi-observer nonlinear observer from model T-S structures also uses the state representation based on the Luenberger type observer.

3.12.2 By Linearization

In this case, we suppose to have a non-linear mathematical model of the physical process that we linearize around various judiciously chosen operating points. Consider the following nonlinear system:

$$\dot{x}(t) = f\big(x(t), u(t)\big) \tag{3.5}$$

Where $f(.) \in C^1$. The linearization the system (3.5) around the arbitrary equilibrium points $(x_i, u_i) \in \mathbb{R}^p \times \mathbb{R}^m$ is:

$$\dot{x}(t) = A_i(x(t) - x_i) + B_i(u(t) - u_i) + f(x_i, u_i) \tag{3.6}$$

Which can be rewritten as:

$$\dot{x}(t) = A_i x(t) + B_i u(t) + d_i \tag{3.7}$$

Where

$$A_i = \left.\frac{\partial f(x,u)}{\partial x}\right|_{\substack{x=x_i \\ u=u_i}}$$

$$B_i = \left.\frac{\partial f(x,u)}{\partial u}\right|_{\substack{x=x_i \\ u=u_i}}$$

$$d_i = f(x_i, u_i) - A_i x_i - B_i u_i \tag{3.8}$$

From a mathematical point of view corresponds to approximate the function $f(.) \in C^1$ by its tangent plant.

3.12.3 Polytopic transformation

We propose to study this transformation in the general case of a nonlinear system refined in the command:

(Continuous case) $$\begin{cases} \dot{x} = f\big(x(t)\big) + B\big(x(t)\big)u(t). \\ y(t) = g\big(x(t)\big) + D\big(x(t)\big)u(t). \end{cases} \tag{3.9}$$

(Discrete-time case) $$\begin{cases} x_{k+1} = f\big(x(k)\big) + B\big(x(k)\big)u(k). \\ y(t) = g\big(x(k)\big) + D\big(x(k)\big)u(k). \end{cases} \tag{3.10}$$

Where $x(.) \in \mathbb{R}^p, u(.) \in \mathbb{R}^m, y(.) \in \mathbb{R}^l, f\big(x(.)\big) \in \mathbb{R}^p, g\big(x(.)\big) \in \mathbb{R}^l, B\big(x(.)\big) \in \mathbb{R}^{p.m}$ and $D\big(x(.)\big) \in \mathbb{R}^{l.m}$.

Tanaka et al [106] initiated the exposed transformation method. It is based on a convex polytopic transformation of scalar functions originating from nonlinearity. The advantage of this method is not to generate an approximation error and to reduce the number of local models compared to the linearization method. Indeed, in the context of stability analysis of T-S models and the synthesis of regulators, the number of matrix constraint is generally reduced by the transformation method, which is synonymous with less conservatism.

The polytopic transformation can be determined by two methods. The first method is based on the bounding of nonlinear terms. The second is command-oriented, it is based on the structure of the input matrices resulting from the transformation.

Chapter 4

Identification and Takagi-Sugeno

4.1 Identification and Takagi Sugeno models

Nonlinear systems identification from experimental data without any prior knowledge of the system parameters is a challenge in control and process diagnostic. It determines mathematical model parameters that are able to reproduce the dynamic behavior of a system. Combing two fundamental research areas: MIMO state space system identification and nonlinear control system produces a technique that leads to robust stabilization of a nonlinear Takagi-Sugeno fuzzy system.

Recent research was developed in the context of the identification of multivariable systems. These researches, however, demonstrates robustness and effectiveness, not only on the theoretical aspect but also in real processes. Thus, complex systems are generally found in the industry, such as in the aluminum foundry, sawmill plant, robot manipulator [10], etc. The application of identification subspace algorithms in this area is promising for inverse diagnostic [169]. In [170], large-scale wind power interfacing to the power grid was studied, and it presents the impact on the stability of the power system. However, with an additional damping controller of the wind generator, new ways for improving system damping and suppressing the low frequency oscillation (LFO) of power systems can be put forward. The N4SID was proposed to identify the state space model of the controlled object. In [171], the N4SID method was used to obtain a dynamical model of the unmanned vehicle, while open-loop and closed-loop control algorithms were implemented on the ArduinoMega controller. In [172], a closed-loop identification method for Multi-Input Multi-Output (MIMO) system has been proposed. The transfer function matrix of the dynamic system is identified in the form of state-space model using N4SID algorithm from the system. The identification in state space, especially for the N4SID algorithm, is widely used in many areas and for various applications. In particular, N4SID is exploited for estimating parameters of industrial systems, as for the detection and

diagnostic analysis of electrical machines. A few studies are mentioned as shown below. The four studies presented in [173] [174, 169], [175] suggested using one of the most recognized algorithms which are: 1) Multivariable Output Error State Space (MOESP) (firstly presented in [176]), and 2) Canonical Variate Analysis (CVA) (firstly presented in [177]). The MOESP uses the techniques of linear algebra and geometry such as singular value decomposition (SVD), LQ factorization (L: Lower triangular matrix; Q: Orthogonal matrix), and matrices projection. This method involves determining the system matrices A and C directly from the extended observability matrix and determining the rest of the system matrices B, D, Q, R, and S. This is done by using the least squares method (a similar approach is presented in [178], [179], and [176]). The CVA, however, is based on statistical arguments and it extensively uses angles and main directions.

In the following, the identification method explained is the Numerical algorithm for Subspace State Space System IDentification (N4SID) [180]. N4SID is based on well-known linear algebra techniques, singular value decomposition, and QR decomposition (Q: orthogonal matrix; R: upper triangular matrix) for numerical implementation. It could estimate state space matrices of deterministic-stochastic systems directly from input and output data. N4SID is convergent and non-iterative, which is numerically stable. Some works are based on a global modelling technique known as generic multiple model approach. The principle of this approach is aimed at reducing the complexity of the system by a decomposition of its operating space into a finite number of operating ranges. Indeed, a local lower-order linear model structure can often be used to describe the dynamic behavior of the system in this local area.

Therefore, one can suggest using T-S model to solve the whole system behavior. This method is well suited for modelling systems from experimental data. In this modelling approach, two families are known according to the structure used to interpolate the local models. The first, called Takagi-Sugeno multiple model, consists of local models sharing a single state vector. The second approach decoupled multiple models, has each model with its own state vector. It has been sufficiently demonstrated by [181], [182], [183], [184], [185], and [186], that the interest in the multiple model of Takagi-Sugeno is the synthesis of control law or estimating state of nonlinear systems. However, from a structural point of view, all these local models, constituting the multiple models, have the same sizes. Then, a single state vector is used. The complexity of these sub-models is therefore constant regardless of the complexity of the system in different areas of operation. Most research has focused on T-S control such as

Autonomous Vehicles control. Perform lane keeping under multiple constraints, roads with unknown curvature, and uncertain lateral wind force for autonomous vehicles is one of the trend and the challenge of research in our time [7]. We cite also [9] who addresses the shared lateral control between a human driver and a lane keeping assist system of intelligent vehicles for both lane keeping and obstacle avoidance. In [187] and [8], the authors got a lot of attention in minimizing the conflict situations between these two driving actors. These authors avoid using quadratic Lyapunov function because of the conservatism seen in their results. Indeed, they used other function like non-quadratic Lyapunov function which is difficult to implement in real life and add more complexity to the studied system. The method of selection of Lyapunov function and the method of LMI's opening is a wonderful field of research which has led to great interest by researchers. In [188] the authors investigated the sliding-mode control problem of T-S fuzzy multi-agent system. Therefore, a cooperative fuzzy-based dynamical sliding-mode controller was designed. The main idea was to transform the fuzzy weighting matrix into a set of scalars by solving LMI's. Furthermore, the energy-coast was studied by using the linear quadratic regulator. We mention as well, the problem of quantized feedback control of nonlinear Markov Jump Systems (MJS's) demonstrated in [189]. Based on T-S fuzzy model, the nonlinear plant was represented by a class of fuzzy (MJS's) with time-varying delay. The quantized states were utilized for the control aim. The sector bound approach was exploited to deal with quantization errors. The Lyapunov function depended both on information and fuzzy basis functions.

On the other hand, in this thesis, we suggest an improved PDC control law for the T-S system to minimize the conservatism and give more relaxation for the results.We present a new design of a new algorithm which combines these two methods previously described. Individually, both methods have very successful results for the robust control of nonlinear systems described by multiple models from N4SID algorithm. We also compare the N4SID and the MOESP algorithms in order to know how our improvement increases the algorithm performances.

This chapter will be organized as follows. Firstly, a review was done on the main algorithms in this field's sub-space N4SID method with other approaches such as polynomial identification, iterative, and even with other sub-space method. Then, the second part presents the selected algorithm for our application, N4SID model, and demonstrates two variations, N4SID 1 and 2, which will be evaluated and tested. The thesis work is focused on the study of

the stabilization of Takagi-Sugeno fuzzy system [175], [190], [191], based on improved Parallel Distributed Compensation (PDC) control law. Finally, the last part of the thesis is dedicated to the synthesis of non-linear observer based on interpolation of linear observer of Luenberger type called multiobserver.

4.2 Related work

Systems identification literature is mainly concerned with computing polynomial models. This method is effective in the case of Single Input Single Output (SISO) systems represented by a linear transfer function. In the case of Multi-input Multi-output (MIMO) systems, when calculating the polynomial model, we are faced with unsolvable mathematical situations. These situations are, however, known to typically give rise to numerically ill-conditioned mathematical problems. Therefore, recent research works have proposed different approaches to solve this issue and minimize the parameterization required. These approaches are called subspace methods which are described in the following sections.

4.3 Iterative identification model

The classical identification algorithms proposed by [192], [193], [170] were a solution for the identification of multivariable systems. However, this method diverges sometimes, as it is an iterative algorithm. Also, iterative algorithms require knowledge of the order, and the observability or controllability indicates that classical algorithms need a parameterization and nonlinear optimizations. To avoid divergence problems, the research works are focused on the non-iterative methods such as N4SID from [180], and also MOESP algorithms presented in [176]. They are both based on geometry and linear algebra and are explained in the next section.

4.4 Subspace identification model

This model was presented to be a powerful alternative to the classical system identification method based on iterative approaches. The key step of this method is the oblique projection of subspaces generated by the block Hankel matrices formed by input and output data of the system. Indeed, in practice, methods of subspaces, whose name reflects that linear

models can be obtained from subspaces of certain matrices, is computed from data inputs and outputs. Then, only the order of the system is needed and it can be determined through input-output, meaning through inspection of the dominant singular value. Moreover, N4SID does not need an extra parameterization of the initial state when estimating a state space from data measured on a plant with a non-zero initial condition.

N4SID and MOESP algorithms are similar. However, the difference is in the numerical implementation level. N4SID use the QR decomposition and MOESP use the LQ decomposition. There is also a difference between these algorithms in the extraction of the system matrices and the convergence speed in addition to the level of the estimation error. Another difference between these two algorithms is related to the kind of employed subspaces projections in the Hankel matrices. These matrices are obviously constituted of the system input/output data. In other words, N4SID uses oblique projection while MOESP is particularly based on the orthogonal projection. Many researches confirm this difference between these two algorithms. For proof purpose we compute the performance indicators usually used to validate a model. They are the mean relative square error (MRSE) and mean related variance (MVAF). These two indicators determine the estimation error and evaluate the accuracy identification between algorithms. This method determines a criterion to measure the distance between the model and the real system. To sum up, we can determine the right choice based on the system aspect and the desired performance like processing time and cross validation [169].

4.5 Contributions

N4SID algorithm and multiple model approach integration, in one algorithm to control a nonlinear multivariable system, should be reflected in an increase of the robustness. The algorithm identifies multi inputs multi outputs (MIMO) systems that are modelled by a state space representation. The algorithm reliably considers the parameters of a deterministic-stochastic, dynamic and linear time invariant multivariable system. It is known that this estimate gives accurate parameters of the process. N4SID is a convergent algorithm and is simple to implement. Our algorithm is used with a nonlinear system in a local area, around an operating point. Multiple model approach will interpolate this local area to cover all nonlinear area. The combined result will yield to an improved nonlinear control. This work is the first that combines these two robust methods to get an efficacy and new technique of nonlinear stabilization.

Firstly, we present a review of the N4SID method. Secondly, we explain the theoretical control part.

4.6 Model description

Given N measurements of the inputs and the outputs generated by the combined stochastic and deterministic system of order n, we considered the following model for identification:

$$x(k+1) = Ax(k) + B\,u(k) + w(k), \tag{4.1}$$

$$y(k) = Cx(k) + Du(k) + v(k), \tag{4.2}$$

where $A \in R^{nxn}$ is the state matrix, $B \in R^{nxm}$ is the control matrix, $C \in R^{lxn}$ is the observation matrix, $D \in R^{lxm}$ is the direct transmission matrix. $v \in R^{lxl}$ and $w \in R^{nxl}$ are both zero-mean Gaussian white noise.

4.6.1 Objective of N4SID method

From the control vectors $u = [u_1\, u_2 \cdots u_n]$; and measurement vectors $y = [y_1\, y_2 \cdots y_n]$ we want to determine the order n of the unknown system, the system matrices A, B, C, D and the noise matrix Q^s, S^s, R^s. E denotes the expected value as operator and $\delta_{kl}$the Kornecker delta. Then we can calculate:

$$E\left[\left(\frac{w_k}{v_k}\right)(w_l^t v_l^t)\right] = \begin{bmatrix}(Q^s) & (S^s)\\ (S^s)^T & (R^s)\end{bmatrix}\delta_{kl} \geq 0^2. \tag{4.3}$$

4.6.2 Decomposition of deterministic-stochastic models

State space representation can be decomposed into two sub-models, deterministic sub-model and stochastic sub-model. Let x_k^d , x_k^s are respectively the deterministic and stochastic components of the state vector represented in equation (4.4) and (4.5). Also, y_k^d , y_k^s are respectively the deterministic and stochastic components of the measurement vector presented in (4.1) and (4.2).

$$x_k = x_k^d + x_k^s \tag{4.4}$$

$$y_k = y_k^d + y_k^s \tag{4.5}$$

However, the system can be decoupled into deterministic and stochastic parts defined as follow:

$$\begin{cases} x_{k+1}^d = Ax_k^d + Bu_k \\ y_k^d = Cx_k^d + Du_k \end{cases}, \tag{4.6}$$

$$\begin{cases} x_{k+1}^s = Ax_k^s + w_k \\ y_k^s = Cx_k^s + v_k \end{cases}. \tag{4.7}$$

4.6.3 Assumption about the deterministic-stochastic model

It is assumed that the pair (A, C) is observable, and the pair $A, B(Q^s)^{\frac{1}{2}}$ is controllable. The controllable pair (A, B) can be stable or unstable. However, the controllable modes $A, (Q^s)^{\frac{1}{2}}$ must be stable. We also assume that the stochastic state x_k^s and stochastic output y_k^s are quasi-stationary. Finally, using this assumption, we can then, in the next section, represent the N4SID algorithm.

4.6.4 N4SID algorithm

In this section, we present two N4SID approach (N4SID 1 and 2 in the following) which the main difference is: N4SID 2 has the same steps as N4SID 1 except that it uses the approximate state $\widetilde{X}_i$ and all the systems matrices. This algorithm determines the state directly from the input and output data and minimizes the number of equations.

First, the N4SID 1 algorithm is explained in Figure 4.1 We have therefore, from a finite number of input-output data (U_k, Y_k), the possibility to form the Hankel matrices (defined in appendix A)$\left(Y_p, Y_f\right)^T$ and $\left(U_p, U_f\right)^T$. In addition, we deduce the oblique projections$(\mathrm{Z_i}, \mathrm{Z_{i-1}})$.

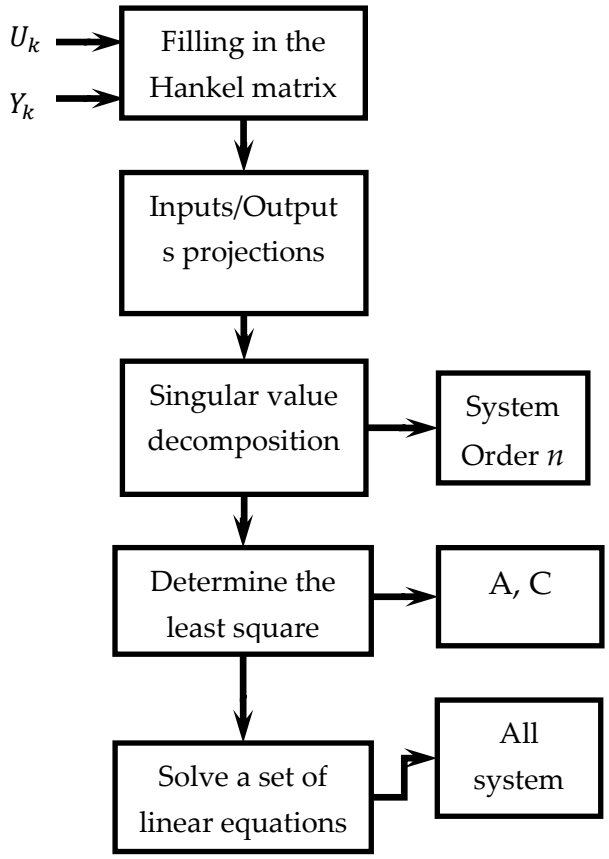

Figure 4. 1 Steps of the N4SID1 algorithm.

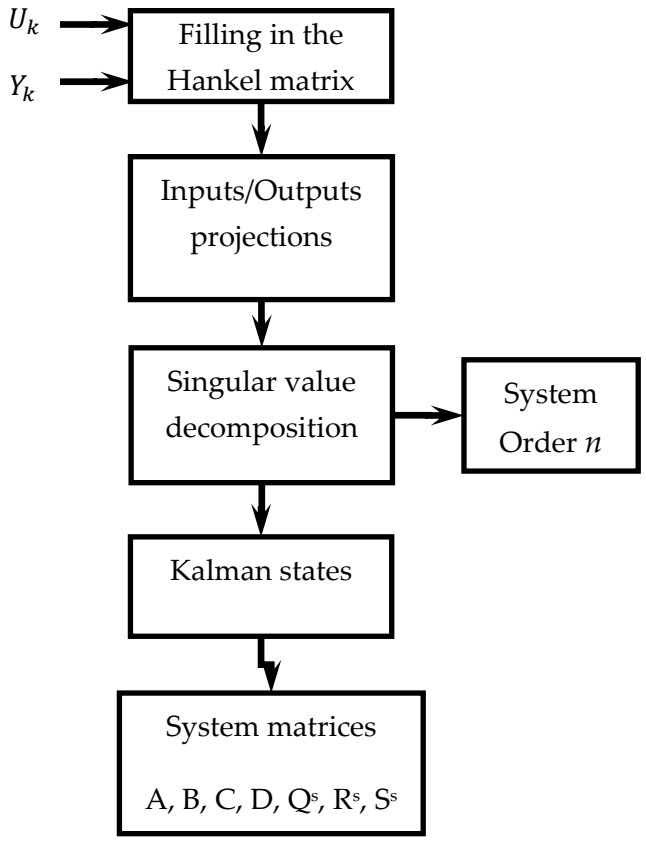

Figure 4. 2 Steps of the N4SID2 algorithm.

These projections are useful in determining the combined system. Indeed, the linear combinations to be made from the input-output block Hankel matrices to generate (Z_i, Z_{i-1}) (projections defined in the appendix C) are functions of the system matrices. Moreover, the system matrices can be retrieved from these linear combinations, as shown in the appendix C.

From input-output we can define the extended observability matrix Γ_i . Trough $\Gamma_i = [C \quad CA \ldots . \quad CA^{i-1}]$, we are able find the *A* and *C* matrices:

Matrix *C*: If we show the extended observability matrix, it is important to note that we can extract directly from the first row of *Γ* the *C* matrix.

Matrix *A*: It is determined from the shift structure of Γ_i, denoting : $\overline{\Gamma_i} = \underline{\Gamma_i} A$; where $\underline{\Gamma_i}$ is the matrix Γ_i without the last l rows: $\underline{\Gamma_i} = (C \quad CA \quad \ldots \quad CA^{i-2})$. $\overline{\Gamma_i}$ is without the first l rows: $\overline{\Gamma_i} = (CA \quad CA^2 \quad \ldots \quad CA^{i-1})$. Therefore, the matrix A is expressed as: $A = \overline{\Gamma_i}^{+} \underline{\Gamma_i}$. Later then, we

determine the rest of system matrices *B*, *D*, Q^s, R^s and S^s from linear regression algorithm and the resolution of linear combination demonstrated in appendix C.

This means N4SID 2 does not need to go through the complicated step 4 shown in Figure 4.1. However, it is clearly explained in the appendix C for determining *B* and *D* matrices as shown in Figure 4.2. Also, the Kalman states are determined as it is explained in [180].

4.7 Takagi Sugeno control

A multiple model or T-S (Takagi-Sugeno) model is a nonlinear system in the form of linear interpolation of n premises. The three methods used for obtaining the multiple model representation are: 1) the identification technique, 2) linearization around different operating points, and 3) polytopic transformation. In the first step, we identify the model parameters based on the given input-output. The second and third steps are assumed to have a nonlinear mathematical model.

Conditions on stability and stabilization of discrete-Time T-S systems are shown in the next section. Stability analysis is derived via quadratic Lyapunov function method and LMIs (Linear Matrix inequalities) formulation, obtained from BMIs (Bilinear Matrix Inequality). Discrete-Time T-S systems using improved PDC (Parallel Distributed Compensation) technique will be applied in order to estimate state with the multi-observer technique.

4.7.1 Discrete-time Takagi-Sugeno system

We considered a Takagi-Sugeno (T-S) model described by fuzzy IF-THEN rules. The ith rule of the model is of the following form:

Rule i

$IF\ F_1(k)\ is\ M_{1i}\ and\ \dots F_n(k) is\ M_{ni}\ THEN$

$$\begin{cases} x(k+1) = A_i x(k) + B_i u(k) \\ y(k) = Cx(k) \end{cases}, \tag{4.8}$$

where $M_{1i}, \ldots . M_{ni}$ are the fuzzy sets and n is the number of the rules. In addition, $x_k \in \mathbb{R}^n$ is the state vector; $u_k \in \mathbb{R}^p$ is the measurable output vector; A_i, B_i and C are the system matrices with appropriate dimension. Then, the premise variables are $Z(k) = [Z_1(k) \ldots . \quad Z_q(k)]$ .Therefore, a T-S model is based on the interpolation between several LTI local models using the following equations:

$$x(k+1) = \sum_{i=1}^{n} \mu_i \left(Z(k)\right)\left(A_i x(k) + B_i u(k)\right) \tag{4.9}$$

and

$$\begin{cases} \sum_{i=1}^{n} \mu_i \left(Z(k)\right) = 1 \\ \mu_i(Z(k)) \geq 0 \end{cases} \quad \text{with,} \tag{4.10}$$

$$\mu_i(Z) = \frac{w_i(Z(t))}{\sum_{i=1}^{n} w_i(Z(t))} \;;\; w_i\big(Z(t)\big) = \prod_{j=1}^{q} M_{ji}(Z(t)).$$

The approach proposed is based on the quadratic Lyapunov function. Choosing a Lyapunov function that guarantee stability in simple terms requires a symmetric matrix which is positively defined. Practically, it is simple to implement using $V(x(k))$ such as:

$$V\big(x(k)\big) = X_k^T P X_k. \tag{4.11}$$

The Discrete-Time T-S fuzzy system is asymptotically stable. If a common matrix $P = P^T > 0$ exists, then the following LMI is feasible [130], [191]:

$$\begin{cases} P > 0\,. \\ A_i^T P A_i - P < 0. \end{cases} \tag{4.12}$$

4.7.2 Stabilization of a discrete-time multiple state feedback

The stabilization technique used in this thesis is the Parallel Distributed Control (PDC) law, which is written as follow:

$$u(k) = -\sum_{i=1}^{n} \mu_i(Z(k)) K_i x(k). \tag{4.13}$$

Using the discrete- time Takagi-Sugeno models previously described in (4.9), a closed loop control law by PDC is given by:

$$\begin{cases} x(k+1) = \sum_{i=1}^{n}\sum_{j=1}^{n} \mu_i\big(Z(k)\big)\mu_j\big(Z(k)\big)\delta_{ij}x(k). \\ \delta_{ij} = A_i - B_iK_j. \end{cases} \tag{4.14}$$

Hypothesis: The two matrices (A_i, B_i) are assumed to be controllable. It is said that the multiple models is locally controllable as described in [194].

The stabilization conditions for discrete-time multiple models using closed-loop PDC control law require a symmetric matrix $P > 0$ and matrices $K_i, \forall i \in I_n$ such as:

$$\begin{cases} l_d(\delta_{ii}, P) < 0, \forall i \in I_n, \\ l_d\big(\delta_{ij}, P\big) \leq 0, \forall i, j \in I_n^2 \ \ and, \\ \mu_i(Z(k))\mu_j(Z(k)) \neq 0. \end{cases} \tag{4.15}$$

$$l_d\big(\delta_{ij}, P\big) = \left[\frac{\delta_{ij}+\delta_{ji}}{2}\right]^T P \left[\frac{\delta_{ij}+\delta_{ji}}{2}\right] - P, \quad with \tag{4.16}$$

$$\delta_{ij} = A_i - B_iK_j.$$

The following conditions are:

$$(A_i - B_iK_i)^T P(A_i - B_iK_i) - P < 0. \tag{4.17}$$

In pre and post multiplying by P^{-1}, we obtain:

$$P^{-1}(A_iP^{-1} - B_iK_iP^{-1})^T P(A_iP^{-1} - B_iK_iP^{-1}) > 0. \tag{4.18}$$

It's assumed that $X = P^{-1}$ and $N_i = K_iP^{-1}$; then we obtain:

$$X(A_iX - B_iK_iX)^T P(A_iX - B_iN_i) > 0. \tag{4.19}$$

Using the Schur complement, the above condition is written in the form of LMI:

$$\begin{bmatrix} X & * \\ A_iX - B_iN_i & X \end{bmatrix} > 0 \ \forall \ i \in I_n. \tag{4.20}$$

By using the same method, the condition $l_d\big(\delta_{ij}, P\big) \leq 0$ is written as:

$$\begin{bmatrix} X & * \\ \frac{A_i+A_j}{2}X - \frac{1}{2}(B_jN_i + B_iN_j) & X \end{bmatrix} \geq 0 \ \forall (i,j) \in I_n^2, i < j. \tag{4.21}$$

Now the discrete-time Takagi-Sugeno models in (4.9) is globally asymptotically stable via improved PDC control law, especially if there are symmetric matrices such as $P = P^T > 0$ and $Q = Q^T \geq 0$ which verifies [195]:

$$\begin{cases} l_d(\delta_{ii}, P) + (r-1)Q < 0, \forall i \in I_n, \\ l_d(\delta_{ij}, P) - Q \leq 0, \forall i, j \in I_n^2, i < j, \\ \mu_i(Z(k))\mu_j(Z(k)) \neq 0. \end{cases} \tag{4.22}$$

$$l_d(\delta_{ij}, P) = \left[\frac{\delta_{ij}+\delta_{ji}}{2}\right]^T P \left[\frac{\delta_{ij}+\delta_{ji}}{2}\right] - P. \tag{4.23}$$

By using matrices Q_{ij} due to the conservatism and pessimism results, we can define the following theorem presented in [194].

Theorem: if matrices $P = P^T > 0$, $Q_{ij} = Q_{ij}^T$ and matrices K_i exists, which verify the equation below:

$$\begin{cases} l_d(\delta_{ii}, P) + (r-1)Q < 0, \forall i \in I_n. \\ l_d(\delta_{ij}, P) - Q \leq 0, \forall i, j \in I_n^2, i < j. \\ \mu_i(Z(k))\mu_j(Z(k)) \neq 0. \end{cases} \tag{4.24}$$

$$Q = \begin{bmatrix} Q_{11} \ldots . & Q_{1n} \\ Q_{1n} \ldots . & Q_{nn} \end{bmatrix}. \tag{4.25}$$

Then the Takagi-Sugeno system in (4.9) is globally asymptotically stable. Thus, the BMIs of the previous theorem can be transformed into LMIs, which gives:

$$\begin{cases} X = P^{-1}. \\ Y_{ii} = XQ_{ij}X. \\ K_i = N_i X^{-1}. \\ \forall i \in I_n. \end{cases} \tag{4.26}$$

4.7.3 Synthesis of multi-observers

Synthesis techniques based on state feedback (PDC control law) need to have the entire state vector $x(k)$, as shown in equations (4.12)-(4.13). Therefore, we need to rebuild the state based system using the following multiobservers:

$$\begin{cases} \hat{x}(k+1) = \mu_i\big(Z(k)\big)\big(A_i\hat{x}(k) + B_i u(k)\big) + L_i\big(y(k) - \hat{y}(k)\big). \\ \hat{y}(k) = \sum_{i=1}^{n} \mu_i\big(Z(k)\big) C_i \hat{x}(k). \end{cases} \tag{4.27}$$

Knowing that the estimation of the state vector error is given by:

$$\tilde{x}(k) = x(k) - \hat{x}(k). \tag{4.28}$$

The dynamics of the estimation error could then be written as:

$$\begin{cases} \hat{x}(k+1) = \sum_{i=1}^{n}\sum_{j=1}^{n} \mu_i\big(Z(k)\big)\mu_j\big(Z(k)\big)\theta_{ij}\tilde{x}(k). \\ \theta_{ij} = A_i - L_i C_j \,, \forall (i,j) \in I_n^2. \end{cases} . \tag{4.29}$$

The synthesis of a multiple observer is used in determining local gains $L_i \in I_n$ to ensure the convergence to zero of the dynamics of the estimation error. We have to ensure that there is $P = P^T > 0$ and matrices $L_i \in I_n$ that verify:

$$\begin{cases} l_d(\theta_{ii}, P) < 0, \forall i \in I_n. \\ l_d\big(\theta_{ij}, P\big) \leq 0, \forall i,j \in I_n^2. \\ \mu_i(Z(k))\mu_j(Z(k)) \neq 0. \end{cases} \tag{4.30}$$

$$l_d\big(\theta_{ij}, P\big) = \left[\frac{\theta_{ij}+\theta_{ji}}{2}\right]^T P \left[\frac{\theta_{ij}+\theta_{ji}}{2}\right] - P. \tag{4.31}$$

Then the estimation error converges to zero. The conditions of the previous theorem can be transformed into LMIs using the Schur complement:

$$\begin{bmatrix} P & * \\ P\,\frac{A_i+A_j}{2} - \frac{1}{2}\big(N_j C_j + N_j C_i\big) & P \end{bmatrix} \geq 0. \tag{4.32}$$

$$\forall (i,j) \in I_n^2 \,, i < j.$$

The previous multiple observers may be improved by the following theorem. The multiple observers is globally asymptotically stable if there exist a symmetric matrices $P > 0$, Q_{ij} and $L_i \in I_n$ that satisfy:

$$\begin{cases} l_d(\theta_{ii}, P) + Q_{ii} < 0, \forall i \in I_n. \\ l_d\big(\theta_{ij}, P\big) + Q_{ij} \leq 0, \forall i,j \in I_n^2. \\ \begin{bmatrix} Q_{11} & Q_{1n} \\ Q_{1n} & Q_{nn} \end{bmatrix}. \\ \mu_i\big(z(k)\big)\mu_j\big(z(k)\big) \neq 0. \\ \theta_{ij} = A_i - L_i C_j \forall (i,j) \in I_n^2. \end{cases} \tag{4.33}$$

The matrix inequalities are written as:

$$\begin{cases} P > 0. \\ \begin{bmatrix} P - Q_{ii} & * \\ PA_i - N_i C_i & P \end{bmatrix} > 0 \ \forall \ i \in I_n. \\ \begin{bmatrix} P - Q_{ij} & * \\ P\frac{A_i + A_j}{2} - \frac{1}{2}(N_i C_j + N_j C_i) & P \end{bmatrix} \geq 0 \ \forall \ i, j \in I_n^2, i < j. \\ Q = \begin{bmatrix} Q_{11} \ldots . & Q_{1n} \\ Q_{1n} \ldots . & Q_{nn} \end{bmatrix}. \\ N_i = PL_i. \end{cases} \tag{4.34}$$

4.8 Takagi- Sugeno stabilization

In this part of the thesis, we are interested in stabilization of the multiple models. In the previous section, we studied only one model with two inputs and two outputs. In this section, we study the stability and stabilization of four MIMO models (each model are LTI with two inputs and two outputs). The T-S is formed by the matrices identified by N4SID2 since the results are more accurate than N4SID1 and MOESP using MSE criterion the tables is present in the fifth chapter of this thesis. The states matrices Ai, represented in equation (4.9), that represent the multiple models, the input vectors, and the output vectors of each local linear model are given as:

$$A_1 = \begin{bmatrix} -1 & 0 & -0.5 & -2 \\ 0 & -2.5 & 0.6 & 1 \\ 0.5 & -1 & -2 & 0.8 \\ 0.2 & 0 & -0.6 & -3 \end{bmatrix}, \quad B_1 = \begin{bmatrix} 1 & 0.5 \\ 0 & 2 \\ 2 & 5 \\ 3 & 2 \end{bmatrix}, \quad C_1 = \begin{bmatrix} 2 & 0 & 5 & 0.3 \\ 3 & 2 & 1 & 0.5 \end{bmatrix}, \quad D_1 = \begin{bmatrix} 0 & 0 \\ 0 & 0 \end{bmatrix}$$

$$A_2 = 0.85 \begin{bmatrix} -1 & 0 & -0.5 & -2 \\ 0 & -2.5 & 0.6 & 1 \\ 0.5 & -1 & -2 & 0.8 \\ 0.2 & 0 & -0.6 & -3 \end{bmatrix}, B_2 = 0.63 \begin{bmatrix} 1 & 0.5 \\ 0 & 2 \\ 2 & 5 \\ 3 & 2 \end{bmatrix}, C_2 = \begin{bmatrix} 2 & 0 & 5 & 0.3 \\ 3 & 2 & 1 & 0.5 \end{bmatrix} D_2 = \bar{0}$$

$$A_3 = 0.8\begin{bmatrix} -1 & 0 & -0.5 & -2 \\ 0 & -2.5 & 0.6 & 1 \\ 0.5 & -1 & -2 & 0.8 \\ 0.2 & 0 & -0.6 & -3 \end{bmatrix}, B_3 = 0.6\begin{bmatrix} 1 & 0.5 \\ 0 & 2 \\ 2 & 5 \\ 3 & 2 \end{bmatrix}, C_3 = \begin{bmatrix} 2 & 0 & 5 & 0.3 \\ 3 & 2 & 1 & 0.5 \end{bmatrix}, D_3 = \begin{bmatrix} 0 & 0 \\ 0 & 0 \end{bmatrix}$$

$$A_4 = 0.6\begin{bmatrix} -1 & 0 & -0.5 & -2 \\ 0 & -2.5 & 0.6 & 1 \\ 0.5 & -1 & -2 & 0.8 \\ 0.2 & 0 & -0.6 & -3 \end{bmatrix}, B_4 = 0.4\begin{bmatrix} 1 & 0.5 \\ 0 & 2 \\ 2 & 5 \\ 3 & 2 \end{bmatrix}, C_4 = \begin{bmatrix} 2 & 0 & 5 & 0.3 \\ 3 & 2 & 1 & 0.5 \end{bmatrix}, D_4 = \bar{0}$$

From (4.27) and (4.34), the feedback gain K_i, the matrix P , and the gain L_i matrix can be obtained as:

$$\begin{cases} P = X^{-1}. \\ K_i = N_i P. \\ N_i = PL_i. \end{cases} \tag{4.35}$$

Solving LMIs system using (4.34) and (4.35), we obtain:

$$P = \begin{bmatrix} 0.6384 & -0.1033 & 0.0320 & -0.0867 \\ -0.1033 & 0.1409 & -0.0300 & -0.0324 \\ 0.0320 & -0.0300 & 0.1888 & 0.0465 \\ -0.0867 & -0.0324 & 0.0465 & 0.6214 \end{bmatrix}, K1 = \begin{bmatrix} -0.1654 & 0.3336 & -0.2190 & -2.2542 \\ -0.3941 & -0.1941 & -0.0100 & 1.1506 \end{bmatrix},$$

$$K2 = \begin{bmatrix} -0.1609 & 0.2250 & -0.0541 & -1.5345 \\ -0.5701 & -0.0491 & -0.1422 & 0.7680 \end{bmatrix}, K3 = \begin{bmatrix} -0.1374 & 0.2276 & -0.1572 & -1.6386 \\ -0.5965 & -0.0446 & -0.0513 & 0.8109 \end{bmatrix},$$

$$K4 = \begin{bmatrix} -0.1687 & 0.4688 & -0.1928 & -2.0304 \\ -0.7914 & -0.1578 & -0.1185 & 1.0189 \end{bmatrix},$$

$$L1 = \begin{bmatrix} -0.2415 & -0.6126 \\ 0.6019 & -1.5255 \\ -0.1902 & 0.2630 \\ 0.1673 & -0.2075 \end{bmatrix}, L2 = \begin{bmatrix} -0.4337 & -0.4415 \\ 1.2732 & -2.9498 \\ -0.3946 & 0.6706 \\ 0.3345 & -0.5000 \end{bmatrix}, L3 = \begin{bmatrix} -0.3757 & -0.5576 \\ 1.3848 & -3.1157 \\ -0.3425 & 0.6031 \\ 0.3256 & -0.4825 \end{bmatrix}, L4 = \begin{bmatrix} -0.5692 & -0.4968 \\ 0.7727 & -1.6519 \\ -0.2834 & 0.2843 \\ 0.1315 & -0.1060 \end{bmatrix}.$$

4.9 Conclusion

In this section of the thesis, we used two N4SID algorithms for the identification of multivariable systems and we compared our proposed algorithm with the MOESP. The N4SID algorithms subspace identification methods differ from other classic identification algorithms in their concept, interpretation, and computational implementation. We demonstrated the efficiency of an improved N4SID algorithm. In the second section of this part, we used the LTI identified model with N4SID2 to build the T-S nonlinear system. After that, we studied various conditions for the global asymptotic stability system. This approach ensures the global asymptotic stability of the closed loop T-S fuzzy systems. Therefore, the stabilization results require the quadratic Lyapunov function and all components of the state vector. For this reason, we constructed a multiobserver to estimate the state vector.

Chapter 5

The design of the new PDC controller based on identification models

5.1 Introduction

Researches nowadays are very interested in developing new ideas and technologies to attain new heights in science, such as the invention of space robots, full autonomous vehicles, Hyperloop and so on. To reach these future technologies, the starting point is developing a new mathematical formulation and equations, which should be realized in practice to translate these ideas into reality.

Discovering and developing new techniques constitute a great impact in both academic and industrial settings. Research always needs innovation to push science to the future path. In this thesis, we used a new system control technique combined with the field of system identification to come up with an improved T-S fuzzy controller. We focus on the case of multi-input/multi-output (MIMO) systems to be identified and controlled. The black box identification, which means no prior knowledge of the system behavior, is the considered identification type.

The goal is to describe a real system dynamics by a mathematical model. This model is created only by the inputs data applied to the system and the recorded outputs, which are the real system response to the previous inputs. The challenge is the necessity of a mathematical model that represents closely and with high accuracy the real system behavior. In our case, we need to identify the system in the form of state space representation as our mathematical model; more clearly, we need to estimate the system matrices. The system state space representation can be identified by two methods:

The subspace system identification and the iterative algorithms. The most common subspace identification algorithms are cited as follows: In [196], the algorithm is based on Markov

parameters with a block Hankel matrix to estimate discrete-time state space model matrices. Indeed, the theory relies on Markov parameters as a starting point, which is very difficult to implement in real process. Papers [197] and [198] are for purely deterministic systems based on two steps: 1) A state space vector sequence is computed from the block Hankel matrix containing the input and output data of the system. 2) The system matrices are extracted from solving a set of linear equations.

The purely stochastic identification is presented in [199] and [200]. In our work, we present and use the identification of MIMO combined stochastic-deterministic systems based on subspace method. We cite the most recognized algorithms in the case of the subspace method: Numerical algorithm for Subspace State Space System. Identification (N4SID), Multivariable Output Error State Space (MOESP), and Canonical Variate Analysis (CVA). On the other side, the most popular iterative algorithm is Prediction Error Method (PEM) [161] and [201]. These two identification methods are different in such points presented in the following:

The subspace identification algorithms are all the time convergent and numerically stable since they are based on linear algebra and geometry tools. They do not need a priori parametrization like the iterative algorithms; only the order of the system is needed, and it can be determined through the computation of the number of the dominant SVD of a matrix that is calculated during the identification. For example, the N4SID is based on both singular value decomposition and QR decomposition (Q: orthogonal matrix; R: upper triangular matrix), while the MOESP uses singular value decomposition (SVD), LQ factorization (L: Lower triangular matrix; Q: Orthogonal matrix), and matrices projection. The CVA, however, treats the problem of combined stochastic-deterministic state space identification from a different point of view, which is purely statistical, and it extensively uses angles and main directions.

The iterative algorithm [161] needs a priori parametrization to start up. It needs a priori knowledge of the system order and the observability or the controllability matrices' indices plus an extra parametrization of the initial state to estimate the state space representation. The convergence is not sure, it can goes into infinite loop with the existence of local minima. In addition, the result can be far from the real value because of a mistake in the initial state estimation. The advantage of PEM compared to the N4SID is that it is more efficient for an input less rich in frequency, e.g. sum of sinusoid; otherwise, the N4SID works better and easily in our case.

We previously mentioned the difference in numerical implementation between N4SID and MOESP, Here; we will briefly explain the algorithms steps. The first part is the same for

both methods. The algorithms begin by determining the extended observability matrix (EOM) and the system order directly from the input-output data by projection. The main difference is that the MOESP determines the A and C matrices directly from the extended observability subspace. The technique used is by shifting the variance of the subspace spanned by the columns of the EOM. This technique was used by [196] in realization theory and in stochastic identification by [120]. The next step of Multivariable Output Error State Space is to compute the remain deterministic and stochastic system matrices respectively B, D and Q, S, R. These matrices are extracted in function of A, C matrices coming from the first step above. Another difference is the projection of input/outputs contained in the Hankel block matrices. N4SID uses the oblique projection, which can lead to ill conditioning subspace problem, while MOESP uses the orthogonal projection, which overcomes the ill conditioning issue seen in the deterministic case in [174].

In this thesis, the N4SID speed of convergence and the accuracy of the estimation are confirmed to be better than the MOESP. This is done by computing the convergence time and the estimation error presented in Table 5.1 and Table 5.2. The N4SID and CVA determine the state sequence implicitly in the function of the EOM established in the first step and the output-input data and then extract all the system matrices in one step by solving a set of linear equations using least square method. So the MOESP extracts the system matrices in two steps, while N4SID and CVA do so in one step. When comparing these three algorithms, the main resemblance is the employment and the exploitation of the same subspace to find the EOM and the system order.

The authors of [202] combined (PEM) and N4SID to directly identify the linear model in continuous-time state-space. They compared a nonlinear physical model of longitudinal car vehicle dynamics to a linear model obtained by system identification techniques. A blind identification method based on N4SID is proposed to identify the disturbances parameters, such as electromechanical modes, harmonics, and forced oscillation in a power system only from measured outputs [203].Flapping Wings Micro Aerial Vehicle (FWMAV) is the result of Unmanned Aerial Vehicle technology development with the mechanism of flapping wings and with the dimensions of the object as small as possible. Modeling of FWMAV dynamics is needed to predict future conditions based on information from current conditions and designed control actions. The FWMAV model uses two system identification algorithms for longitudinal and lateral dynamic. The results obtained show that the N4SID is more accurate than the State Space Estimation (SSEST) algorithm [204]. Subsequently, we compared between two versions

of N4SID, which are N4SID 1, 2, and MOESP algorithms. The control design will be based on the Linear Time Invariant (LTI) matrices produced by the N4SID 1 & 2, as we will show subsequently.

The T-S model is a nonlinear model constructed by local linear models or matrices $(\mathrm{A_i}, \mathrm{B_i}, \mathrm{C_i}, \mathrm{D_i})$, $i = 1 \dots n$, sharing a single state vector. The nonlinearity comes from the interpolation function, which is the membership function. These matrices in our work come from the identification using N4SID algorithm in its two versions. In this thesis, the contribution is presented as an improvement of the Parallel Distributed Compensation control law that leads to a remarkable enhancement of the nonlinear Takagi-Sugeno fuzzy systems stabilization in term of convergence speed and relaxation. This contribution never existed in the literature until now. This improved formulation of the PDC control law is developed and discussed based on mathematical theory applied to discrete-time T-S fuzzy system and validated by simulations, in order to show the effectiveness and robustness of the improved fuzzy controller based on PDC law, knowing that the discrete-time T-S fuzzy model is based on subspace identification algorithms, which are N4SID 1 and 2.

We support our idea by comparing between the classical T-S controller presented in [45] and our improved T-S model results in terms of relaxation and stabilization time convergence. The results confirm the effectiveness and the clear impact of the improved PDC formulation for the stabilization purpose of the discrete-time T-S model.

Many research works in high-tech fields are focused on T-S fuzzy systems, e.g. the development of new controllers for autonomous vehicles [6]. The author developed a lateral controller based on T-S fuzzy system to perform lane keeping under various constraints like steering saturation and uncertain lateral wind. Many steering controllers have been developed to solve the path tracking issues [6] [7] [8]. The authors of [205] combined the fuzzy logic and the PID control and suggested a new lateral control system architecture. Several studies have focused on steering system control, especially fuzzy control systems [6] [7] [8]. These authors achieved very interesting results regarding lateral control based on Takagi–Sugeno models. They used a non-quadratic Lyapunov function, which is complicated in terms of implementation because of quadratic Lyapunov function conservatism. They also used assumptions and approximations to compute the state vector containing six state variables. In addition, scientists trying to improve the T-S fuzzy system in terms of convergence speed have published many new theories. Paper [206] reports a robust fuzzy predictive control (RFPC) method based on T-S model for the nonlinear uncertain process in the presence of the unknown

disturbances and time-varying delay.

The authors designed fuzzy rules, the nonlinear process represented by some linear sub-models, to increase the convergence speed and the regulative ability with regard to the developed controller. The output tracking error is introduced into the T-S model to improve the control law. In [126], the stability analysis and controller design for delayed T–S fuzzy systems are investigated. In order to be suitable for triple integral terms, an improved matrix inequality is proposed to estimate both strictly and nonstrictly rational proper functions.

We organized this part in the following order. First, we reviewed the main algorithms in the state space field, N4SID method and other approaches. The second section shows the three candidate algorithms steps. The next part, presents the discrete-time T-S systems control architecture and steps, which include the stability and the stabilization condition and process development. The last two parts are the results and the discussion of those results.

5.2 Numerical algorithm for subspace State Space identification

The discrete –time LTI state space identification model is presented as follow:

$$x_{k+1} = A_i x_k + B_i u_k + w_k, \tag{5.1}$$

$$y_k = C x_k + D u_k + v_k, \tag{5.2}$$

This model is absolutely based on input-output data. This model is a stochastic-deterministic system of n order.

Where $A \in R^{nxn}$, $B \in R^{nxm}$, $C \in R^{lxn}$, $D \in R^{lxm}$, $v \in R^{lxl}$, and $w \in R^{nxl}$ are both zero-mean Gaussian white noise.

5.2.1 N4SID Algorithms 1 and 2 Steps

In this section, we will be explaining the two N4SID versions algorithm's steps. We started with the N4SID 1 Algorithm Steps [180]:

We start by filling the Hankel matrix with input/output measurements. Then, we define the input/output projections. After that, we calculate the singular value that gives us the system order and the EOM. Then, we solve the least square solution to extract our system *A* and *C*

matrices. Finally, we find the rest of the system matrices by linear equations resolution. The second version of the N4SID Algorithm [180] steps are the same as the first one except the 4th and 5th points which are respectively:

The calculation of the states *Xi / Xi+1* called the Kalman states and resolving a bunch of linear equations to come up with the system matrices *A, B, C, D, Q, R, and S.*

5.2.2 MOESP Algorithm and Steps

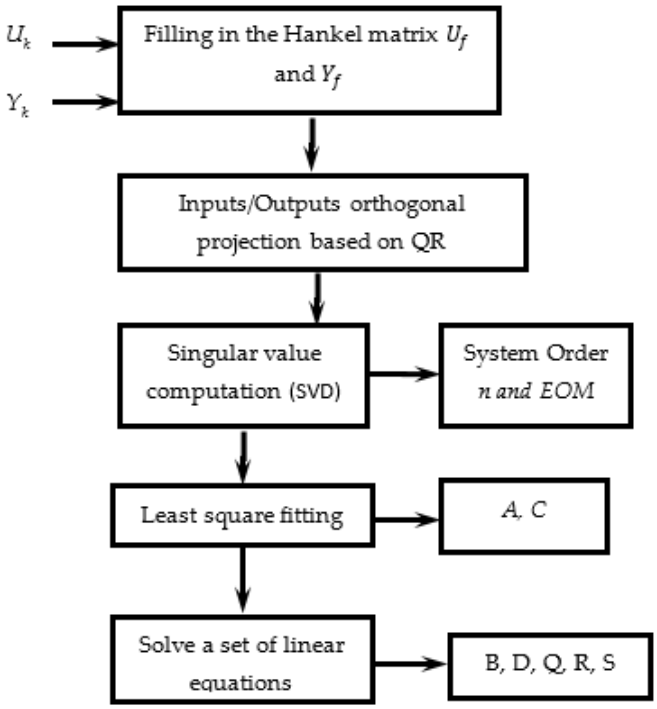

Figure 5. 1 MOESP algorithm steps.

5.3 Discrete-time Takagi-Sugeno Systems control architecture and steps

This section of the thesis treats and discuss the stability and the stabilization conditions of the T-S system based on the quadratic Lyapunov function in the form of linear matrix inequalities. The stabilization theory is based on the feedback state control, more precisely on the improved Parallel Distributed Compensation control law formulation. The last part of this section focus on the theory that leads us to compute the entire system state vector, which is the

Luenberger nonlinear observer. This state vector is applied in the stabilization formula for the system control purpose.

5.3.1 Discrete-time Takagi-Sugeno System

The following discrete-time (T-S) system is described by fuzzy IF-THEN rules.

The Rule i is of the form:

IF $\varphi_1(\mathrm{k})$ is τ_1^i and ... $\varphi_{\mathrm{q}}(\mathrm{k})$is τ_q^i THEN

$$\begin{cases} x_{k+1} = \mathrm{A_i} x_k + \mathrm{B_i} u_k. \\ y_k = \mathrm{C_i}\, x_k. \end{cases} \tag{5.3}$$

Where τ_1^i …. τ_q^i are the fuzzy sets, and n is the number of the rules. In addition, $x_k \in \mathbb{R}^n$ is the state vector; $u_k \in \mathbb{R}^p$ is the control vector and y_k is the measurable output vector; A_i, B_i and C_i are the system matrices with appropriate dimension, In addition, the premise variables are represented by the vector $\varphi(k) = [\varphi_1(k) \ldots . \quad \varphi_q(k)]$. The discrete-time T-S fuzzy system is presented as follows:

$$x_{k+1} = \sum_{\mathrm{i}=1}^{\mathrm{n}} \xi_{\mathrm{i}} \big(\varphi(\mathrm{k})\big)\big(\mathrm{A_i} x_k + \mathrm{B_i} u_k + B_i^w \mathrm{w(k)}\big). \tag{5.4}$$

The convexity conditions are:

$$\begin{cases} \sum_{\mathrm{i}=1}^{\mathrm{n}} \xi_{\mathrm{i}} \big(\varphi(\mathrm{k})\big) = 1 \\ \xi_{\mathrm{i}}(\varphi(\mathrm{k})) \geq 0. \end{cases} \tag{5.5}$$

With

$$\xi_{\mathrm{i}}(\varphi(\mathrm{k})) = \frac{\lambda_{\mathrm{i}}(\varphi(\mathrm{k}))}{\sum_{\mathrm{i}=1}^{\mathrm{n}} \lambda_{\mathrm{i}}(\varphi(\mathrm{k}))} \; ; \; \lambda_{\mathrm{i}}\big(\varphi(\mathrm{k})\big) = \prod_{\mathrm{j}=1}^{\mathrm{q}} \tau_j^i(\varphi(\mathrm{k})).$$

$\xi_{\mathrm{i}}(\varphi(\mathrm{k}))$, $i = 1,2, \ldots, n$, are the normalized grades of membership.

$\tau_j^i\big(\varphi(\mathrm{k})\big), \mathrm{j} = 1,2,.., \mathrm{q}$, are the grades of membership corresponding to the fuzzy term τ_j^i.

The open loop discrete-time T-S fuzzy system is:

$$x_{k+1} = \sum_{\mathrm{i}=1}^{\mathrm{n}} \xi_{\mathrm{i}} \big(\varphi(\mathrm{k})\big)\, \mathrm{A_i} x_k. \tag{5.6}$$

The proposed Lyapunov function $\mathrm{V(x_k)}$ is:

$$V(x_k) = X_k^T F\, X_k. \tag{5.7}$$

We choose this Quadratic Lyapunov candidate function because it is easy in real implementation contrary to other Lyapunov function.

The T-S expressed in equation (5.6) is Quadratically asymptotically stable in case a common symmetric matrix $F = F^T > 0$ exists, such that the following LMIs are feasible [130] [191]:

$$\begin{cases} F > 0. \\ A_i^T F\, A_i - F < 0. \quad \forall\, i \in I_n. \end{cases} \tag{5.8}$$

To say that $V(x_k) = X_k^T F\, X_k$ is a Lyapunov function we must validate these three conditions that are the stability conditions in (5.8):

- $V > 0,\ V(0) = 0.$
- $V(k+1) - V(k) < 0.$

So $V > 0$ gives $F > 0$, because $X_k^T X_k > 0$ which is the first condition in equation (5.8), $V(0) = 0$, which is validate as well. $V(k+1) - V(k) < 0$ which gives the second equation of (5.8).

The above LMIs are the sufficient asymptotic stability conditions obtained by the application of the Quadratic Lyapunov function (5.7) along the trajectory of the discrete-time T-S presented in (5.6).

The existence of matix *F* depends on two main conditions that are [207]:

1. Every matrice must be a Schur matrix.

2. The product $\prod_{i=1}^{n} A_i$ must belong to Schur condition.

We said *A* is a Schur matrix when the module of each Eigen values of matrix *A* belong to the disc of center (0, 0) and radius 1.

5.3.2 Discrete-time Takagi-Sugeno Stabilization

The improved feedback control law precisely the PDC control law is written as follows:

$$u_k = -\sum_{i=1}^{n} \xi_i(\varphi(k))[G_i x_k] - [S_i x_{k+1}].$$

Where $S_i = G_i$.

$$u_k = -\sum_{i=1}^{n} \xi_i(\varphi(k))[G_i x_k] - [G_i x_{k+1}]. \tag{5.9}$$

Applying a PDC control law on the closed loop discrete-time T-S fuzzy system described in (5.7) we get:

$$\begin{cases} x_{k+1} = \sum_{i=1}^{n} \sum_{j=1}^{n} \xi_i(\varphi(k)) \xi_j(\varphi(k)) \vartheta_{ij} x_k - B_i G_j x_{k+1}. \\ \vartheta_{ij} = (A_i - B_i G_j). \end{cases} \tag{5.10}$$

Hypothesis: In this case the two system matrices (A_i, B_i) are supposed to be controllable. It is said that the T-S models are locally controllable as described in [194].

The closed loop of the discrete-time T-S fuzzy system (5.4) via PDC control law is globally asymptotically stable if exist a symmetric matrice $F > 0$ and a matrices $G_i, i \in I_n$ such as [208]:

$$C_{discrete}(\vartheta_{ii}, F) < 0 \quad , \ \forall\, i \in I_n \tag{5.11}$$

$$C_{discrete}(\vartheta_{ij}, F) \leq 0 \quad \forall\, (i,j) \in I_n^2 \quad i < j \tag{5.12}$$

$$\xi_i(\varphi(k))\, \xi_j(\varphi(k)) \neq 0. \tag{5.13}$$

$$C_{discrete}(\vartheta_{ij}, F) = \left[\frac{\vartheta_{ij}+\vartheta_{ji}}{2}\right]^T F \left[\frac{\vartheta_{ij}+\vartheta_{ji}}{2}\right] - F\ . \tag{5.14}$$

The first closed loop stabilization condition is $C_{discrete}(\vartheta_{ii}, F) < 0, \forall i \in I_n$ we substitute *ij* in equation (5.14) by *ii* we get the condition:

$$(A_i - B_i G_i)^T F (A_i - B_i G_i) - F < 0. \tag{5.15}$$

Multiplying (18) in pre and post by F^{-1}, we conclude the following inequality:

$$F^{-1}(A_i - B_i G_i)^T F (A_i - B_i G_i) F^{-1} - F^{-1} F F^{-1} < 0 \tag{5.16}$$

$$(A_i F^{-1} - B_i G_i F^{-1})^T F (A_i F^{-1} - B_i G_i F^{-1}) - F^{-1} < 0. \tag{5.17}$$

We want to write this inequality as LMI. We used the Schur complement as follow:

Let the matrices $Q = Q^T$ and $R = R^T$.

The following matrix inequalities are equivalent:

$$R < 0\,, Q - SR^{-1}S^T > 0, \tag{5.18}$$

$$\begin{pmatrix} Q & S^T \\ S & R \end{pmatrix} > 0. \tag{5.19}$$

So we simply make (-1) as a common factor in equation (5.17) to get the Schur LMI form desired form (5.18) we get:

$$-(F^{-1} - (A_i F^{-1} - B_i G_i F^{-1})^T F (A_i F^{-1} - B_i G_i F^{-1})) < 0. \tag{5.20}$$

$$F^{-1} - (A_i F^{-1} - B_i G_i F^{-1})^T F (A_i F^{-1} - B_i G_i F^{-1}) > 0. \tag{5.21}$$

Until now we get the Schur desired form but still we have bilinearity which is the multiplication of two unknown variables $G_i F^{-1}$. The solution is to use a simple variable change as follow:

It's supposed that $X = F^{-1}$ and $H_i = G_i F^{-1}$, thus we get the following Linear Matrix Inequality:

$$X - (A_i X - B_i H_i)^T F (A_i X - B_i H_i) > 0. \tag{5.22}$$

Applying the Schur complement, we get the LMI:

$$\begin{pmatrix} X & * \\ A_i X - B_i H_i & X \end{pmatrix} > 0. \tag{5.23}$$

Using the same method for the following stabilization condition coming from the Quadratic Lyapunov function [129] when we apply

$$V(k+1) - V(k) < 0. \tag{5.24}$$

$$C_{discrete}\left(\vartheta_{ij}, F\right) \leq 0\,, \forall\, (i,j) \in I_n^2 \quad i < j. \tag{5.25}$$

We get:

$$\begin{pmatrix} X & * \\ \frac{A_i+A_j}{2}X - \frac{1}{2}\left(B_jH_i + B_iH_j\right) & X \end{pmatrix} \geq 0 \ . \tag{5.26}$$

We apply the theorem described in [194] to reduce the conservatism of the previous stabilization conditions presented as LMIs. The theorem uses a several matrices M_{ij} instead of a common matrice M.

Theorem: if there exist matrices $F = F^T > 0$, $M_{ij} = M_{ij}^T$ and matrices G_i which verifies:

$$\begin{cases} C_{discrete}(\vartheta_{ii}, F) + M_{ii} < 0, \forall i \in I_n, \\ C_{discrete}\left(\vartheta_{ij}, F\right) + M_{ij} \leq 0, \forall i, j \in I_n^2 \\ \xi_i\left(\varphi(k)\right)\xi_j(\varphi(k)) \neq 0. \end{cases} \tag{5.27}$$

Where,

$$\begin{bmatrix} M_{11} & \cdots & M_{1n} \\ \vdots & \ddots & \vdots \\ M_{1n} & \cdots & M_{nn} \end{bmatrix} > 0. \tag{5.28}$$

And ,

$\vartheta_{ij} = \left(A_i - B_iG_j\right)$, so the discrete-time closed loop system (5.10) is globally asymptotically stable.

The inequality (5.22) can be expressed in the LMI form by applying the Schur complement and the last theorem, we get:

$$\begin{pmatrix} X - Y_{ii} & * \\ A_iX - B_iH_i & X \end{pmatrix} > 0 \quad \forall\, i \in I_n \tag{5.29}$$

By applying the same approach and the same steps, the condition $C_{discrete}\left(\vartheta_{ij}, F\right) \leq 0$ is given by:

$$\begin{pmatrix} X - Y_{ij} & * \\ \frac{A_i+A_j}{2}X - \frac{1}{2}\left(B_jN_i + B_iH_j\right)X & X \end{pmatrix} > 0 \quad \forall\, (i,j) \in I_n^2 \quad i < j \tag{5.30}$$

The first Lyapunov function condition is $V > 0$ gives $F > 0$, because $X_k^T X_k > 0$.

Which means $F > 0$ is a stability and stabilization condition. We multiply as we said pre and post by F^{-1} gives:

$F^{-1}\,FF^{-1} > 0$; gives $F^{-1} > 0$ which means $X > 0$.

Since $X = F^{-1}$.

$$X > 0; \tag{5.31}$$

$$\begin{pmatrix} Y_{11} & \cdots & Y_{1n} \\ \vdots & \ddots & \vdots \\ Y_{1n} & \dots & Y_{nn} \end{pmatrix} > 0 \; ; \tag{5.32}$$

$$\begin{pmatrix} M_{11} & \cdots & M_{1n} \\ \vdots & \ddots & \vdots \\ M_{1n} & \dots & M_{nn} \end{pmatrix} > 0 \quad ; \tag{5.33}$$

$$\begin{cases} X = F^{-1}. \\ Y_{ij} = XM_{ij}X. \\ G_i = H_i X^{-1}. \\ \forall i \in I_n. \end{cases} \tag{5.34}$$

5.4 Nonlinear Luenberger Observer Design

The role of the nonlinear observer is crucial in the control process especially in the case of state feedback control. In many cases, the system state vector cannot be read or it is partially read because of the disturbances and noises. The nonlinear Luenberger observer ensure the compute and the existence of the discrete-time T-S system state vector as we will explain in this section. The state vector $x(k)$ is used for the state feedback control (PDC) see equation (5.10).

$$\begin{cases} \hat{x}_{k+1} = \sum_{i=1}^{n} \xi_{\mathrm{i}}\big(\varphi(\mathrm{k})\big)\big((\mathrm{A_i}\hat{x}_k + \mathrm{B_i}u_k) + \mathrm{N_i}(y_k - \hat{y}_k)\big). \\ \hat{x}_{k+1} = \sum_{i=1}^{n} \xi_i\big(\varphi(\mathrm{k})\big)\Big([I + B_i G_i]^{-1}(\mathrm{A_i} - \mathrm{B_i G_i})\,\hat{x}_k + \mathrm{N_i}\big((y_k - \hat{y}_k)\big)\Big). \\ \hat{\mathrm{y}}(\mathrm{k}) = \sum_{\mathrm{i}=1}^{\mathrm{n}} \xi_{\mathrm{i}}\,\big(\varphi(\mathrm{k})\big)\mathrm{C_i}\hat{x}_k. \end{cases} \tag{5.35}$$

The estimation error of the state vector is written as:

$$\tilde{x}_k = x_k - \hat{x}_k. \tag{5.36}$$

Considering that, the dynamics of the state vector error is given by:

$$\begin{cases} \tilde{x}_{k+1} = \sum_{i=1}^{n} \sum_{j=1}^{n} \xi_i(\varphi(k)) \xi_j(\varphi(k)) \alpha_{ij} \tilde{x}_k. \\ \alpha_{ij} = A_i - N_i C_j \, , \forall (i,j) \in I_n^2. \end{cases} \tag{5.37}$$

The design of the nonlinear observer must validate the following conditions to ensure the migration to zero of the state vector dynamics. The conditions are: It must exists $F = F^T > 0$ and matrices $N_i \in I_n$ valid the following conditions:

$$\begin{cases} C_{discrete}(\alpha_{ii}, F) < 0, \forall i \in I_n. \\ C_{discrete}(\alpha_{ij}, F) \leq 0, \forall i, j \in I_n^2. \\ \xi_i(\varphi(k)) \, \xi_j(\varphi(k)) \neq 0. \end{cases} \tag{5.38}$$

$$C_{discrete}(\alpha_{ij}, F) = \left[\frac{\alpha_{ij}+\alpha_{ji}}{2}\right]^T F \left[\frac{\alpha_{ij}+\alpha_{ji}}{2}\right] - F. \tag{5.39}$$

The conditions (5.38) and (5.39) guarantee the convergence of the state error dynamics, which means the estimate state vector, converges to the real state. These conditions can be expressed as Linear Martix Inequalities applying the Schur complement:

$$\begin{bmatrix} F & * \\ F\frac{A_i+A_j}{2} - \frac{1}{2}(H_j C_j + H_j C_i) & F \end{bmatrix} \geq 0 \tag{5.40}$$

When $i < j$.

The Luenberger observers may be enhanced by the next theorem: the multiple Luenberger observers are globally asymptotically stable if there exist symmetric matrices $F > 0$, M_{ij} and $N_i \in I_n$ that satisfy:

$$\begin{cases} C_{discrete}(\alpha_{ii}, F) + M_{ii} < 0, \forall i \in I_n. \\ C_{discrete}(\alpha_{ij}, F) + M_{ij} \leq 0, \forall i, j \in I_n^2. \\ \begin{pmatrix} M_{11} & \cdots & M_{1n} \\ \vdots & \ddots & \vdots \\ M_{1n} & \ldots & M_{nn} \end{pmatrix} > 0 \\ \xi_i(\varphi(k)) \, \xi_j(\varphi(k)) \neq 0. \\ \alpha_{ij} = A_i - N_i C_j \, , \forall (i,j) \in I_n^2. \end{cases} \tag{5.41}$$

The LMIs are given by:

$$\begin{cases} F > 0. \\ \begin{bmatrix} F - M_{ii} & * \\ FA_i - H_iC_i & F \end{bmatrix} > 0 \ \forall \ i \in I_n. \\ \begin{bmatrix} F - M_{ij} & * \\ F\frac{A_i + A_j}{2} - \frac{1}{2}(H_iC_j + H_jC_i) & F \end{bmatrix} \geq 0 \ \forall \ i < j. i, j \in I_n^2 . \\ M = \begin{pmatrix} M_{11} & \cdots & M_{1n} \\ \vdots & \ddots & \vdots \\ M_{1n} & \dots & M_{nn} \end{pmatrix} > 0. \\ H_i = FN_i. \end{cases} \tag{5.42}$$

5.5 Results

The first part of this section compares 3 subspace algorithms, which are N4SID 1, 2 and MOESP. The comparison focused on the convergence time and estimation error; the results show that the two versions of N4SID are better in both criteria mentioned before.

In the second part, we first construct the T-S fuzzy model formed by 4 submodels from the N4SID 1 and 2 identification algorithms. Secondly, we compared the discrete-time Takagi-Sugeno of [45] and our improved PDC control law design. The results demonstrate the robustness and effectiveness of the improved PDC control law formula. This idea is original and has not been used before. From (5.25) and (5.32), the feedback gain G_i, the matrix F, and the gain $\mathrm{N_i}$ are of the form:

$$\begin{cases} F = X^{-1}. \\ G_i = H_iF. \\ H_i = FN_i. \end{cases} \tag{5.34}$$

The system matrices and gains are:

$$A_1 = \begin{bmatrix} -1 & 0 & -0.5 & -2 \\ 0 & -2.5 & 0.6 & 1 \\ 0.5 & -1 & -2 & 0.8 \\ 0.2 & 0 & -0.6 & -3 \end{bmatrix}, B_1 = \begin{bmatrix} 1 & 0.5 \\ 0 & 2 \\ 2 & 5 \\ 3 & 2 \end{bmatrix}, C_1 = \begin{bmatrix} 2 & 0 & 5 & 0.3 \\ 3 & 2 & 1 & 0.5 \end{bmatrix}, D_1 = \bar{0}$$

$$A_2 = 0.85\begin{bmatrix} -1 & 0 & -0.5 & -2 \\ 0 & -2.5 & 0.6 & 1 \\ 0.5 & -1 & -2 & 0.8 \\ 0.2 & 0 & -0.6 & -3 \end{bmatrix}, B_2 = 0.63\begin{bmatrix} 1 & 0.5 \\ 0 & 2 \\ 2 & 5 \\ 3 & 2 \end{bmatrix}, C_2 = \begin{bmatrix} 2 & 0 & 5 & 0.3 \\ 3 & 2 & 1 & 0.5 \end{bmatrix}, D_2 = \bar{0}$$

$$A_3 = 0.8\begin{bmatrix} -1 & 0 & -0.5 & -2 \\ 0 & -2.5 & 0.6 & 1 \\ 0.5 & -1 & -2 & 0.8 \\ 0.2 & 0 & -0.6 & -3 \end{bmatrix}, B_3 = 0.63\begin{bmatrix} 1 & 0.5 \\ 0 & 2 \\ 2 & 5 \\ 3 & 2 \end{bmatrix}, C_3 = \begin{bmatrix} 2 & 0 & 5 & 0.3 \\ 3 & 2 & 1 & 0.5 \end{bmatrix}, D_3 = \bar{0}$$

$$A_4 = 0.6\begin{bmatrix} -1 & 0 & -0.5 & -2 \\ 0 & -2.5 & 0.6 & 1 \\ 0.5 & -1 & -2 & 0.8 \\ 0.2 & 0 & -0.6 & -3 \end{bmatrix}, B_4 = 0.4\begin{bmatrix} 1 & 0.5 \\ 0 & 2 \\ 2 & 5 \\ 3 & 2 \end{bmatrix}, C_4 = \begin{bmatrix} 2 & 0 & 5 & 0.3 \\ 3 & 2 & 1 & 0.5 \end{bmatrix}, D_4 = \bar{0}$$

$$N_1 = \begin{bmatrix} -0.2415 & -0.6126 \\ 0.6019 & -1.5255 \\ -0.1902 & 0.2630 \\ 0.1673 & -0.2075 \end{bmatrix}, N_2 = \begin{bmatrix} -0.4337 & -0.4415 \\ 1.2732 & -2.9498 \\ -0.3946 & 0.6706 \\ 0.3345 & -0.5000 \end{bmatrix}$$

$$N_3 = \begin{bmatrix} -0.3757 & -0.5576 \\ 1.3848 & -3.1157 \\ -0.3425 & 0.6031 \\ 0.3256 & -0.4825 \end{bmatrix}, N_4 = \begin{bmatrix} -0.5692 & -0.4968 \\ 0.7727 & -1.6519 \\ -0.2834 & 0.2843 \\ 0.1315 & -0.1060 \end{bmatrix}.$$

$$F = \begin{bmatrix} 0.6384 & -0.1033 & 0.0320 & -0.0867 \\ -0.1033 & 0.1409 & -0.0300 & -0.0324 \\ 0.0320 & -0.0300 & 0.1888 & 0.0465 \\ -0.0867 & -0.0324 & 0.0465 & 0.6214 \end{bmatrix}$$

In case of N4SID2 the gains are:

$$G_1 = \begin{bmatrix} -0.1654 & 0.3336 & -0.2190 & -2.2542 \\ -0.3941 & -0.1941 & -0.0100 & 1.1506 \end{bmatrix}$$

$$G_2 = \begin{bmatrix} -0.1609 & 0.2250 & -0.0541 & -1.5345 \\ -0.5701 & -0.0491 & -0.1422 & 0.7680 \end{bmatrix}$$

$$G_3 = \begin{bmatrix} -0.1374 & 0.2276 & -0.1572 & -1.6386 \\ -0.5965 & -0.0446 & -0.0513 & 0.8109 \end{bmatrix}$$

$$G_4 = \begin{bmatrix} -0.1687 & 0.4688 & -0.1928 & -2.0304 \\ -0.7914 & -0.1578 & -0.1185 & 1.0189 \end{bmatrix}$$

In case of N4SID1 the gains are:

$$S1 = \begin{bmatrix} -30.2159 & 8.4949 & -1.3444 & -63.6708 \\ 7.0015 & -4.1881 & 2.5946 & 31.3355 \end{bmatrix},$$

$$S2 = \begin{bmatrix} -11.5722 & 10.3269 & -7.4245 & -71.61 \\ -4.7249 & -4.3694 & 0.0180 & 34.5519 \end{bmatrix},$$

$$S3 = \begin{bmatrix} -9.8733 & 11.3026 & -8.1181 & -76.382 \\ -5.9746 & -4.6472 & 0.2152 & 36.7503 \end{bmatrix},$$

$$S4 = \begin{bmatrix} -11.5635 & -4.0802 & -7.5605 & -54.89 \\ -8.8555 & 3.6893 & 0.8954 & 26.5195 \end{bmatrix}.$$

Table 5. 1 Subspace algorithms convergence time.

N4SID 1	N4SID 2	MOESP
0.2969	0.5625	0.6250

Table 5. 2 Estimation error.

N4SID 1	N4SID 2	MOESP
2.4940	0.5745	0.6820

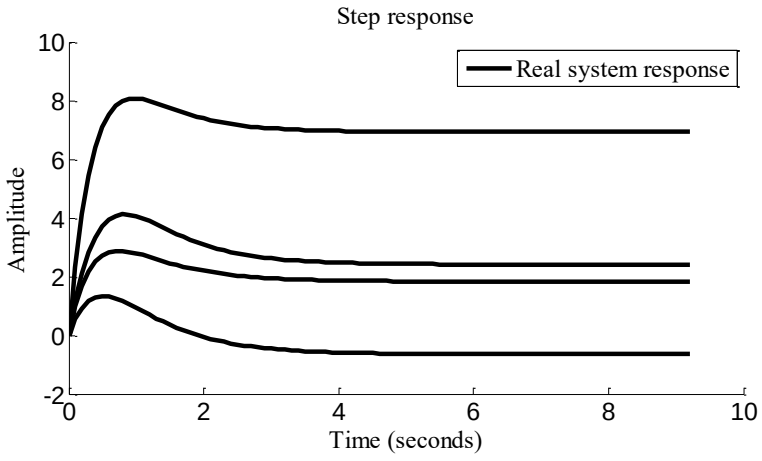

Figure 5. 2 Real continuous system step response.

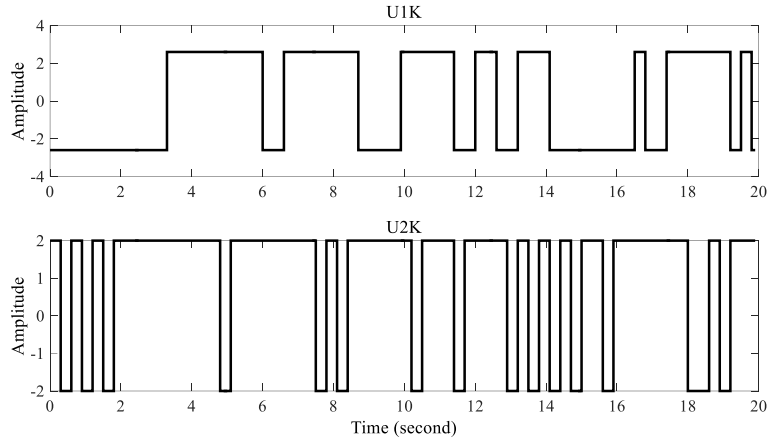

Figure 5. 3 Generation of two PRBS for identification of 2 input system.

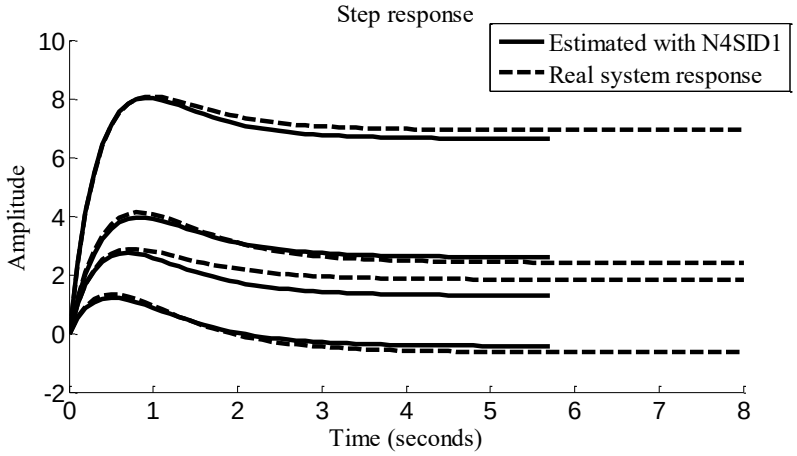

Figure 5. 4 N4SID1 identification algorithm and real system step response.

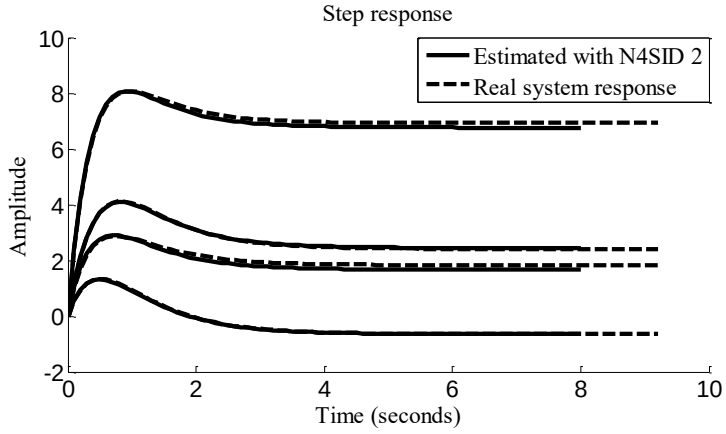

Figure 5. 5 N4SID2 identification algorithm and real system step response.

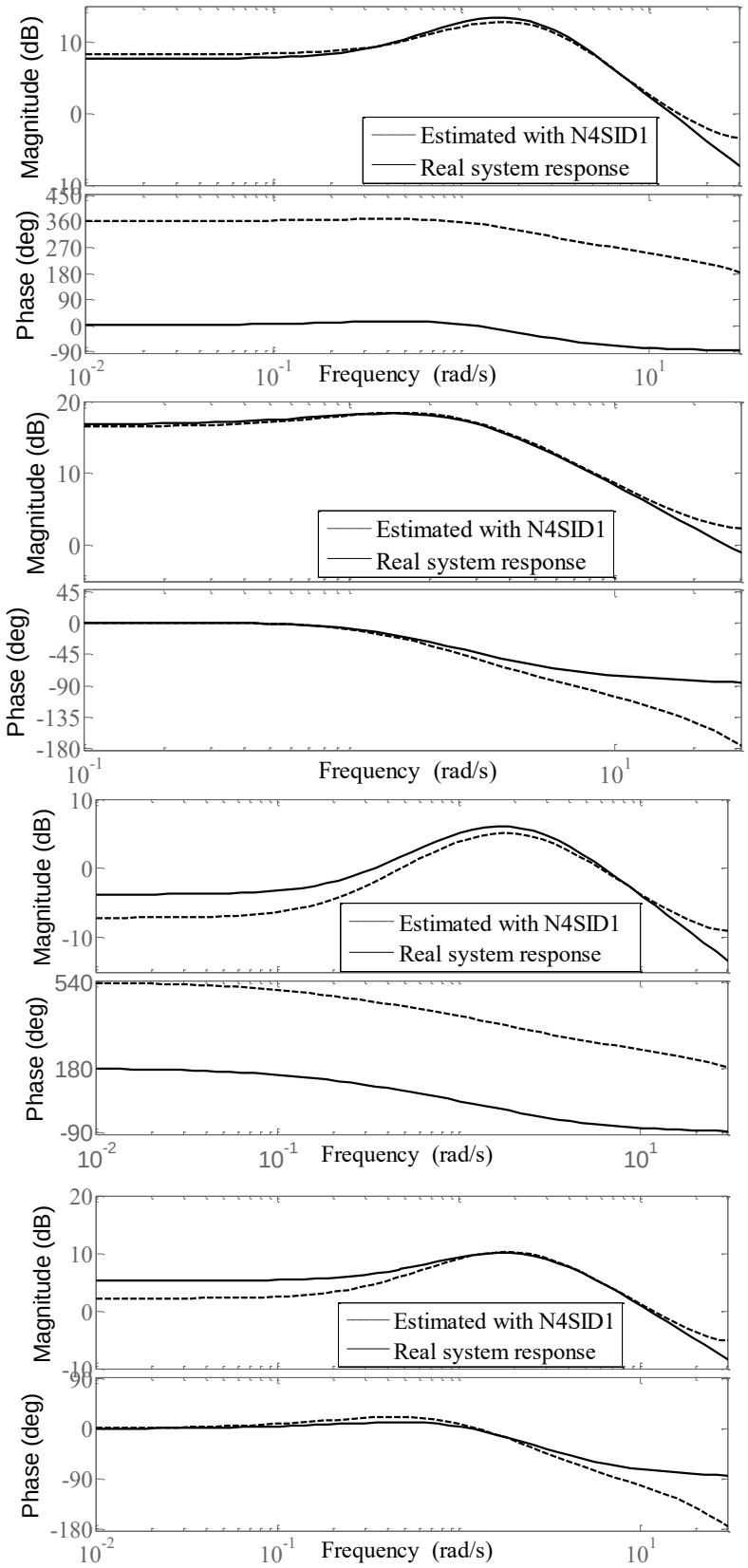

Figure 5. 6 N4SID1 identification algorithm and real system frequency response.

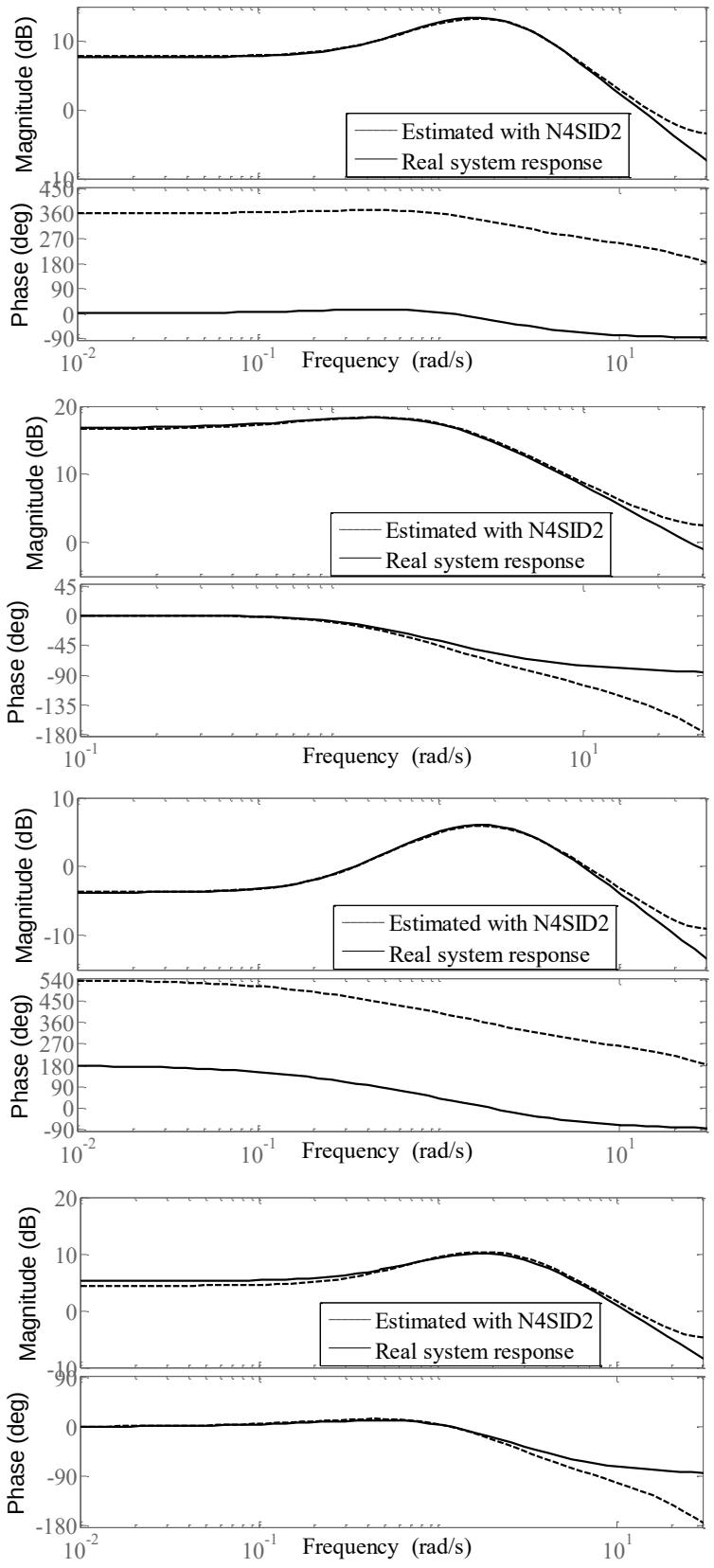

Figure 5. 7 N4SID 2 identification algorithm and real system frequency response.

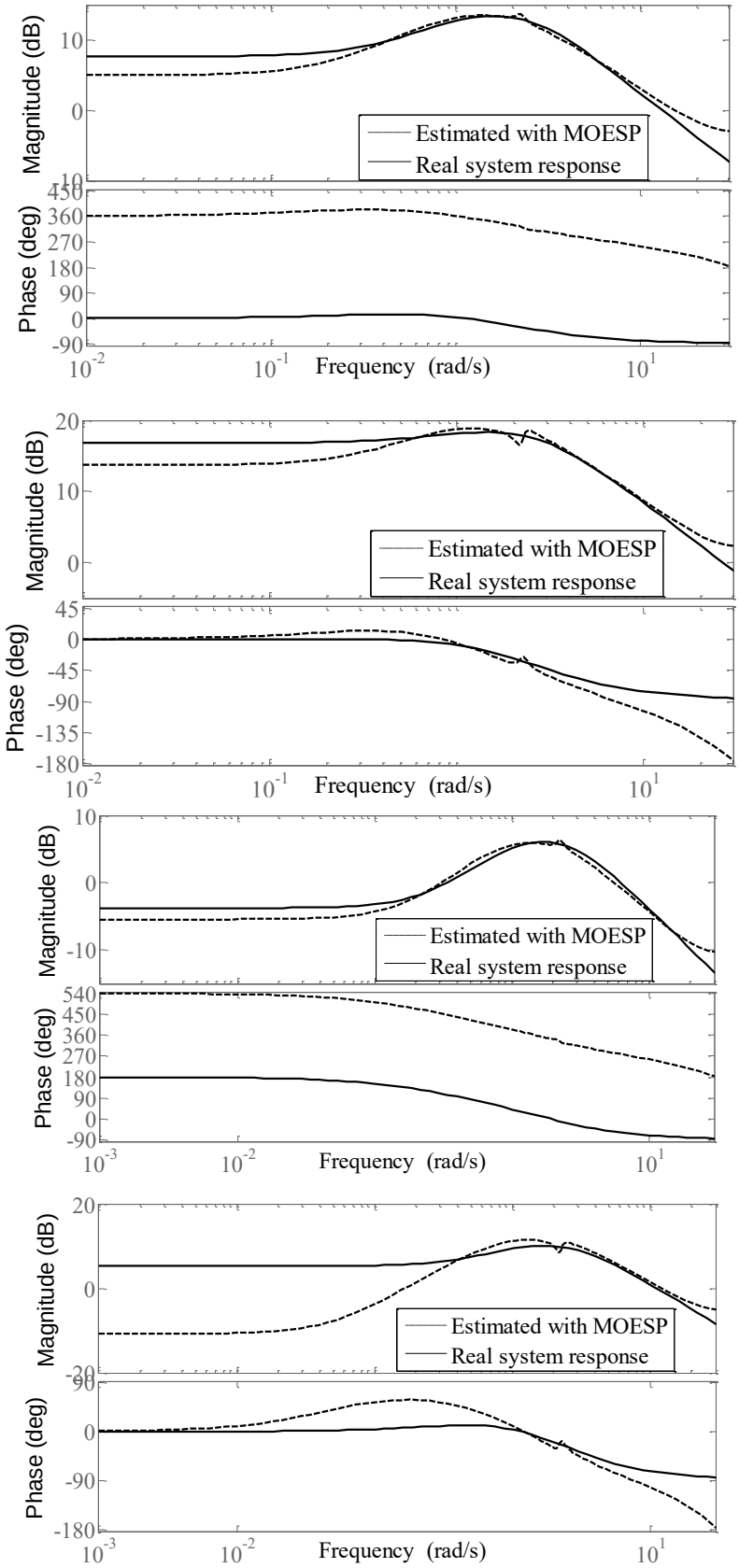

Figure 5. 8 MOESP identification algorithm and real system frequency response.

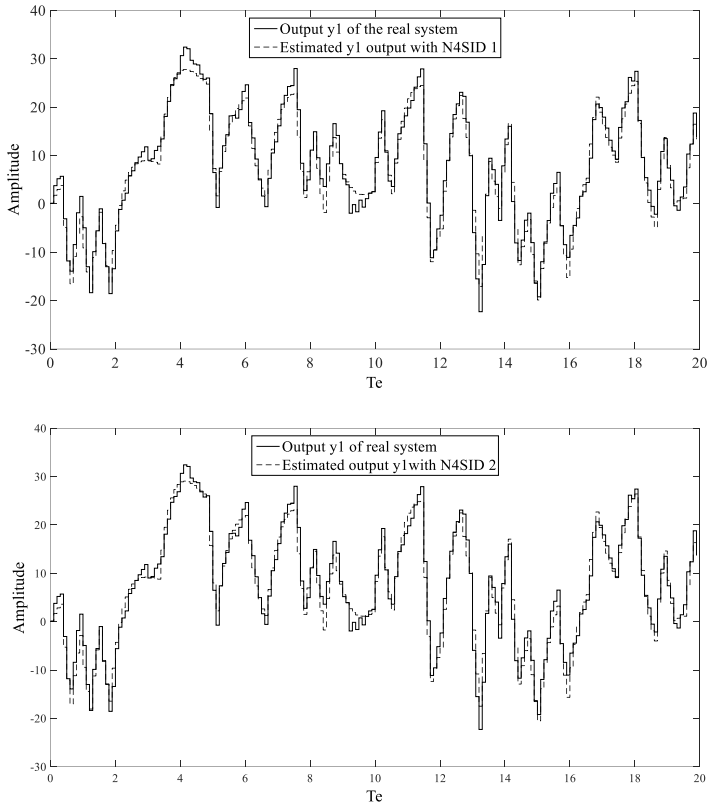

Figure 5. 9 Zoom on the samples [1,200] showing the N4SID1 and N4SID2 identification of the first output.

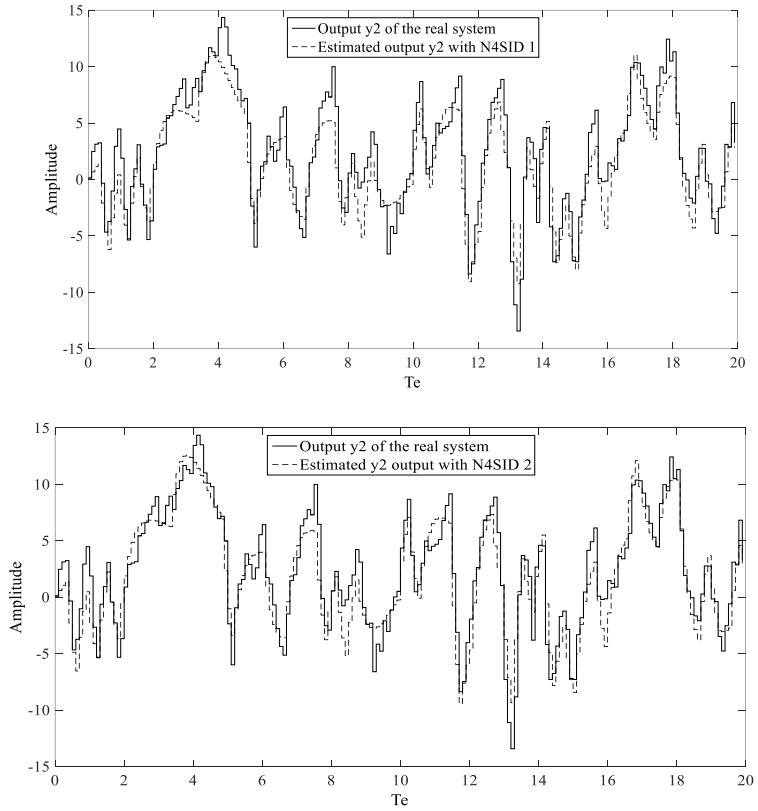

Figure 5. 10 Zoom on the samples [1,200] showing N4SID1 and N4SID2 identification of the second output.

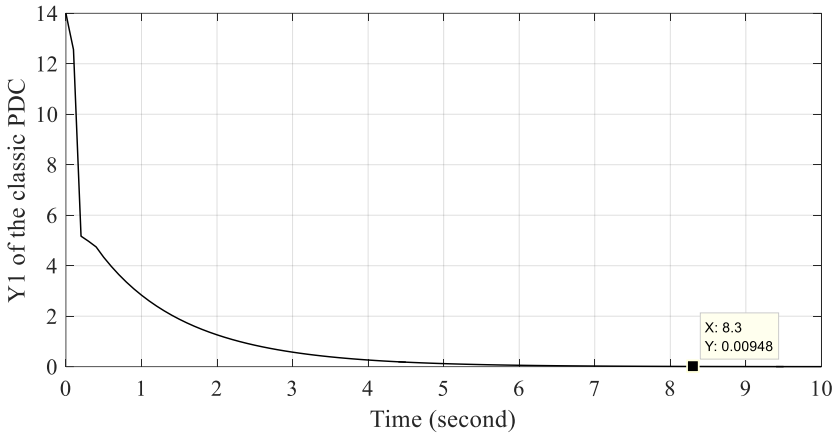

Figure 5. 11 Y1 output of classic PDC control.

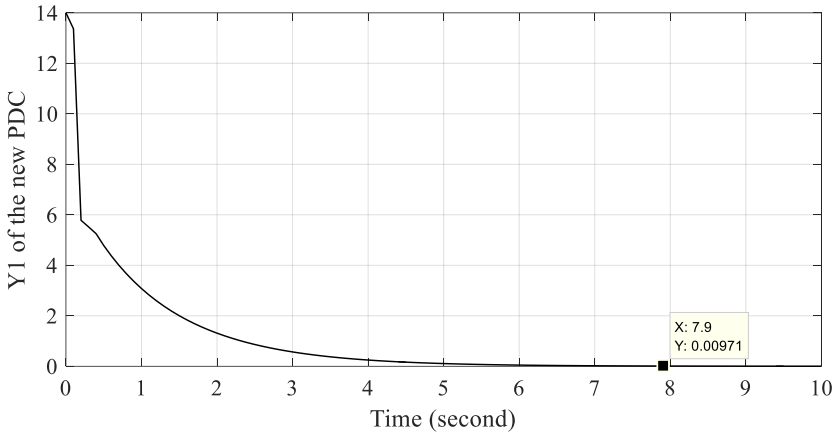

Figure 5. 12 Y1 output of improved PDC control.

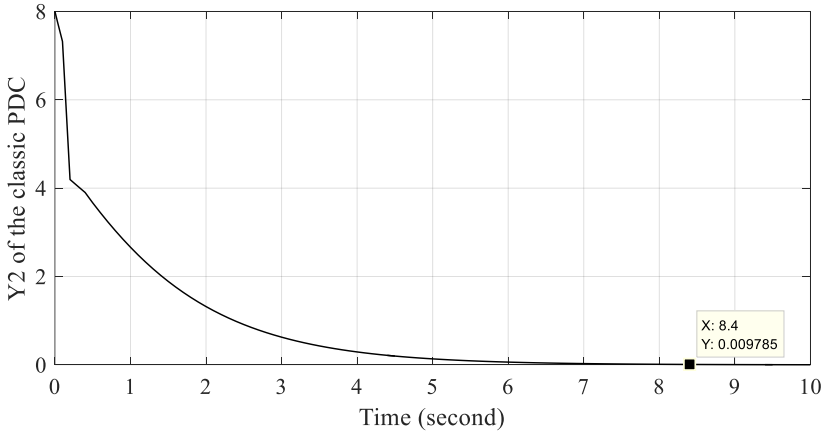

Figure 5. 13 Y2 output of classic PDC control.

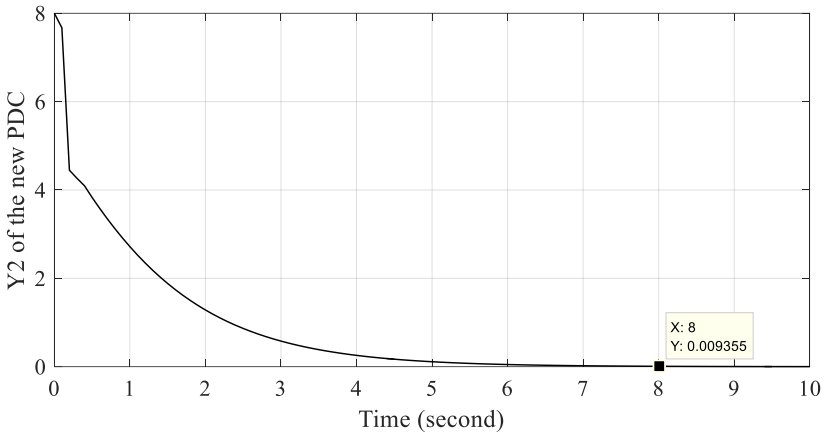

Figure 5. 14 Y2 output of improved PDC control.

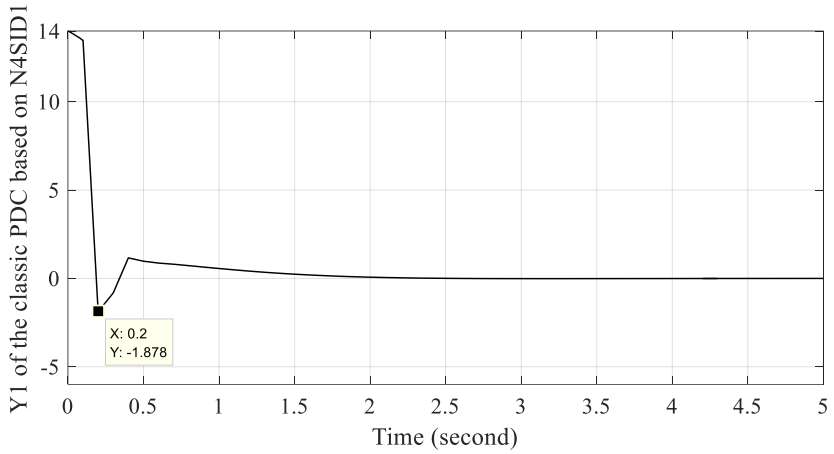

Figure 5. 15 Y1 output using PDC control for T-S based on N4SID1.

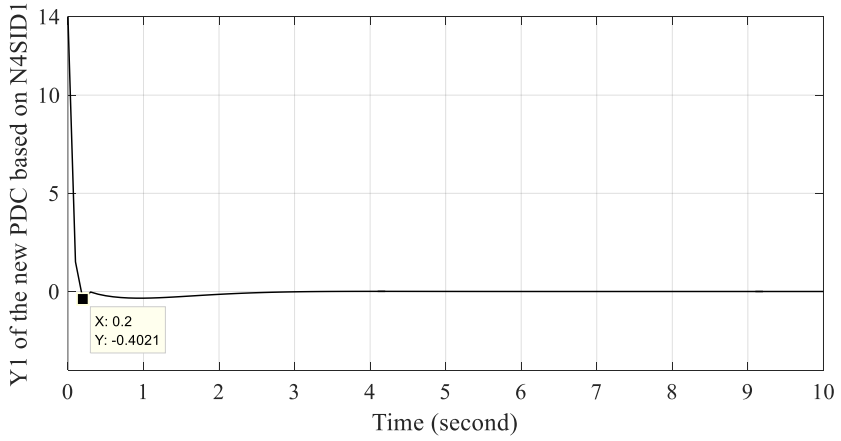

Figure 5. 16 Y1 output improved PDC control for T-S based on N4SID1.

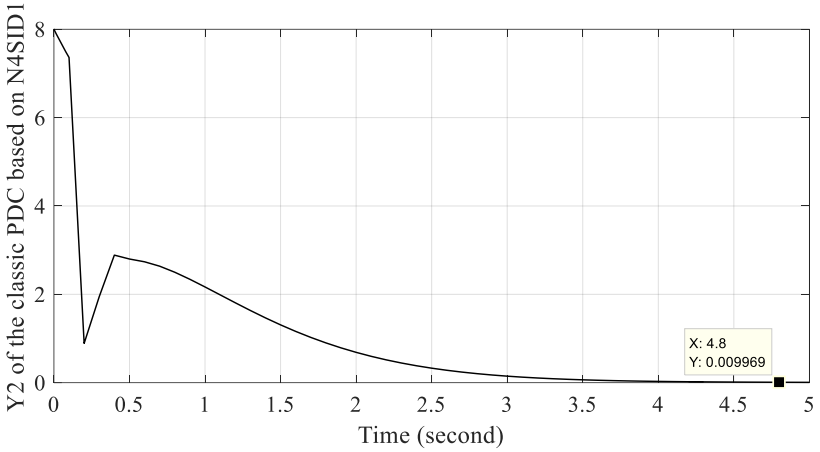

Figure 5. 17 Y2 output using PDC control for T-S based on N4SID1.

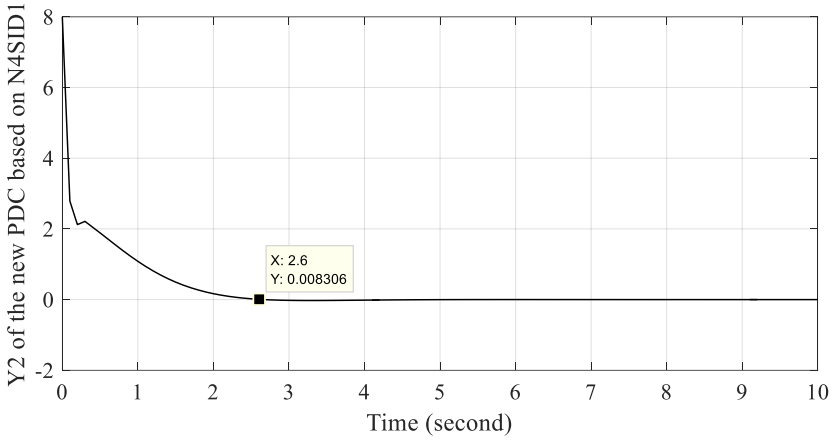

Figure 5. 18 Y2 output using improved PDC control for T-S based on N4SID1.

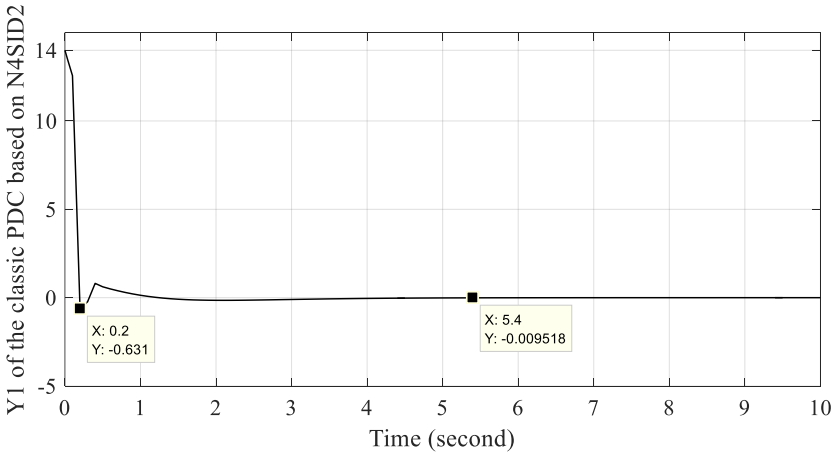

Figure 5. 19 Y1 output using PDC control for T-S based on N4SID2.

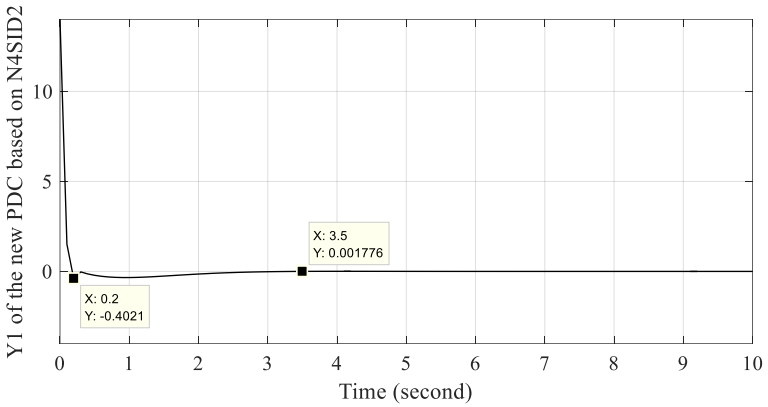

Figure 5. 20 Y1 output using improved PDC control for T-S based on N4SID2.

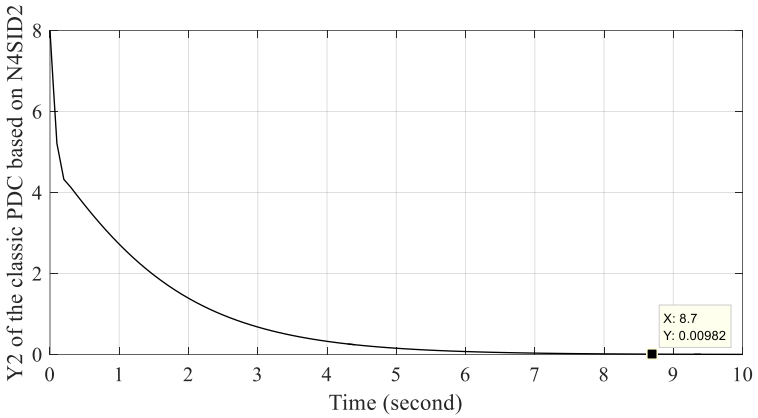

Figure 5. 21 Y2 output using PDC control for T-S based on N4SID2.

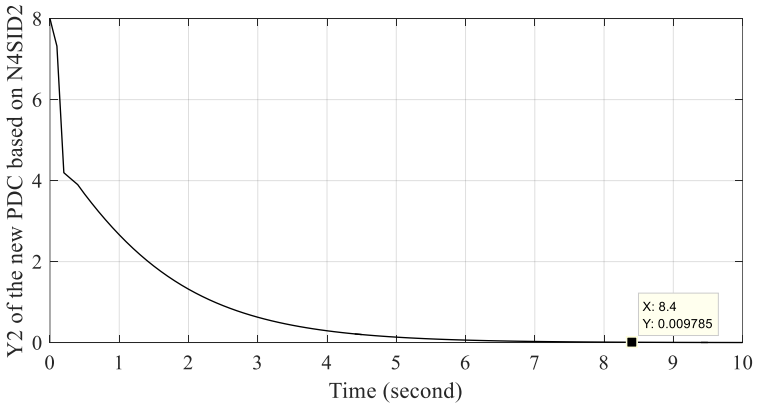

Figure 5. 22 Y2 output using improved PDC control for T-S based on N4SID2.

5.6 Discussion

In Figure 5.2, we show the real system step response as a reference that allows us to see

the identification algorithms' efficiency and the fidelity to reproduce a real dynamic behavior of a MIMO system.

Our system is a two inputs and two outputs system, which is known as a MIMO system; In Figure5. 3, we present two Pseudo Random Binary Signal (PRBS) as an input rich in frequency to ensure a good identification process.

In Figure 5.4, the estimated MIMO system with the N4SID1 presents four step responses that are graphically very close to the step response of the real studied system. On the other hand, the Figure 5.5 shows graphically more and more accuracy in the estimation than N4SID1 using the N4SID2 identification algorithm. Figs. 5.6- 5.8 show the Bode diagram in magnitude and phase. As we can see graphically, the N4SID2 is the most accurate comparing to N4SID1 and MOESP. The confirmation of the graphic results can be seen by calculation in Table 5.1 and 5.2. Figures 5.9 and 5.10 indicate a zoom on the outputs y1 and y2. Figures 5.11 and 5.12 represent the y1 output of the real system without any identification. We applied the classic T-S controller of [45] and the new proposed method to see the difference between these two controllers in terms of convergence speed and relaxation.

In Figure 5.11, when we applied the classic PDC law or controller, we observed that the stabilization time was 8.3 seconds, while when we applied the new formulation of the T-S and PDC law, we found that the stabilization time was 7.9 seconds. In Figures 5.13 and 5.14, we applied the same controller for the real system output y2; we found that the stabilization time for the classic case was 8.4 seconds, while for the new controller, it was only 8 seconds.

In Figures 5.15 and 5.16, when we applied the PDC classic control based on N4SID 1 for the y1 output, we got 0.2 second convergence speed with an overshoot of -1.878, while the new controller gave 0.2 second as well for the stabilization time but with a relaxed curve and a small overshoot of -0.4021.

For the y2 output of the system identified with N4SID 1, see Figures 5.17 and 5.18. The classic PDC control has 4.8 seconds as the convergence speed, while the new one has only 2.6 seconds with more relaxation, as shown in Fig. 17 and 18. Figs. 19 and 20 are dedicated to the N4SID 2 identified system. These figures show that the output y1 has a 5.4 second stabilization time and an overshoot of -0.631, while the new controller has only 3.5 seconds and -0.4021 overshoot, which means more relaxation.

Figures 5.21 and 5.22 represent the y2 output of the system identified with N4SID 2; the classic T-S control has 8.7 seconds as the convergence speed, and the new T-S control was 8.4 second. We can see that the new controller is better in terms of stabilization speed and

relaxation.

5.7 Conclusion

In this chapter, we first presented and explained state space identification, which could be subspace identification or classical identification. Then, we focused on subspace identification because of its advantages compared to iterative algorithms. We compared three algorithms, which are N4SID1, N4SID2 and the MOESP, for MIMO systems.

The second part was the control process based on the two versions of N4SID. We showed that they are more accurate and have better convergence speed than the MOESP. We then built the T-S system with both N4SID 1 and 2.Wich means we have two discrete-time T-S. After that, we applied the improved PDC control law for the discrete-time T-S fuzzy system based on N4SID1 and2 models. In addition, we applied a classical PDC controller to the same T-S system. Finally, we compared the control results between the classic and the improved PDC controller applied to the same discrete-time T-S fuzzy system.

The results prove that the improved PDC control law formulation is more robust and efficient since it gives more relaxation with a minimum overshoot for the results plus a higher convergence speed.

Chapter 6

The new PDC control applied to Autonomous vehicles control

6.1 Introduction

In recent years, lateral control of autonomous vehicles has attracted great attention from academic [123] and industrial communities [37], [209] and many results have been reported [6] [7] [8]. Some authors suggest new lateral control system architecture by combining the fuzzy logic and PID control [205]. Others focused on stabilizing lateral dynamics with considerations of parameters uncertainties and control saturation through robust yaw control. A robust yaw-moment controller design for improving vehicle handling and stability with consideration of parameters uncertainties and control saturation has been developed [79]. However, the state vector contains only two parameters to be controlled, which are the yaw rate and the sideslip angle; in this case, there is not enough information about the state of the vehicles that allows for their control in a tight way. Sun et al. [42] present a non-model-based controller for vehicle dynamics systems to improve lateral stability, where output tracking control and adaptive dynamic programing approaches are employed to track the desired yaw rate and, at the same time, mitigate the sideslip angle, roll angle, and roll rate of the vehicle. Considering Sun et al. [42], the proposed idea does not have a mathematical model, which means there are no mathematical stability and stabilization conditions to get access to the system control.

On the other hand, some authors investigated the vision-based autonomous driving with deep learning and reinforcement learning methods. Different from the end-to-end learning method, this method breaks the vision-based lateral control system down into a perception module and a control module [43]. Nonetheless, there are no constraints in the model, e.g. lateral wind force applied to the vehicles, unknown road curvature and steering physical saturation. This implies that the introduced method is still far from real world driving situations. For instance, an asymptotic stabilization problem for a class of nonlinear under-actuated systems was studied by Jiang and Astolfi [40]. Its solution, together with the back stepping and the forward control design

methods, is exploited in the control of the nonlinear lateral dynamics of a vehicle. This technique proved that with the established controller, a vehicle is able to track any feasible reference at a constant speed and the lateral deviation converges to zero. The issues in this case are: there is a constant longitudinal vehicle speed and only one intern variable that can be controlled.

The lateral control of an autonomous and connected vehicle (ACV), especially in emergencies, is important from safety point of view. The trajectory to be followed by an ACV must either be planned in real-time or be communicated from its preceding vehicle, which was introduced by Liu et al. [210].Yet, this technique has a constant longitudinal velocity and no internal variables. Zhang and Wang [44] investigated the combined active front wheel steering/direct yaw moment control for the improvement of a vehicle lateral stability and vehicle handling performance. The authors' more particular assumption [44] is that the longitudinal velocity is not constant but it varies within a range. Both the nonlinear tyre model and the variation of the longitudinal velocity are considered in vehicle system modelling. To track the system reference, a generalized proportional-integral (PI) control law is proposed. There is still the problem of no constraints on the model. Besides, a robust non-linear control was discussed. It uses barrier Lyapunov function under lateral offset called deviation error as a constraint for the lateral control of autonomous vehicles [211], [212]. Nevertheless, there is only one intern variable on the state vector that can be controlled, there are no constraints and no sweeping into longitudinal velocity. In addition, only partial state information is available for real-time control implementation. All the above lateral control methods do not use an observer to compute the entire vehicle state vector to ensure an efficient and accurate control scheme.

The first motivation came from the above issues in lateral control of autonomous vehicles. Based on the above discussion, the T-S fuzzy control method is further investigated. The T-S fuzzy control gives the possibility to sweep in large vehicles' speed variation range. Furthermore, this feature helps to improve the closed loop performance of the autonomous vehicles under different constraints. The T-S fuzzy control systems are efficient and successful because they can describe nonlinear systems in a convex form with local and simple consequents. However, the T-S fuzzy systems control approach belongs to the state feedback control, that is, they require the entire system state to be available. Getting more information about the vehicle states indeed is of paramount importance for efficient control. Some methods are developed for the vector state estimation. We cite Tong et al. [140]'s work, where a novel observer based adaptive fuzzy output-feedback back stepping control is designed; thus the unmeasurable states are estimated based on

the designed fuzzy state observer. Moreover, a novel integral sliding mode control is designed for the T-S fuzzy model based on Semi Markovian Jump System with immeasurable premise variables [141].

Recently, several studies have focused on steering system control, especially fuzzy control systems [6], [9], and [8]. These authors achieved very interesting results regarding lateral control based on Takagi–Sugeno models. Various constraints such as road with unknown curvature, steering saturation and lateral wind force, sweeping into large range of vehicle longitudinal speed and exploiting an approximated vector state containing six intern variables for effective control were fully used in their work. However, the authors used a non-quadratic Lyapunov function to reduce the conservatism caused by the use of common quadratic Lyapunov functions. On the other hand, the proposed non-quadratic Lyapunov function is complicated and complex in implementation, which arise more complexity to the system. Nevertheless, even when a nonquadratic Lyapunov is used for the T-S control scheme combined with the PDC control law, for example, the solution is a set of bilinear matrix inequalities. In addition, the conservatism will always exist. Due to this complexity, the authors were forced to use approximations and assumptions for the control purpose. Using assumptions and approximations in the automatic control signifies that there are still problems in the model and it needs more improvements to represent the desired system dynamics. The second and main motivation is based on the lacks introduced by Nguyen et al. [6], Nguyen et al. [9], and Sentouh et al. [8]. This work is based on the following summarized contributions:

- A Quadratic Lyapunov function is considered to simplify the implementation of the system and minimize the system complexity.
- An Improved PDC controller is designed. We introduce a new mathematical term in the classic PDC control law; this term is composed by the optimized gains times the gradient term of the state vector. This is to make it slides faster to the global minimum of the ellipsoid shape created by the Lyapunov function applied to the T-S system to make the results more relaxed.
- Contrary to Nguyen et al. [6], Nguyen et al. [9], and Sentouh et al. [8] and others in the first motivation mentioned, the state vector will not be approximated. It will be measured and it contains six real state variables values using Luenberger multiobserver.
- First time application of Jemmali et al. [45]'s technique for the autonomous vehicles.

This chapter is summarized as follows. The second section presents the vehicle modelling. The third part presents the control design for discrete-time T-S systems, which focuses on the stabilization of discrete-time T-S fuzzy system based on the new Parallel Distributed Compensation (PDC) control law and the synthesis of multiobservers. The fourth section is devoted to application in the steering control. Finally, the last part presents the new results and compares them with previous results.

6.2 Vehicle modeling

This section presents the different steps used for the vehicle modeling. First, the vehicle parameters are introduced and presented in Table 6.1:

Table 6. 1 Definition of parameters

Parameter	Description	Value
B_s	Steering system damping	5.73
C_f	Front cornering stiffness	57000 N/rad
C_r	Rear cornering stiffness	59000 N/rad
I_s	Steering system moment of inertia	0.02 kgm2
I_z	Vehicle yaw moment of inertia	2800 kgm2
K_p	Manual steering column coefficient	0.5
l_f	Distance from the CG to the front axle	1.3 m
l_r	Distance from the CG to the rear axle	1.6 m
l_s	Look-ahead distance	5 m
l_w	Distance from the CG to the impact center of the wind force	0.4 m
M	Mass of the vehicle	2025 kg
R_s	Steering gear ratio	16
σ_t	Tyre length contact	0.13 m

6.2.1 Lateral dynamics model of the vehicle

Extracting from the well-known bicycle model presented by Rajamani [4], the obtained model of the vehicle lateral dynamics is expressed as:

$$\begin{bmatrix}\dot{\beta}\\ \dot{r}\end{bmatrix} = \begin{bmatrix}a_{11} & a_{12}\\ a_{21} & a_{22}\end{bmatrix}\begin{bmatrix}\beta\\ r\end{bmatrix}\delta + \begin{bmatrix}e_1\\ e_2\end{bmatrix} f_w. \tag{6.1}$$

Where β is the sideslip angle at the center of gravity (CG), and the yaw rate is r shown in Figure 6. 1. As represented in equation (6.1), fw is the lateral wind force, and the system matrices elements are written as follows:

$$a_{11} = -2\frac{(C_r + C_f)}{m\vartheta_x}\,;\; a_{12} = 2\frac{(l_r C_r - l_f C_f)}{m\vartheta_x^2} - 1\,;$$

$$a_{21} = 2\frac{(l_r C_r - l_f C_f)}{I_z}\,;\; a_{22} = -2\frac{\left(l_r^2 C_r + l_f^2 C_f\right)}{I_z \vartheta_x}.$$

$$b_1 = \frac{2C_f}{m\vartheta_x}\,;\; b_2 = \frac{2l_f C_f}{I_z}\,;\; e_1 = \frac{1}{m\vartheta_x}\,;\; e_2 = \frac{l_w}{I_z}\,.$$

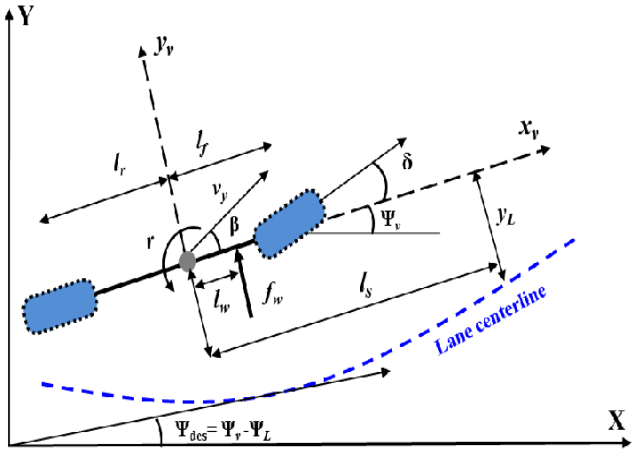

Figure 6. 1 Lateral vehicle dynamics modeling [6].

6.2.2 Road-vehicle positioning

The vehicle positioning dynamics on the road is described by [4]:

$$\begin{cases} \dot{y}_L = \vartheta_x \beta + \dot{l}_s r + \vartheta_x \psi_L. \\ \dot{\psi}_L = r - \vartheta_x \rho_r. \end{cases} \quad (6.2)$$

Where y_L is the lateral deviation error from the centerline of the lane projected forward a look-ahead distance l_s and ψ_L are the heading error between the tangent to the road and the vehicle orientation. The road curvature is indicated by ρ_r.

6.2.3 Steering system model

The electronic power steering system is given as follows [137]:

$$\ddot{\delta} = 2\frac{K_p C_f \sigma_t}{R_S^2 I_s}\beta + 2\frac{K_p C_f \sigma_t}{R_S^2 I_s}\frac{l_f}{\vartheta_x} r \cdots - 2\frac{K_p C_f \sigma_t}{R_S^2 I_s}\delta - \frac{B_s}{I_s}\dot{\delta} + \frac{1}{R_s I_s} T_s. \quad (6.3)$$

Where T_s is the steering torque, δ is the steering angle, l_s is the inertia moment of the steering column, B_s is the damping factor of the column, R_s is the reduction ratio of the column, σ_t is the width of the tyre contact finally, the manual steering column coefficient is K_p.

6.2.4 Vehicle control-based model

From the previous models (6.1), (6.2) and (6.3), the road-vehicle continuous-time model utilized for the aim of system control is written as follows:

$$\dot{x}(t) = A_c x(t) + B_c u(t) + B_{cw} w(t). \quad (6.4)$$

Where

$x = \left[\beta\ r\ \psi_L\ y_L\ \delta\ \dot{\delta}\right]^T$ is the vehicle vector state,

$w = [f_w\ \rho_r]^T$ is the disturbance vector,

and $u = T_s$ is the input vector.

The control-based system matrices in (6.4) are expressed as:

$$A_c = \begin{bmatrix} a_{11} & a_{12} & 0 & 0 & b_1 & 0 \\ a_{21} & a_{22} & 0 & 0 & b_2 & 0 \\ 0 & 1 & 0 & 0 & 0 & 0 \\ v_x & l_s & v_x & 0 & 0 & 0 \\ 0 & 0 & 0 & 0 & 0 & 1 \\ a_{61} & a_{62} & 0 & 0 & a_{65} & a_{66} \end{bmatrix}; B_{cw} = \begin{bmatrix} e_1 & 0 \\ e_2 & 0 \\ 0 & -v_x \\ 0 & 0 \\ 0 & 0 \\ 0 & 0 \end{bmatrix}; B_c = \begin{bmatrix} 0 \\ 0 \\ 0 \\ 0 \\ 0 \\ \frac{1}{R_s I_s} \end{bmatrix}.$$

We have:

$$a_{61} = 2\frac{K_p C_f \sigma_t}{R_s^2 I_s}, a_{62} = 2\frac{K_p C_f \sigma_t}{R_s^2 I_s}\frac{l_f}{v_x},$$

$$a_{65} = -2\frac{K_p C_f \sigma_t}{R_s^2 I_s}, a_{66} = -\frac{B_s}{I_s}.$$

Therefore, the control design in this thesis is based on the following discrete-time system (6.5).

$$x_{k+1} = A\,x_k + B\,u_k + B_w w(k) \tag{6.5}$$

Te $= 0.01$ second is the discretization time.

6.3 Control design for discrete-time T-S systems

In this part, the new PDC controller design is developed. The stability and the stabilization conditions are demonstrated.

6.3.1 Discrete-time Takagi-Sugeno system

The following discrete-time T-S system is described by fuzzy IF-THEN rules.

Rule i is of the form:

$$\text{IF } \varphi_1(\mathrm{k}) \text{ is } \tau_1^{\mathrm{i}} \text{ and } \ldots \varphi_{\mathrm{q}}(\mathrm{k}) \text{is } \tau_{\mathrm{q}}^{\mathrm{i}} \text{ then}$$

$$\begin{cases} x_{k+1} = A_i x_k + B_i u_k. \\ y_k = C_i\, x_k. \end{cases} \tag{6.6}$$

Where τ_1^i $\ldots.\tau_q^i$ are the fuzzy sets, and n is the number of the rules. In addition, $x_k \in \mathbb{R}^n$ is the state vector; $u_k \in \mathbb{R}^p$ is the control vector and y_k is the measurable output vector; A_i, B_i *and* C_i are the system matrices with appropriate dimension. The premise variables are represented by the vector $\varphi(k) = [\varphi_1(k) \ldots. \quad \varphi_q(k)]$.

Consider the discrete-time T-S fuzzy model:

$$x_{k+1} = \sum_{i=1}^{n} \xi_i \left(\varphi(k)\right)(A_i x_k + B_i u_k + B_i^w w_k). \tag{6.7}$$

The convexity conditions are:

$$\begin{cases} \sum_{i=1}^{n} \xi_i \left(\varphi(k)\right) = 1 \\ \quad \xi_i(\varphi(k)) \geq 0. \end{cases} \tag{6.8}$$

With

$$\xi_i(\varphi(k)) = \frac{\lambda_i(\varphi(k))}{\sum_{i=1}^{n} \lambda_i(\varphi(k))} \;;\; \lambda_i\big(\varphi(k)\big) = \prod_{j=1}^{q} \tau_j^i(\varphi(k)).$$

$\xi_i(\varphi(k))\,, i = 1,2, \ldots, n$, are the normalized grades of membership.

$\tau_j^i\big(\varphi(k)\big), j = 1,2,..,q$, are the grades of membership corresponding to the fuzzy term τ_j^i.

The open loop discrete-time T-S fuzzy system is:

$$x_{k+1} = \sum_{i=1}^{n} \xi_i \left(\varphi(k)\right) A_i x_k. \tag{6.9}$$

The candidate Lyapunov quadratic function is:

$$V(x_k) = x_k^T F\, x_k. \tag{6.10}$$

Theorem 6.1: The discrete-time T-S fuzzy system presented in equation (6.9) is quadratically asymptotically stable if there exists a common symmetric matrix $F = F^T > 0$ such that the following LMIs are feasible [21] [191]:

$$\begin{cases} F > 0. \\ A_i^T F\, A_i - F < 0. \quad \forall\, i \in I_n. \end{cases} \tag{6.11}$$

Where I_n is a set of natural numbers ranging from *1 to n*.

To say that $V(x_k) = x_k^T F\, x_k$ is a Lyapunov function we must validate these three conditions that are the stability conditions in (6.11):

- $V > 0$,
- $V(0) = 0$,
- $V(x_{k+1}) - V(x_k) < 0$.

Proof 1:

$V > 0$ gives $F > 0$, because $x_k^T . x_k > 0$, for non-zero vector x_k , which is the first condition in equation (6.11),

$V(0) = 0$, which is validated as well.

$V(x_{k+1}) - V(x_k) < 0$ gives the second equation of (6.11).

Proof 2:

Using the equation (6.9) and equation (6.10):

$V(x_{k+1}) - V(x_k) = x_{k+1}^T F\, x_{k+1} - x_k^T F\, x_k$

$= \left[\sum_{i=1}^n \xi_i\left(\varphi(k)\right) A_i x_k\right]^T F \sum_{i=1}^n \xi_i\left(\varphi(k)\right) A_i x_k - x_k^T F\, x_k$

$= \left[\sum_{i=1}^n \xi_i\left(\varphi(k)\right) {x_k}^T {A_i}^T\right] F \left[\sum_{i=1}^n \xi_i\left(\varphi(k)\right) A_i x_k\right] - x_k^T F\, x_k$

$= {x_k}^T\left[\sum_{i=1}^n \sum_{j=1}^n \xi_i(\varphi(k))\xi_j(\varphi(k))\left(A_i^T F A_j\right)\right] x_k - x_k^T F\, x_k.$

Let $F = \sum_{i=1}^n \sum_{j=1}^n \xi_i(\varphi(k))\xi_j(\varphi(k))\, F$

$= {x_k}^T\left[\sum_{i=1}^n \sum_{j=1}^n \xi_i(\varphi(k))\xi_j(\varphi(k))\left(A_i^T F A_j\right)\right] x_k - x_k^T\left[\sum_{i=1}^n \sum_{j=1}^n \xi_i\left(\varphi(k)\right)\xi_j\left(\varphi(k)\right) F\right] x_k$

${x_k}^T\left[\sum_{i=1}^n \sum_{j=1}^n \xi_i(\varphi(k))\xi_j(\varphi(k))\left(A_i^T F A_j - F\right)\right] x_k \le {x_k}^T\left[\sum_{i=1}^n \xi_i\left(\varphi(k)\right)\left(A_i^T F A_j - F\right)\right] x_k.$

The last two lines called number of inequality reduction.

- Number of inequality reduction:

If $n = 2$*:*

$\sum_{i=1}^2 \sum_{j=1}^2 \xi_i(\varphi(k))\xi_j(\varphi(k))\left(A_i^T F A_j - F\right)$

$= \xi_1\xi_1(A_1^T F A_1 - F) + \xi_1\xi_2(A_1^T F A_2 - F) + \xi_2\xi_1(A_2^T F A_1 - F) + \xi_2\xi_2(A_2^T F A_2 - F)$

$\sum_{i=1}^2 \xi_i\left(A_i^T F A_j - F\right) = \xi_1(A_1^T F A_1 - F) + \xi_2(A_2^T F A_2 - F)$

$= \xi_1\xi_1(A_1^T F A_1 - F) + \xi_1\xi_2(A_1^T F A_1 - F) + \xi_2\xi_1(A_2^T F A_2 - F) + \xi_2\xi_2(A_2^T F A_2 - F).$

If $n = 2$*:*

$\sum_{i=1}^{2} \xi_i \left(A_i^T F A_i - F\right) - \sum_{i=1}^{2} \xi_i \xi_j \left(A_i^T F A_j - F\right) = \xi_1 \xi_2 (A_1^T F A_1 - F) + \xi_2 \xi_1 (A_2^T F A_2 - F) -$

$\{\xi_1 \xi_2 (A_1^T F A_2 - F) + \xi_2 \xi_1 (A_2^T F A_1 - F)\}$

$= \xi_1 \xi_2 \{(A_1^T F A_1 + A_2^T F A_2) - (A_1^T F A_2 + A_2^T F A_1)\}.$

$(A_1 - A_2)^T F (A_1 - A_2)^T > 0$

Means

$A_1^T F A_1 - A_1^T F A_2 - A_2^T F A_1 - A_2^T F A_1 > 0$

Means

$\sum_{i=1}^{2} \xi_i \left(\varphi(k)\right)(A_i^T F A_i - F) - \sum_{i=1}^{2} \sum_{j=1}^{2} \xi_i\left(\varphi(k)\right) \xi_j\left(\varphi(k)\right)\left(A_i^T F A_j - F\right) > 0$

Means

$V(x_{k+1}) - V(x_k) \leq x_k{}^T \left[\sum_{i=1}^{n} \xi_i\left(\varphi(k)\right)(A_i^T F A_i - F)\right] x_k.$

If the condition $A_i^T F A_i - F < 0$ *holds,* $V(x_{k+1}) - V(x_k) < 0$ *and* $A_i^T F A_i - F < 0.$

The above LMIs are the sufficient asymptotic stability conditions obtained by the application of the Quadratic Lyapunov function (6.10) along the trajectory of the discrete-time T-S presented in (6.9).

The existence of matrix *F* depends on two main conditions that are [124]:

1. Every matrix *A* must be a Schur matrix.
2. The matrix product $\prod_{i=1}^{n} A_i$ must be Schur.

A is a Schur matrix when the module of each eigen values of matrix *A* belongs to the disc of center (0, 0) and radius 1.

6.3.2 Autonomous vehicles' stabilization

Considering the new PDC formula:

$$u_k = -\sum_{i=1}^{n} \xi_i\left(\varphi(k)\right)[G_i x_k] - [S_i x_{k+1}].$$

Where $S_i = G_i$.

$$u_k = -\sum_{i=1}^{n} \xi_i\left(\varphi(k)\right)[G_i x_k] - [G_i x_{k+1}]. \quad (6.12)$$

Applying a PDC control law on the closed loop discrete-time T-S fuzzy system described in (6.7) we get:

$$\begin{cases} x_{k+1} = \sum_{i=1}^{n} \sum_{j=1}^{n} \xi_i(\varphi(k)) \xi_j(\varphi(k)) \vartheta_{ij} x_k - B_i G_j x_{k+1}. \\ \vartheta_{ij} = (A_i - B_i G_j). \end{cases} \tag{6.13}$$

Hypothesis: In this case, the two system matrices (A_i, B_i) are supposed to be controllable. It is said that the T-S models are locally controllable as described by Euntai and Lee [58].

Theorem 6.2: The closed loop of the discrete-time T-S fuzzy system (6.7) via PDC control law is globally asymptotically stable if there exists a symmetric matrix $F > 0$ and matrices $G_i, i \in I_n$ such as [58]:

$$C_{discrete}(\vartheta_{ii}, F) < 0 \qquad \forall\, i \in I_n \tag{6.14}$$

$$C_{discrete}(\vartheta_{ij}, F) \leq 0 \qquad \forall\, (i,j) \in I_n^2 \quad i < j \tag{6.15}$$

$$\xi_i(\varphi(k))\, \xi_j(\varphi(k)) \neq 0. \tag{6.16}$$

$$C_{discrete}(\vartheta_{ij}, F) = \left[\frac{\vartheta_{ij} + \vartheta_{ji}}{2}\right]^T F \left[\frac{\vartheta_{ij} + \vartheta_{ji}}{2}\right] - F\,. \tag{6.17}$$

The first closed loop stabilization condition is $C_{discrete}(\vartheta_{ii}, F) < 0, \forall i \in I_n$. ij in equation (6.17) is substituted with ii to get the condition:

$$(A_i - B_i G_i)^T F (A_i - B_i G_i) - F < 0. \tag{6.18}$$

Multiplying (18) in pre and post by F^{-1}, the following inequality is obtained:

$$F^{-1}(A_i - B_i G_i)^T F (A_i - B_i G_i) F^{-1} - F^{-1} F F^{-1} < 0 \tag{6.19}$$

$$(A_i F^{-1} - B_i G_i F^{-1})^T F (A_i F^{-1} - B_i G_i F^{-1}) - F^{-1} < 0. \tag{6.20}$$

This inequality will be written as LMI. The Schur complement is used as follows:

Let the matrices be $Q = Q^T \; and \;\; R = R^T$.

The following matrix inequalities are equivalent:

$$R < 0 \, , Q - SR^{-1}S^T > 0, \tag{6.21}$$

$$\begin{bmatrix} Q & S^T \\ S & R \end{bmatrix} > 0. \tag{6.22}$$

So (-1) is made as a common factor in equation (6.20) to get the Schur LMI desired form (6.21) as follows:

$$-(F^{-1} - (A_i F^{-1} - B_i G_i F^{-1})^T F (A_i F^{-1} - B_i G_i F^{-1})) < 0. \tag{6.23}$$

$$F^{-1} - (A_i F^{-1} - B_i G_i F^{-1})^T F (A_i F^{-1} - B_i G_i F^{-1}) > 0. \tag{6.24}$$

Until now we get the Schur desired form, but there is still bilinearity which is the multiplication of two unknown variables $G_i F^{-1}$. The solution is to use a simple variable change as follows:

It is supposed that $X = F^{-1}$ and $H_i = G_i F^{-1}$; thus we get the following Linear Matrix Inequality:

$$X - (A_i X - B_i H_i)^T F (A_i X - B_i H_i) > 0. \tag{6.25}$$

Applying the Schur complement, we get the LMI:

$$\begin{bmatrix} X & * \\ A_i X - B_i H_i & X \end{bmatrix} > 0. \tag{6.26}$$

Using the same method for the following stabilization condition coming from the Quadratic Lyapunov function when we apply:

$$V(x_{k+1}) - V(x_k) < 0. \tag{6.27}$$

$$C_{discrete}\left(\vartheta_{ij}, F\right) \leq 0 \, , \forall \, (i,j) \in I_n^2 \quad i < j. \tag{6.28}$$

We get:

$$\begin{bmatrix} X & * \\ \frac{A_i + A_j}{2} X - \frac{1}{2}\left(B_j H_i + B_i H_j\right) & X \end{bmatrix} \geq 0 \tag{6.29}$$

We apply the following theorem described by Euntai and Lee [58].The aim of this theorem is to reduce the conservatism of the previous stabilization conditions presented as LMIs. The theorem uses a several matrices M_{ij} instead of a common matrix M.

Theorem 6.3: if there exists matrices $F = F^T > 0$, $M_{ij} = M_{ij}^T$ and matrices G_i which verifies:

$$\begin{cases} C_{discrete}(\vartheta_{ii}, F) + M_{ii} < 0, \forall i \in I_n, \\ C_{discrete}(\vartheta_{ij}, F) + M_{ij} \leq 0, \forall i, j \in I_n^2 \\ \xi_i(\varphi(k))\, \xi_j(\varphi(k)) \neq 0. \end{cases} \quad (6.30)$$

Where,

$$\begin{bmatrix} M_{11} & \cdots & M_{1n} \\ \vdots & \ddots & \vdots \\ M_{1n} & \cdots & M_{nn} \end{bmatrix} > 0. \quad (6.31)$$

And ,

$\vartheta_{ij} = (A_i - B_i G_j)$, so the discrete-time closed loop system (6.13) is globally asymptotically stable.

The LMI (6.26) can be relaxed by using theorem 6.3:

$$\begin{bmatrix} X - Y_{ii} & * \\ A_i X - B_i H_i & X \end{bmatrix} > 0 \quad \forall\, i \in I_n \quad (6.32)$$

The LMI (29) by using the condition $C_{discrete}(\vartheta_{ij}, F) \leq 0$ and theorem 6.3 is:

$$\begin{bmatrix} X - Y_{ij} & * \\ \frac{A_i + A_j}{2} X - \frac{1}{2}(B_j N_i + B_i H_j) X & X \end{bmatrix} > 0 \quad \forall\, (i,j) \in I_n^2 \quad i < j \quad (6.33)$$

The first Lyapunov function condition is $V > 0$ gives $F > 0$, because $x_k^T . x_k > 0$.

This means $F > 0$ is a stability and stabilization condition.

Multiplying pre and post by F^{-1} gives:

$F^{-1} F F^{-1} > 0$; gives $F^{-1} > 0$, which implies X > 0. Since $X = F^{-1}$.

$$X > 0; \quad (6.34)$$

$$\begin{bmatrix} Y_{11} & \cdots & Y_{1n} \\ \vdots & \ddots & \vdots \\ Y_{1n} & \dots & Y_{nn} \end{bmatrix} > 0 \; ; \tag{6.35}$$

$$\begin{bmatrix} M_{11} & \cdots & M_{1n} \\ \vdots & \ddots & \vdots \\ M_{1n} & \dots & M_{nn} \end{bmatrix} > 0 \quad ; \tag{6.36}$$

$$\begin{cases} X = F^{-1}. \\ Y_{ij} = XM_{ij}X. \\ G_i = H_iX^{-1}. \\ \forall i \in I_n. \end{cases} \tag{6.37}$$

6.3.3 Developing of nonlinear Luenberger observer

Consider the following Luenberger nonlinear observer as follow:

$$\begin{cases} \hat{x}_{k+1} = \sum_{i=1}^{n} \xi_i\big(\varphi(k)\big)\big((A_i\hat{x}_k + B_iu_k + B_i^w w_k) + N_i(y_k - \hat{y}_k)\big). \\ \hat{y}(k) = \sum_{i=1}^{n} \xi_i\left(\varphi(k)\right)C_i\hat{x}_k. \end{cases} \tag{6.38}$$

The estimation error of the state vector is written as:

$$\tilde{x}_k = x_k - \hat{x}_k. \tag{6.39}$$

Knowing that, the dynamics of the state vector error is given by equation (6.7) and (6.38):

$$
\begin{cases}
\tilde{x}_{k+1} = x_{k+1} - \hat{x}_{k+1} = \sum_{i=1}^{n} \xi_i\big(\varphi(k)\big)[(A_i x_k + B_i u_k + B_i^w w_k)] - \\
\qquad \sum_{i=1}^{n} \xi_i\big(\varphi(k)\big)[(A_i \hat{x}_k + B_i u_k + B_i^w w_k) + N_i(y_k - \hat{y}_k)] \\
= \sum_{i=1}^{n} \xi_i\,[A_i x_k + B_i u_k + B_i^w w_k - A_i \hat{x}_k - B_i u_k - B_i^w w_k - N_i y_k + N_i \hat{y}_k] \\
\qquad = \sum_{i=1}^{n} \xi_i\big(\varphi(k)\big)[A_i x_k - A_i \hat{x}_k + N_i \hat{y}_k - N_i y_k] \\
\quad = \sum_{i=1}^{n} \xi_i\big(\varphi(k)\big)\left[A_i(x_k - \hat{x}_k) + N_i\left(\begin{matrix}\sum_{j=1}^{n} \xi_j\big(\varphi(k)\big) C_j \hat{x}_k \\ -\sum_{i=1}^{n} \xi_i\big(\varphi(k)\big) C_j x_k\end{matrix}\right)\right] \\
\qquad = \sum_{i=1}^{n} \xi_i\big(\varphi(k)\big)\left[A_i \tilde{x}_k + N_i \sum_{j=1}^{n} \xi_j\big(\varphi(k)\big) C_j(\hat{x}_k - x_k)\right] \\
\qquad = \sum_{i=1}^{n} \xi_i\big(\varphi(k)\big)\left[A_i \tilde{x}_k - N_i \sum_{j=1}^{n} \xi_j\big(\varphi(k)\big) C_j(x_k - \hat{x}_k)\right] \\
\qquad\quad = \sum_{i=1}^{n} \xi_i\big(\varphi(k)\big)\left[A_i \tilde{x}_k - N_i \sum_{j=1}^{n} \xi_j\big(\varphi(k)\big) C_j \tilde{x}_k\right] \\
\qquad\qquad \sum_{i=1}^{n} \sum_{j=1}^{n} \xi_i\big(\varphi(k)\big)\xi_j\big(\varphi(k)\big)\alpha_{ij}\tilde{x}_k. \\
\qquad\qquad\quad \alpha_{ij} = A_i - N_i C_j\,, \forall (i,j) \in I_n^2.
\end{cases}
\tag{6.40}
$$

Indeed, the synthesis of Luenberger observers consists of computing local gains $N_i \in I_n$ to guarantee the convergence of the estimation error dynamics of the state vector to 0. In addition, $F = F^T > 0$ and matrices $N_i \in I_n$ should make the following conditions valid:

$$
\begin{cases}
C_{discrete}(\alpha_{ii}, F) < 0, \forall i \in I_n. \\
C_{discrete}\big(\alpha_{ij}, F\big) \le 0, \forall i,j \in I_n^2. \\
\xi_i\big(\varphi(k)\big)\,\xi_j(\varphi(k)) \neq 0.
\end{cases}
\tag{6.41}
$$

$$
C_{discrete}\big(\alpha_{ij}, F\big) = \left[\tfrac{\alpha_{ij}+\alpha_{ji}}{2}\right]^T F \left[\tfrac{\alpha_{ij}+\alpha_{ji}}{2}\right] - F. \tag{6.42}
$$

The conditions (6.41) and (6.42) secure global convergence of the state error vector, In addition, these conditions can be written as LMI:

$$
\begin{bmatrix} F & * \\ F\,\frac{A_i+A_j}{2} - \frac{1}{2}\big(H_j C_j + H_j C_i\big) & F \end{bmatrix} \ge 0 \tag{6.43}
$$

When $i < j$.

The Luenberger observers may be enhanced by the next theorem.

Theorem 6.4: the multiple Luenberger observers are globally asymptotically stable if there exists symmetric matrices $F > 0$, M_{ij} *and* $N_i \in I_n$ that satisfy:

$$\begin{cases} C_{discrete}(\alpha_{ii}, F) + M_{ii} < 0, \forall i \in I_n. \\ C_{discrete}(\alpha_{ij}, F) + M_{ij} \leq 0, \forall i, j \in I_n^2. \\ \begin{bmatrix} M_{11} & \cdots & M_{1n} \\ \vdots & \ddots & \vdots \\ M_{1n} & \dots & M_{nn} \end{bmatrix} > 0 \\ \xi_i(\varphi(k))\, \xi_j(\varphi(k)) \neq 0. \\ \alpha_{ij} = A_i - N_i C_j \,, \forall (i,j) \in I_n^2. \end{cases} \tag{6.44}$$

The LMIs are given by:

$$\begin{cases} F > 0. \\ \begin{bmatrix} F - M_{ii} & * \\ FA_i - H_i C_i & F \end{bmatrix} > 0 \;\forall\, i \in I_n. \\ \begin{bmatrix} F - M_{ij} & * \\ F\frac{A_i + A_j}{2} - \frac{1}{2}(H_i C_j + H_j C_i) & F \end{bmatrix} \geq 0 \;\forall\, i < j. i, j \in I_n^2 \\ M = \begin{bmatrix} M_{11} & \cdots & M_{1n} \\ \vdots & \ddots & \vdots \\ M_{1n} & \dots & M_{nn} \end{bmatrix} > 0. \\ H_i = FN_i. \end{cases} \tag{6.45}$$

6.4 Application of the lateral control for autonomous vehicles

This part will present the T-S model for simulation purpose. It is clear in (6.5) that the system matrices are nonlinearly linked to the vehicle speed. This velocity is measured and bounded as follows: $v_{min} \leq v_x \leq v_{max}$, $v_{min} = 10\ m/s$, $v_{max} = 25\ m/s$.

The vector variables of the measured premise to achieve the vehicle T-S model are as follows:

$$\theta = \begin{bmatrix} v_x & \frac{1}{v_x} & \frac{1}{v_x^2} \end{bmatrix}^T \in R^3.$$

Indeed, by following the description part of the nonlinearity approach of Tanaka and Wang [143], a right choice will guide us to an exact T-S representation of system (6.5) with eight linear subsystems. Nevertheless, the acquired T-S fuzzy system would be massive for control purposes, mainly for real-time control implementation. Therefore, the factorization of Taylor will be applied to fully benefit from the relationship between v_x, $\frac{1}{v_x}$, *and* $\frac{1}{v_x^2}$; consequently, the numerical difficulty of the suggested control technic can be notably decreased as follows:

$$\begin{aligned} \frac{1}{v_x} &= \frac{1}{v_0} + \frac{1}{v_1}\Delta_x \,, \\ v_x &= v_0\left(1 - \frac{v_0}{v_1}\,\Delta_x\right), \\ \frac{1}{v_x^2} &= \frac{1}{v_0^2}\left(1 + 2\frac{v_0}{v_1}\,\Delta_x\right). \end{aligned} \tag{6.46}$$

The new measured time-varying parameter $\Delta_x \in [-1,\ \ 1]$ is used to describe the variation of v_x between its lower and upper bounds v_{min}, v_{max}.
The two constants v_0 and v_1 in (6.46) are given by:

$$v_0 = 2\,\frac{v_{min}\,v_{max}}{v_{min}+v_{max}}, v_1 = 2\,\frac{v_{min}\,v_{max}}{v_{min}-v_{max}}\,. \tag{6.47}$$

Replacing relations (6.46) in system (6.5), the premise variable of this system will be expressed as $\theta_* = \Delta_x$. The T-S fuzzy presented in (6.7) of system (6.5) has two linear subsystems $(A_i,\ B_i,\ B_i^w)$. The following membership functions related to the obtained T-S system are given by:

$$\begin{aligned} \xi_1 &= \frac{1-\Delta_x}{2}. \\ \xi_2 &= 1 - \xi_1. \end{aligned} \tag{6.48}$$

6.5 Results

In this section, we compare between the discrete-time T-S of [45] and our new PDC control law design applied to the lateral control for autonomous vehicles. The results

demonstrate the robustness and effectiveness of the improved PDC control law formula. This idea is original and has not been used before. From (6.37) and (6.45), the feedback gain G_i, the matrix F, and the gain N_i are of the form:

$$\begin{cases} F = X^{-1}. \\ G_i = H_i F. \\ H_i = F N_i. \end{cases} \tag{6.49}$$

In this part, we present the results of the lateral control of autonomous vehicles for T-S presented by [45], the methods used by [6], [9], [8] and the new formulation of the PDC control law. Based on (6.49), we get the following gains and matrices:

$$F = e^{-03}\begin{bmatrix} 0.0513 & 0.0139 & 0.0693 & 0.0120 & 0.1275 & 0.0070 \\ 0.0139 & 0.0062 & 0.0235 & 0.0041 & 0.0400 & 0.0025 \\ 0.0693 & 0.0235 & 0.1267 & 0.0196 & 0.21158 & 0.0121 \\ 0.0120 & 0.0041 & 0.0196 & 0.0051 & 0.0368 & 0.0019 \\ 0.1275 & 0.0400 & 0.2158 & 0.0368 & 0.4979 & 0.0266 \\ 0.0070 & 0.0025 & 0.0121 & 0.0019 & 0.0266 & 0.0029 \end{bmatrix}$$

$$G_1 = [\,538.7210 \;\; 88.1555 \;\; 137.5593 \;\; 21.1442 \;\; -146.3325 \;\; -56.7097].$$

$$G_2 = [545.2576 \;\; 58.9360 \;\; 139.5243 \;\; 21.1255 \;\; -148.8607 \;\; -56.7512].$$

For multi-observer gains we have:

$$N1 = e^{03}\begin{bmatrix} 0.0116 & 0.0007 \\ 0.0828 & -0.0020 \\ 0.0285 & -0.0003 \\ 0.2673 & -0.0020 \\ -0.0196 & -0.0273 \\ 9.3447 & 7.3696 \end{bmatrix}, \quad N2 = e^{04}\begin{bmatrix} 0.0026 & 0.0000 \\ 0.0152 & -0.0001 \\ 0.0076 & -0.0000 \\ 0.0624 & -0.0001 \\ 0.0074 & -0.0023 \\ -1.2496 & 0.6264 \end{bmatrix}.$$

The following figures present a combined scenario applied for the autonomous vehicles. Firstly, we test the control input saturation, which means that we make the assumption that the vehicle system will not start from the origin. The state vector $x_0 = [0; 0.01; 0.02; 0; 0; 0.3]$, which is not the system equilibrium points, for example, the lane centreline. It can clearly be observed that our two T-S systems converge all the state variables to zero, but the new PDC control law formulation converges faster and shows more robustness than the first T-S controller. The six states given by the classic PDC controller are compared as illustrated in Figures 6.4-6.9 with Figures 6.12 - 6.17 of the new PDC control design. On the other hand, our model is tested in terms of disturbance mitigation. The system dynamic is subjected to a lateral

wind force of 500 Newton. Figure 6.2 and Figure 6.3, of the classic PDC controller and Figure 6.10, and Figure 6.11 show a remarkable robust stabilization. Our model showed robustness and effectiveness against the disturbances.

As shown in the following figures, the new PDC controller stabilizes the state vector variable faster than the classic PDC controller.

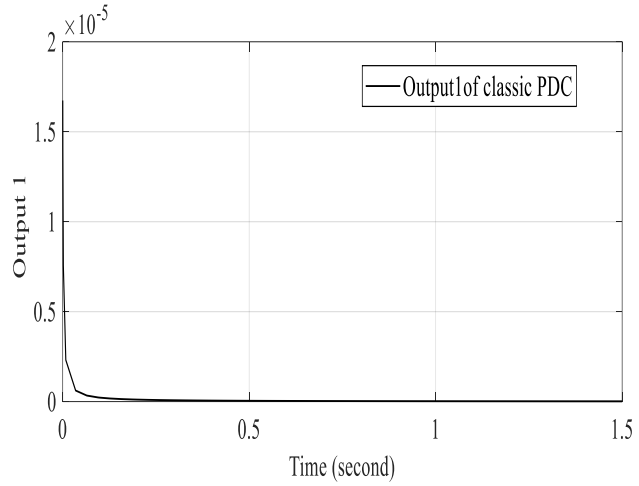

Figure 6. 2 Output1 of the lateral control using the classic PDC law.

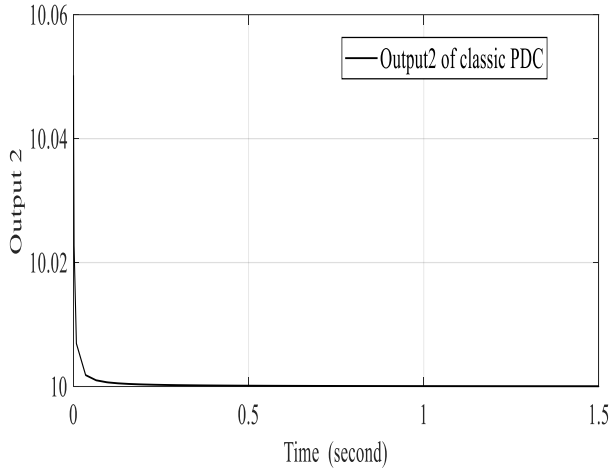

Figure 6. 3 Output2 of the lateral control using the classic PDC law.

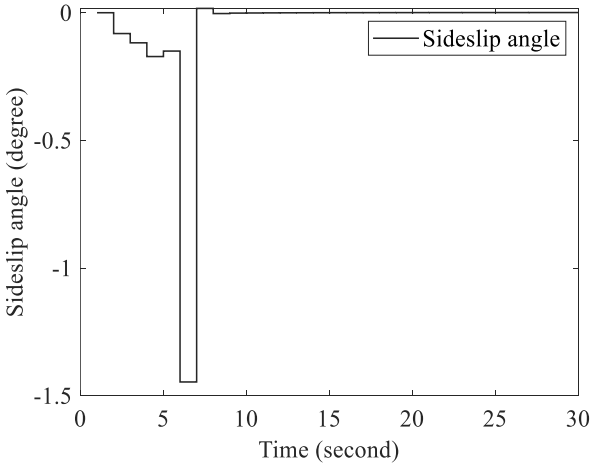

Figure 6. 4 Sideslip using the classic PDC law.

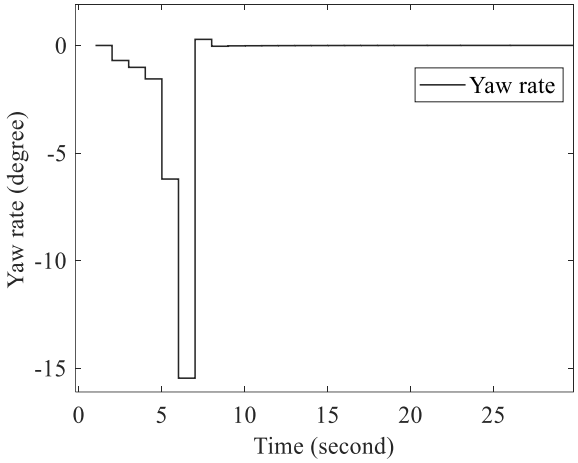

Figure 6. 5 Yaw rate using the classic PDC law.

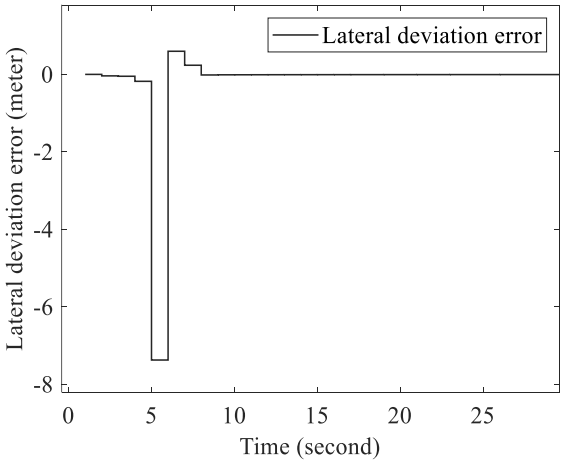

Figure 6. 6 Lateral deviation error using the classic PDC law.

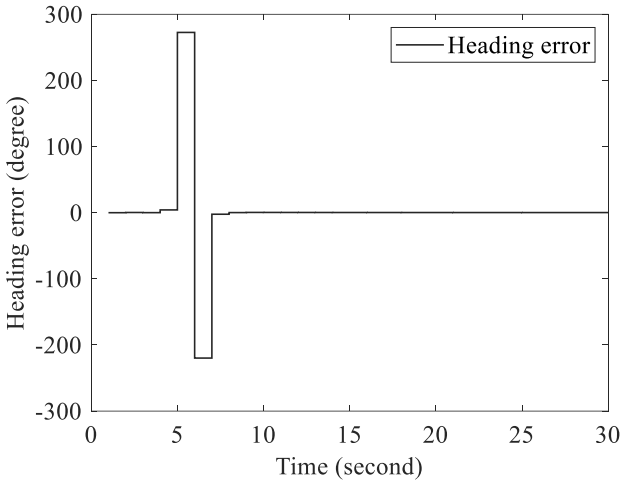

Figure 6. 7 Heading error using the classic PDC law.

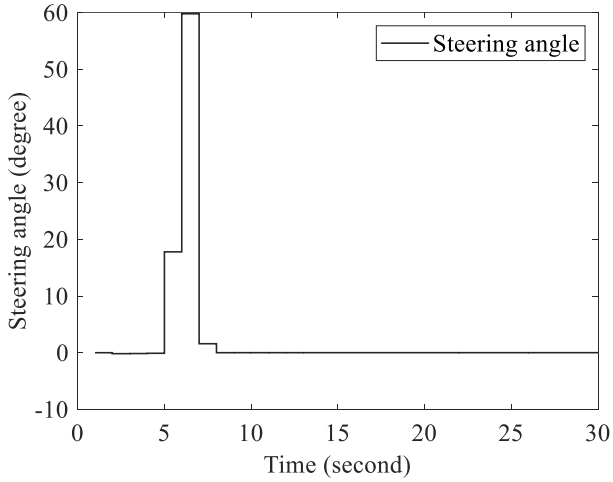

Figure 6. 8 Steering angle using the classic PDC law.

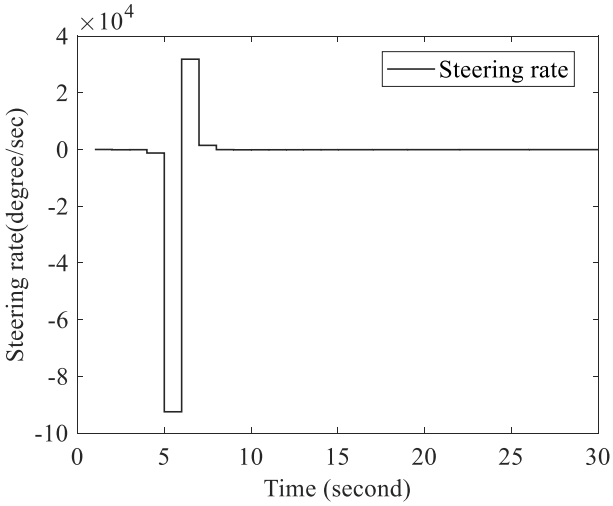

Figure 6. 9 Steering rate using the classic PDC law.

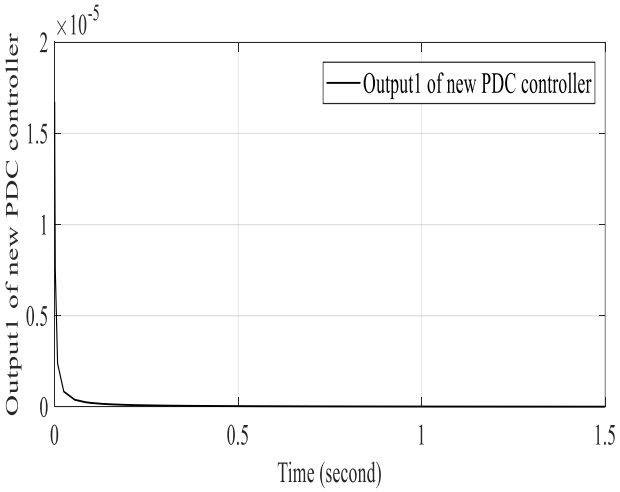

Figure 6. 10 Output1 of the new PDC controller.

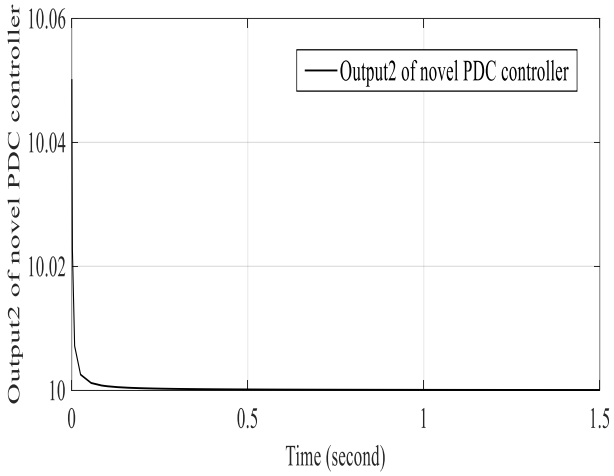

Figure 6. 11 Output2 of the new PDC controller.

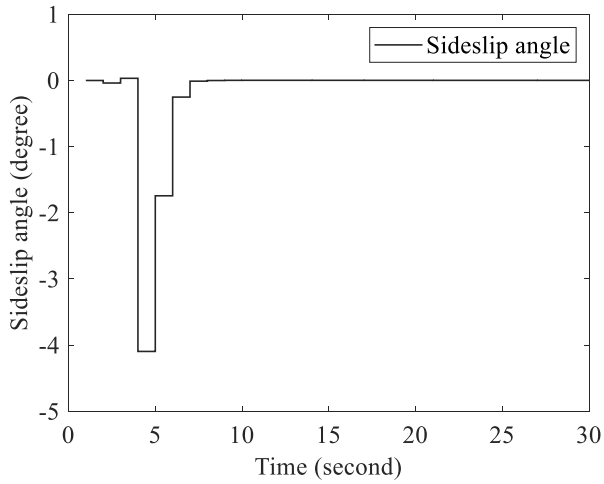

Figure 6. 12 Sideslip of the new PDC controller.

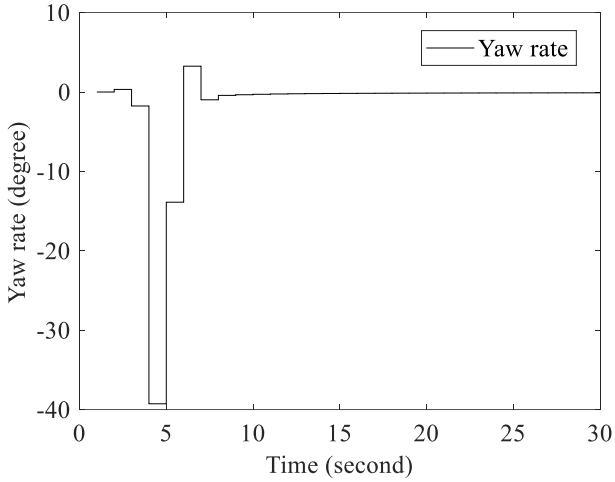

Figure 6. 13 Yaw rate of the new PDC controller.

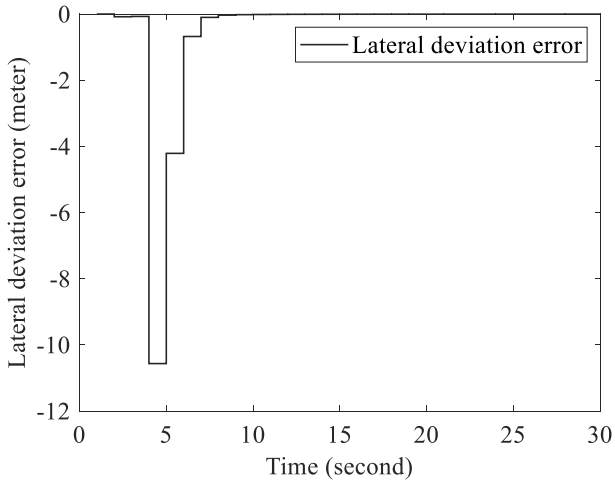

Figure 6. 14 Lateral deviation error of the new PDC controller.

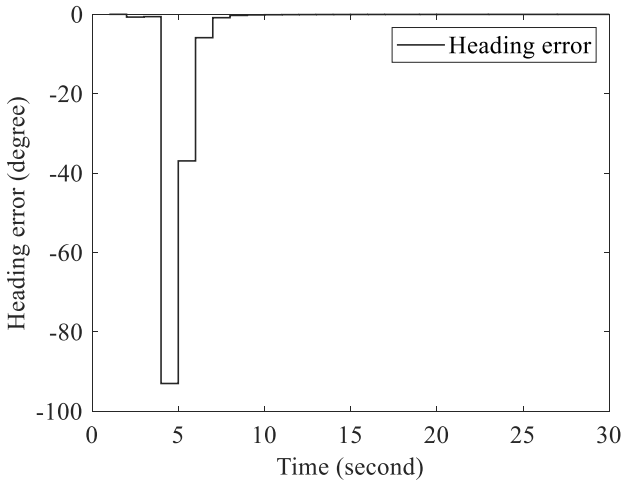

Figure 6. 15 Heading error of the new PDC controller.

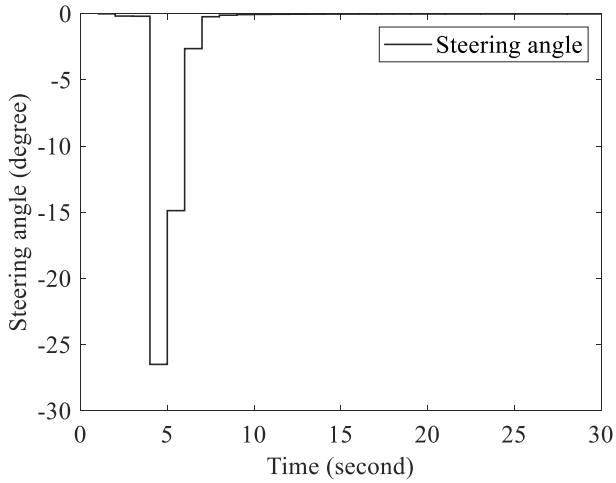

Figure 6. 16 Steering angle of the new PDC controller.

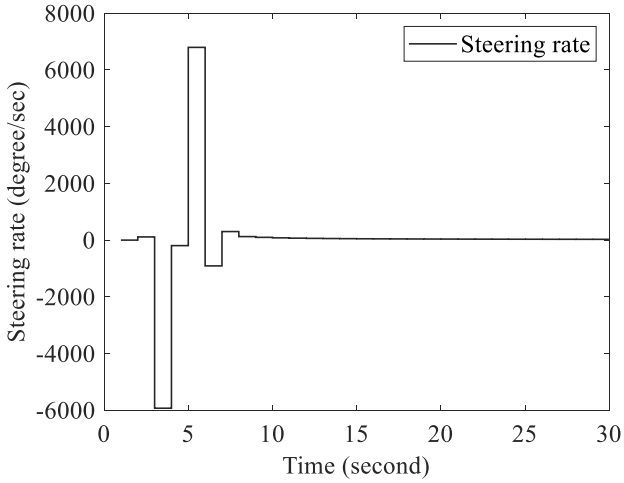

Figure 6. 17 Steering rate of the new PDC controller.

Table 6.2 below shows that the sideslip angle converges to zero. It takes 10 seconds when using the classic PDC controller and 7 seconds when using the new PDC controller design. The yaw rate converges in 12 seconds using the classic PDC controller while it takes 11 seconds using the new PDC controller. The lateral deviation and the heading error share the same time for both cases as well as the steering angle; but it can be observed that the behavior of the lateral deviation error of the new PDC controller is better than the classic one, because we do not have an overshoot in this case. As seen in Figure 6.7, the heading error was 290 degree using the classic PDC controller, while in Figure 6.15; the heading error is only 95 degree using the new PDC controller. This implies a reduction of 67.24 percent. On the other hand, the steering rate takes 8 seconds for the classic PDC, while it takes 10 seconds for the new PDC design. Nevertheless, the improvement is in the term of degree per second, which is better than the case of the new PDC controller.

Table 6. 2 Comparison between states time convergence

States	**Classic PDC (second)**	**New PDC (second)**
Sideslip	10	7
Yaw rate	12	11
Lateral deviation	8	8
Heading error	8	8
Steering angle	8	8
Steering rate	8	10

These results confirm the robustness and the effectiveness in terms of stabilization and improvement of lateral control as shown in the previous figures. We notice also that all trajectories of the vehicle T-S fuzzy system converge to zero.

6.6 Conclusion

We proposed in this chapter a new formulation of Parallel Distributed Compensation law for lateral control purpose, suggesting new steering control architecture of autonomous

vehicles. The vehicle system has been defined by discrete-time T-S model. This method relies on the use of a quadratic Lyapunov function, which is easy to implement, and LMIs techniques to get the matrices and gains values. We also computed the true values of the state vector using multiple Luenberger observers. Moreover, in this chapter, we compared the lateral control results given by the new formulation of the PDC law with the improved classic one [45]. As shown, the two lateral controllers converge the autonomous vehicles states to the equilibrium point and ensure the lane keeping under various constraints. In this chapter, we showed that the conservatism is minimized, the pessimism of the quadratic Lyapunov function is reduced and the results are more relaxed. The effectiveness of the proposed method is clearly illustrated via different figures.

Chapter 7

Autonomous vehicle path following

7.1 Introduction

This chapter is about autonomous ground vehicle path following control. This common motion control problem tries to construct steering control rules to reach and follow a chosen path without a precise time constraint [213].

Path following control for autonomous cars is gaining popularity, as seen by [214], [215] and references thereto.[216] proposes a vision-based lane maintaining controller with successful experimental validation on highways with unpredictable curvature using two separate PID nested loops. [214] presents a current assessment with a specific focus on motion planning and feedback control of self-driving urban cars, in which a variety of control strategies, such as pure pursuit, feedback linearization, control Lyapunov design, and model predictive control (MPC).

Tagne et al. [217] present an intriguing study highlighting the benefits and downsides of three lateral controllers based on sliding mode control, the immersion and invariance concept, and the system passivity characteristic. Another notable comparison analysis on the performance limits and tradeoffs (in terms of lane tracking, stability robustness, and passenger comfort) of three controllers, including PID, linear-quadratic Gaussian, and H∞, was recently given in [218]. Furthermore, obstacle avoidance control is critical for autonomous cars. In [219], a two-stage nonlinear nonconvex control technique for obstacle avoidance is devised, consisting of an outer-loop nonlinear MPC and an inner-loop linear feedback control.

Attia et al. [220] propose a mixed longitudinal lateral control method for autonomous vehicle guiding in which a nonlinear MPC technique is employed for lateral control and another Lyapunov-based control rule ensures longitudinal speed tracking. Other MPC-based control techniques have been used for autonomous vehicle route following and obstacle avoidance,

[221], [222]. However, the MPC approach necessitates tackling online optimizations, which imposes a significant computing cost, particularly for nonlinear MPC problems, as described in [221]. Furthermore, the majority of existing results on vehicle path following control necessitate full state-information for feedback schemes.

However, due to the high expense of vehicle sensors, measurements of particular vehicle states, such as lateral speed and/or sideslip angle, are not accessible on series-production cars [223], [72]. An output feedback control method must be employed in this real circumstance [224]. It is emphasised that the output feedback MPC technique is still an unresolved subject that requires a moving horizon estimation [225].

Furthermore, due to the use of a genetic algorithm for the design method and the excessive amount of linear submodels of the vehicle polytopic system, it may be difficult to attain realistically good route following performance using the technique in [213]. Motivated by the theoretical and practical challenges discussed above, in this thesis, The Takagi-Sugeno (T-S) fuzzy control approach [106], [70] is used to account for the time-varying character of vehicle speed. To decrease conservatism, the physical limits of speed are explicitly showed in the control design.

The following is the structure of this thesis. Section 2 is dedicated to lane keeping aims, section 3 is dedicated to simulation design, section 4 is devoted to simulation findings, and the final section is related to the conclusion.

7.2 Lane keeping goals for autonomous vehicles

The majority of the vehicles are equipped with an inertial navigation system to measure the yaw rate r and an odometer for the measurement of the vehicle speed v_x. The steering angle δ is obtained from an optical encoder. The look-ahead lateral deviation y_L and the heading error ψ_L can be measured by a video camera. The lateral speed v_y and the sideslip angle β can be measured by dual antenna GPS systems or Correvit optical sensors. Unfortunately, due to their excessive costs, the measurements of β and v_y are unavailable for real-time implementation in practice [213], [74]. Furthermore, the proposed TS fuzzy observer effectively estimates both the unknown steering angle and the effective engine torque.

This section proposes a systematic route following control mechanism that can address this key practical difficulty. The following design needs are specifically examined.

• Only low-cost sensors from series-production cars may be used for real-time control implementation.

• For practical use, the control structure must be basic with low numerical complexity.

• Under unknown curvatures, a suitable path following performance with better transient responsiveness is obtained.

• Lyapunov stability arguments ensure the performance and resilience of closed-loop control.

In this Ph.D. thesis, this scenario attempts to demonstrate the proposed controller's lane-keeping performance in the case when the road is made up of many sections with varying curvature amplitudes. For this reason, we used Matlab toolboxes for simulation.

- Note that the lateral wind force is applied on Simulink as external disturbance. It is addressed by the feedback controller part of the PDC.
- The curvature is considered as external disturbance of the vehicle control issue.
- To set limitations on the actuator, we used saturation blocks in Simulink. These blocks allow us to specify the maximum and minimum values for the actuator signals, effectively limiting their range of operation. By incorporating these saturation blocks into the control system model, we can ensure that the actuator commands stay within the desired range and satisfy the physical limitations of the actuator.

7.3 Road - vehicle modelling for path following

The vehicle modelling for path tracking control is shown in Figure. 7.1. Table 7.1 contains the terminology.

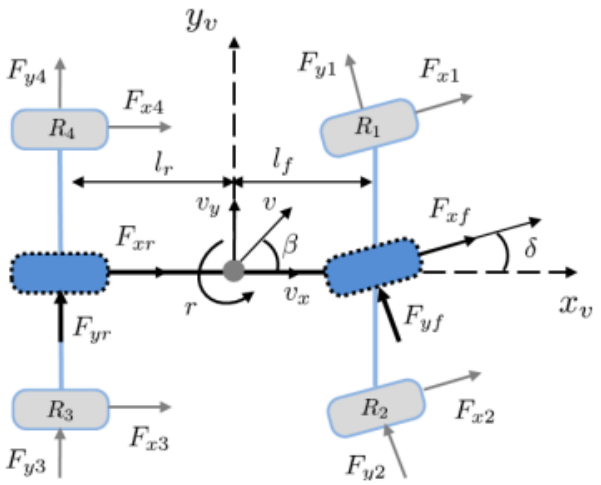

Figure 7. 1 Modelling of vehicle lateral dynamics [93].

Table 7. 1: Table Nomenclature

Parameter	Description	Value
$\mathbf{B_s}$	Steering system damping	5.73
$\mathbf{C_f}$	Front cornering stiffness	57000 N/rad
$\mathbf{C_r}$	Rear cornering stiffness	52000 N/rad
$\mathbf{I_s}$	Steering system moment of inertia	0.02 kgm2
$\mathbf{I_z}$	Vehicle yaw moment of inertia	2400 kgm2
$\mathbf{K_p}$	Manual steering column coefficient	0.55
$\mathbf{l_f}$	Distance from the CG to the front axle	1.3 m
$\mathbf{l_r}$	Distance from the CG to the rear axle	1.6 m
$\mathbf{l_s}$	Look-ahead distance	6 m
$\mathbf{l_w}$	Distance from the CG to the impact center of the wind force	0.45 m
M	Mass of the vehicle	2000 kg
$\mathbf{R_s}$	Steering gear ratio	14
$\boldsymbol{\sigma_t}$	Tyre length contact	0.13 m

Assuming low slip angles and a minimal contribution of longitudinal friction forces. The vehicle movements are represented by a nonlinear single track model, as shown in Figure 7. 1. This model represents the basic vehicle dynamics, which are described in [216], [226]:

$$M(\dot{v}_x - rv_y) = F_{xf}\, cos\delta - F_{yf}\, sin\delta + F_{xr}.$$

$$M(\dot{v}_y - rv_y) = F_{xf}\, sin\delta + F_{yf}\, cos\delta + F_{yr} + f_w.$$

$$I_z\dot{r} = l_f(F_{xy}\, sin\delta + F_{yf}\, cos\delta) - l_r F_{yr} + l_w f_w. \tag{7.1}$$

The longitudinal forces in the front and rear *Fxi* as well as lateral forces *Fyi* are calculated using Pacejka's formula called magic formula [226]:

$$F_{ki}(\alpha_i) = D_i sin(C_i\, arctan\, \xi_i)$$

$$\xi_i = (1 - E_i)B_i\alpha_i + E_i\, arctan(B_i\alpha_i)$$

Where $k \in \{x, y\}$ *and* $i \in \{f, r\}$. The Pacejka parameters *Bi, Ci, Di, and Ei* are affected by the tyre, road, and vehicle operating circumstances. The front and rear tyre sideslip angles are provided by:

$$\alpha_r = \delta - arctan\left(\frac{v_y + l_f r}{v_x}\right);$$

$$\alpha_f = arctan\left(\frac{l_f r - v_y}{v_x}\right).$$

Because we are focusing on path following, information on the vehicle position relative to the lane centerline is essential for control design (see Figure 7.1). The lateral error y_L at the look-ahead distance and the heading error ψ_L can be used to describe this information. [216] gives the dynamics of these variables as:

$$\dot{y}_L = \beta v_x + l_s r + \psi_L v_x$$

$$\psi_L = r - l_r v_x \tag{7.2}$$

Where *ρr* is the road curvature.

The nonlinear vehicle (7.1) is simplified for lateral control. The following conventional presumptions are taken into account [9]. First, the forces generated by longitudinal dynamics and aerodynamics are disregarded. Second, the lateral tire forces are proportional to the sideslip angles of each axle. Third, the assumption of small angles is used. As a result, the simplified representation of the vehicle's lateral dynamics is:

$$\begin{bmatrix}\dot{\beta}\\ \dot{r}\end{bmatrix} = \begin{bmatrix}a_{11} & a_{12}\\ a_{21} & a_{22}\end{bmatrix}\begin{bmatrix}\beta\\ r\end{bmatrix}\delta + \begin{bmatrix}e_1\\ e_2\end{bmatrix} f_w. \tag{7.3}$$

Where β is the sideslip angle at the center of gravity (CG), and the yaw rate is *r* shown in Figure 6. 1. As represented in equation (6.1), *fw* is the lateral wind force, and the system matrices elements are written as follows:

$$a_{11} = -2\frac{(C_r + C_f)}{m\vartheta_x}\,;\; a_{12} = 2\frac{(l_r C_r - l_f C_f)}{m\vartheta_x^2} - 1\,;$$
$$a_{21} = 2\frac{(l_r C_r - l_f C_f)}{I_z}\,;\; a_{22} = -2\frac{\left(l_r^2 C_r + l_f^2 C_f\right)}{I_z \vartheta_x}.$$
$$b_1 = \frac{2C_f}{m\vartheta_x}\,;\; b_2 = \frac{2l_f C_f}{I_z}\,;\; e_1 = \frac{1}{m\vartheta_x}\,;\; e_2 = \frac{l_w}{I_z}.$$

The control objective is to ensure that autonomous cars can follow a path even when the road is curved. As a result, the road model ought to reflect the curvature's a priori knowledge. The curved trajectory is predicted using the generator model listed below:

$$\begin{cases}\dot{x}_w = A_w x_w + B_w \theta_w\\ y_w = C_w x_w\end{cases} \tag{7.4}$$

Where $x_w = \rho_r$, $A_w = \frac{1}{\tau_r}$, $B_w = \frac{-1}{\tau_r}$ *and* $C_w = 1$. The disturbance θ_w is an irreducible signal such as impulse or white noise.

Be aware that a curved trajectory cannot be accurately predicted using model (7.4). But thanks to the time constant τ_r *= 1* [s], this predictor model offers a priori knowledge about the dynamics of the road curvature. In the majority of real-world driving scenarios, the latter is reasonable for the prediction of the road curvature. After that, the developed controller may make use of this data to predict and anticipate the system's evolution in order to enhance the overall closed-loop behaviours.

Note that the controller's design is based on three key models: the vehicle's lateral dynamics model, road vehicle positioning, and the steering system model. In Chapter 6, the controller architecture is described in depth. There are minor changes to the vehicle specifications, as shown in Table 7.1.

7.4 Simulation design

In this part, we explain the simulation design, we describe each Simulink block separately and we discuss the overall control architecture as well as the connection between each block. In this chapter of the thesis. The Simulink diagram is divided into three major sections.

1) The path planning.

2) The T-S lateral controller.

3) The autonomous vehicle to be controlled.

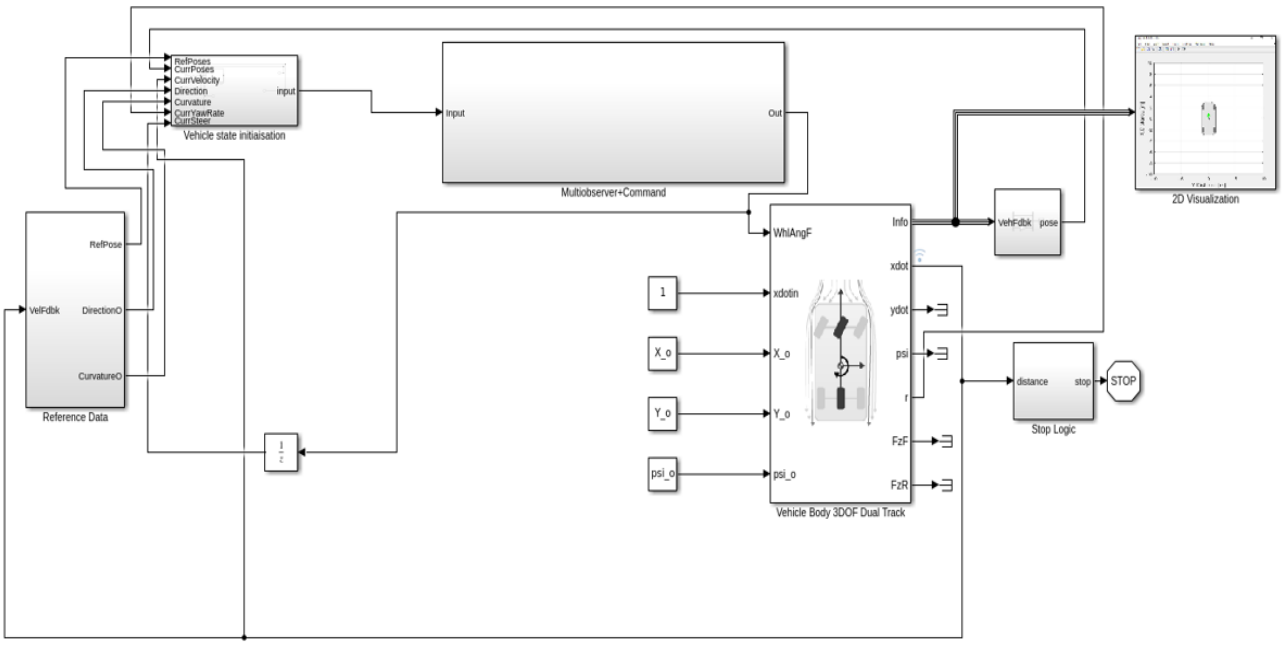

Figure 7. 2 Simulation design.

1) Path planning block:

The role of the path planning is the generation of a path as a reference for the autonomous vehicle. We used the scenario application of Matlab to draw several path shapes. These outputs were discussed extensively in the controller block section. It should be noted that this programme is part of the Matlab automated driving toolbox and MathWorks. Reference trajectories are generated to define the desired state for the lane keeping. Using the block vehicle state initialisation, this block compute the error between the current states and the desired one, these errors are the input of the multiobserver of the block "Multiobserver+ Command".

2) Controller Block:

Given the vehicle's current velocity and direction, the T-S Lateral Controller computes the Torque, which modifies the current posture of a vehicle to match a reference position. This instruction is computed by the controller utilising method described in chapter 6 of this thesis whose control rule is based on kinematic bicycle model. The controller block called "Multiobserver + Command".

The inputs:

The controller's inputs are separated into inputs from the first block on the Simulink diagram (path planner), other inputs come from the third block (vehicle dynamics), as illustrated in Figure 7.1.

Reference pose:

Pose of reference, expressed as a [x, y, theta] vector. x and y are measured in metres, whereas theta is measured in degrees. The reference point to guide the vehicle toward is specified by x and y. The orientation angle of the route at this reference point is specified by theta and is positive in the anticlockwise direction. The reference point for a forward-moving vehicle is the point on the path closest to the centre of the vehicle's front axle.

Driving direction of vehicle: The driving direction determines the position error and angle error used to compute the steering angle command.

Curvature of path:

Curvature of the path at the reference point, in radians per meter, specified as a real scalar. Note that the above three inputs of the controller are the path planner outputs, and the following inputs are the outputs of the vehicle dynamics block.

Current pose:

The vehicle's current pose is given as a [x, y, theta] vector x and y are measured in metres, whereas is measured in degrees x and y define the vehicle's position, which is defined as the centre of the vehicle's rear axle. Theta specifies the vehicle's orientation angle at position (x, y) and is positive in the anticlockwise direction.

Current longitudinal velocity:

Current longitudinal velocity of the vehicle, specified as a real scalar. Units are in meters per second.

Current yaw rate:

Current yaw rate of the vehicle, in degrees per second, specified as a real scalar. The current yaw rate is the rate of change in the angular velocity of the vehicle.

Current steering angle:

Current steering angle of the vehicle, in degrees, specified as a real scalar. This value is positive in the counter clockwise direction.

Parameters:

The parameters are referred to table 7.1. To compute the **s**teering torque command, the controller minimizes the position error and the angle error of the current pose with respect to the reference pose based on the optimization algorithm noted as Linear Matrix Inequality. The driving direction of the vehicle determines these error values based on observer called Luenberger multiobserver. Note that when the vehicle is in forward motion (Direction parameter is 1).The position error is the lateral distance from the center of the front axle to the

reference point on the path. The angle error is the angle of the front wheel with respect to reference path.

3) Vehicle body 3DOF (3 Degree Of Freedom) subsystem:

The Vehicle Body 3DOF block calculates longitudinal, lateral, and yaw motion using a rigid two-axle vehicle body model. The block takes into consideration body mass as well as aerodynamic drag between the axles caused by acceleration and steering. When vehicle pitch, roll, and vertical motion are not relevant, use this block in vehicle dynamics and autonomous driving studies to mimic nonholonomic vehicle motion. It should be noted that this programme is part of the Matlab Vehicle dynamics blockset toolbox and MathWorks.

- **Input Signals and Parameter:**

X-0: Initial longitudinal position: Initial vehicle CG displacement along the earth-fixed X-axis, in m.

Y-0: Initial lateral position: Initial vehicle CG displacement along the earth-fixed Y-axis, in m

xdot_in: Initial longitudinal velocity: Initial vehicle CG velocity along the vehicle-fixed x-axis, in m/s.

psi_0: Initial yaw angle: Initial rotation of the vehicle-fixed frame about the earth-fixed Z-axis (yaw), in rad

WhlAngF: Front wheel steering.

- **The Output of vehicle dynamics block:**

Info: Bus signal

xdot: Vehicle longitudinal velocity**:** Vehicle CG velocity along the vehicle-fixed x-axis, in m/s.

ydot :Vehicle lateral velocity: Vehicle CG velocity along the vehicle-fixed y-axis, in m/s.

Psi: Yaw**:** Rotation of the vehicle-fixed frame about the earth-fixed Z-axis (yaw), in rad.

r: Yaw rate**:** Vehicle angular velocity, r, about the vehicle-fixed z-axis (yaw rate), in rad/s.

FzF: Normal force on front wheels: Normal force on front wheels, FzF, along the vehicle-fixed z-axis, in N. not used.

FzR: Normal force on rear wheels: Normal force on rear wheels, FzR, along the vehicle-fixed z-axis, in N. not used.

7.5 Simulation results

This section presents several situations of autonomous vehicle path tracking. These situations are based on roads shapes difficulties and different longitudinal velocities. We increase the level of difficulty on each chosen path.

We show the most significant scenarios, that we can observe the most convergent autonomous vehicle tracking case and the worst path following, and this for each selected road at different levels of velocities .This simulation does not take time into account. Note that the red color is the reference path and the black color is dedicated for the autonomous vehicle path.

- **Scenario 1:** In the first scenario, we display four distinct figures at four different speeds, beginning with the best case at 10 km/h (Figure7.3) or less and ending with the worst situation at 100 km/h (Figure7.6) and higher.

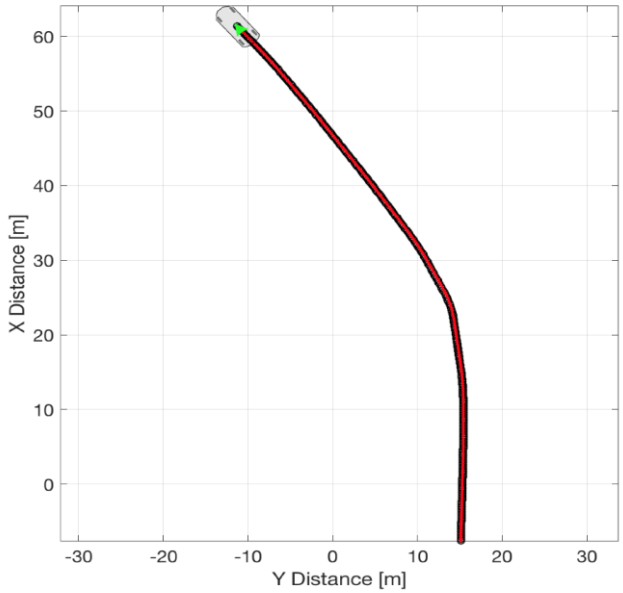

Figure 7. 3 Autonomous vehicle path tracking1 at 10km/h.

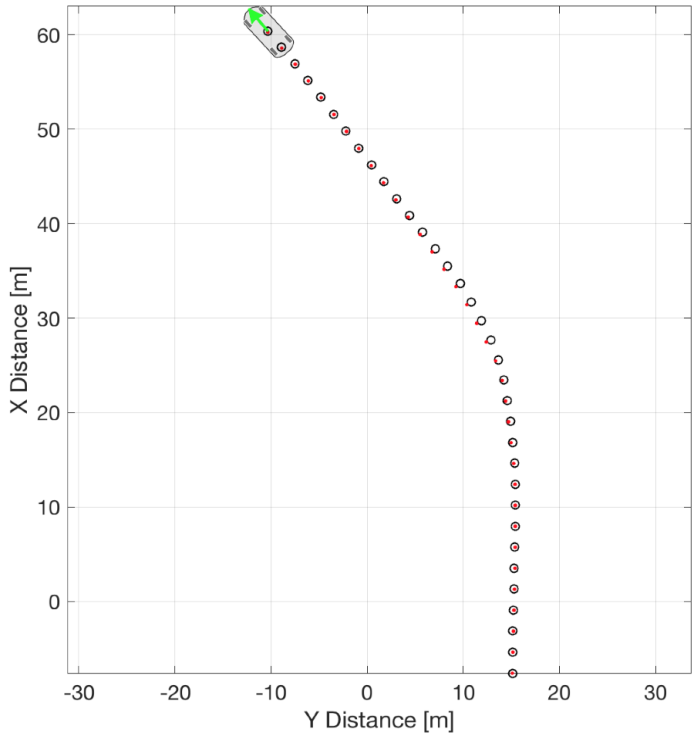

Figure 7. 4 Autonomous vehicle path tracking1 at 40km/h.

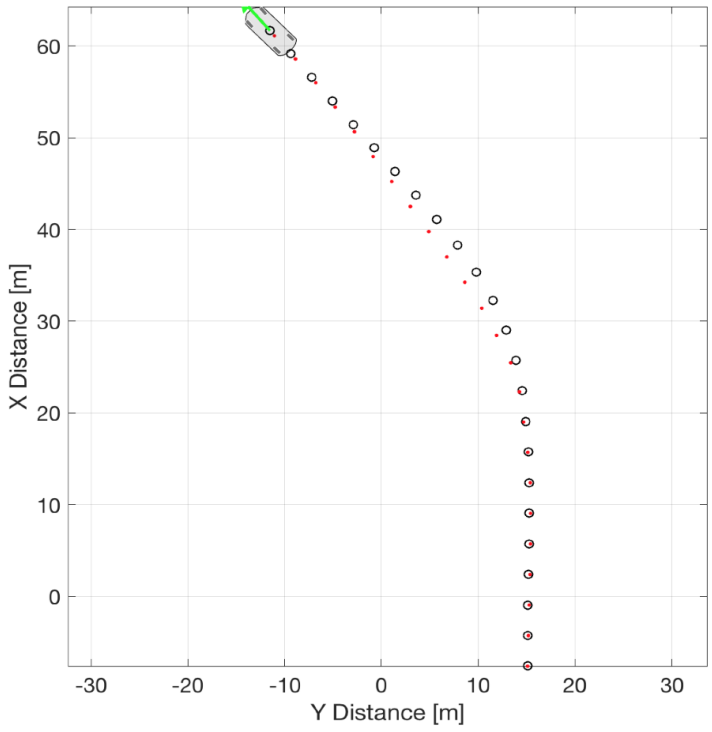

Figure 7. 5 Autonomous vehicle path tracking1 at 60km/h.

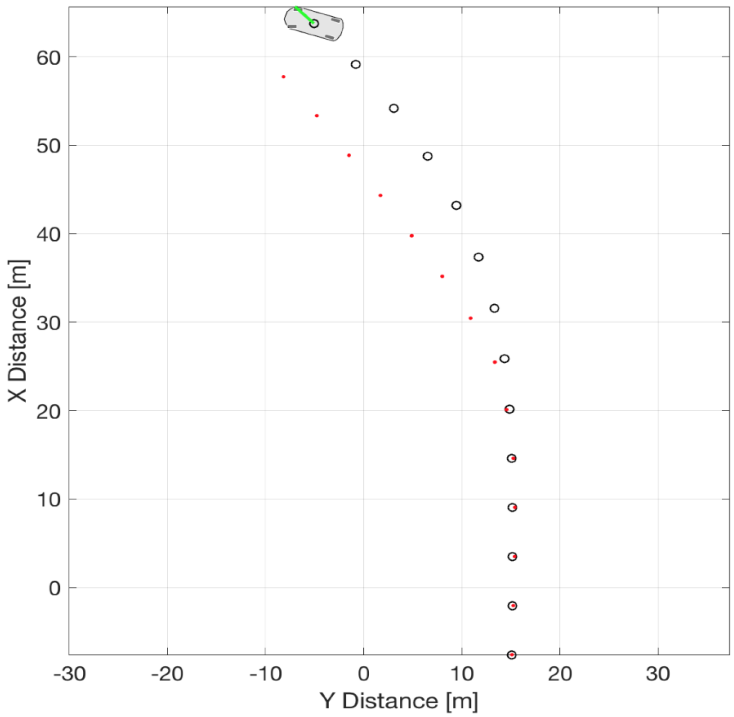

Figure 7. 6 Autonomous vehicle path tracking1 at 100km/h.

At 40 km/h, we can observe that there is a tiny difference between the reference path and the autonomous vehicle path (Figure 7.4). At 60 km/h (Figure 7.5), the error is easily visible with the naked eye. However, at 100 km/h (Figure 7.6), the autonomous car obviously diverges while turning left.

- **Scenario 2:** In second scenario, we display three distinct figures at three different speeds, beginning with the best case at 10 km/h (Figure 7.7) or less and ending with the worst situation at 55 km/h (Figure 7.9).

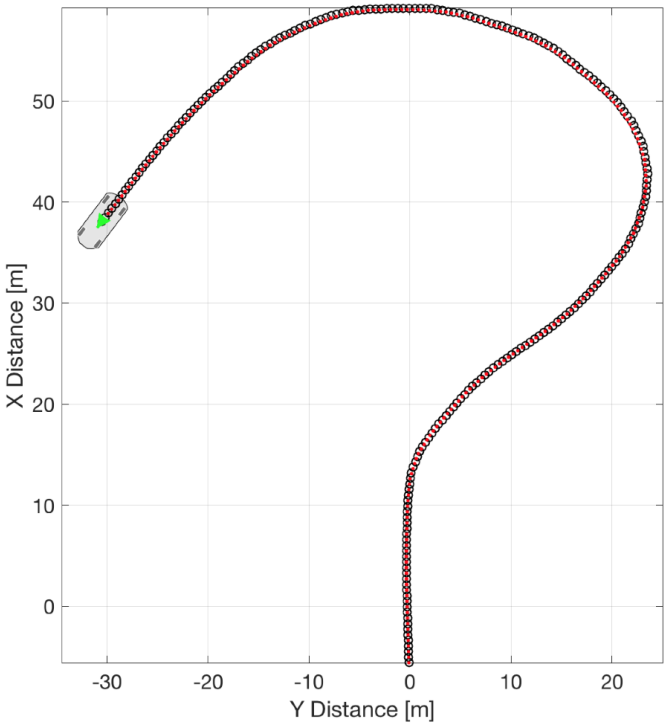

Figure 7. 7 Autonomous vehicle path tracking2 at 10km/h.

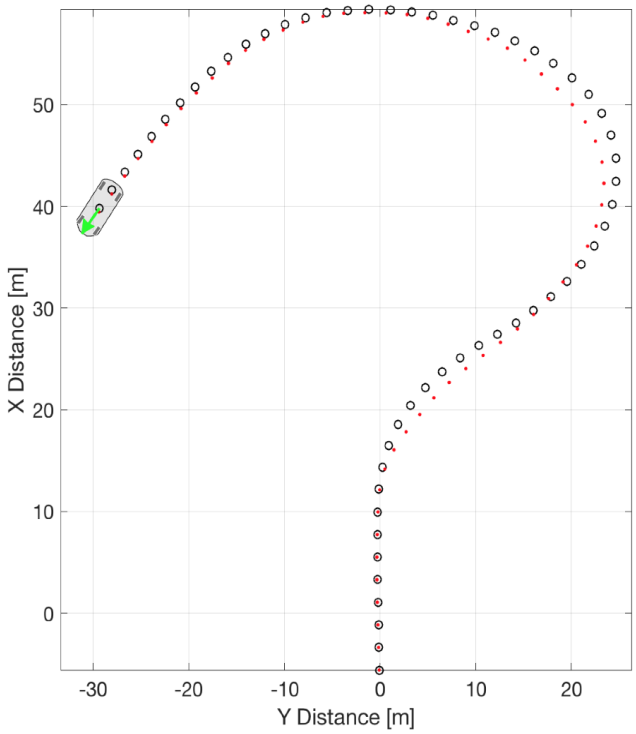

Figure 7. 8 Autonomous vehicle path tracking2 at 30km/h.

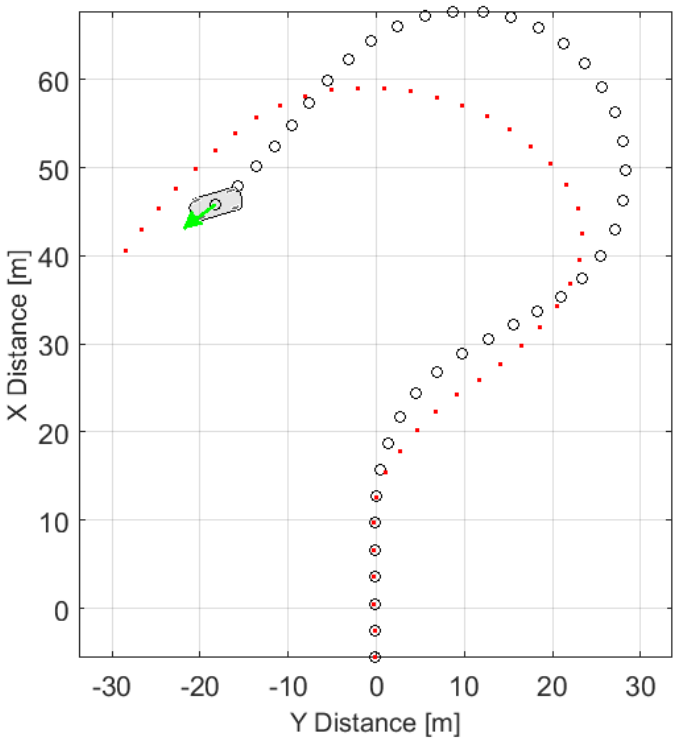

Figure 7. 9 Autonomous vehicle path tracking2 at 55km/h.

At 30 km/h, there is a little deviation between the reference path and the autonomous vehicle path (Figure 7.8). However, at 55 km/h (Figure 7.9), the error is easily visible and. the autonomous car obviously diverges when turning left.

- **Scenario 3:** In the third scenario, three separate results will be displayed at three different speeds, beginning with the best case at 10 km/h and ending with the worst situation at 55 km/h.

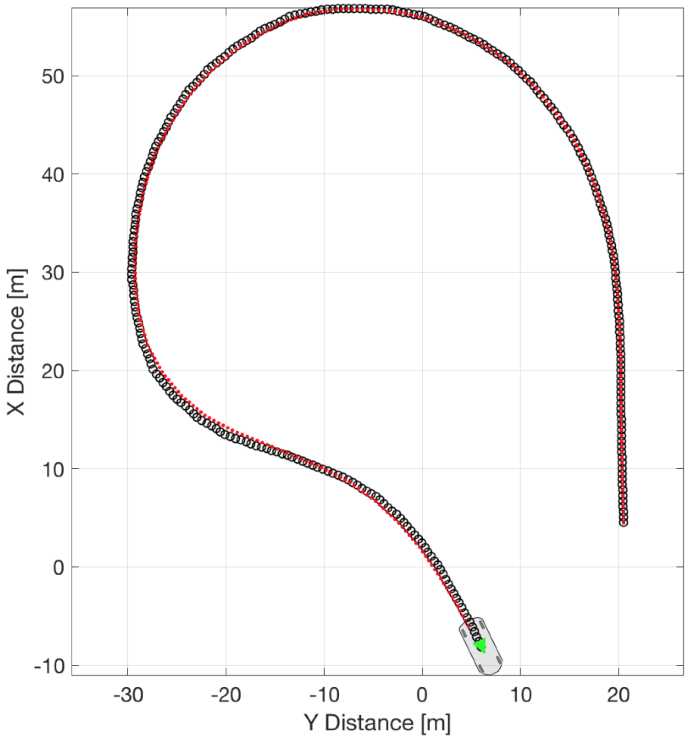

Figure 7. 10 Autonomous vehicle path tracking3 at 10km/h.

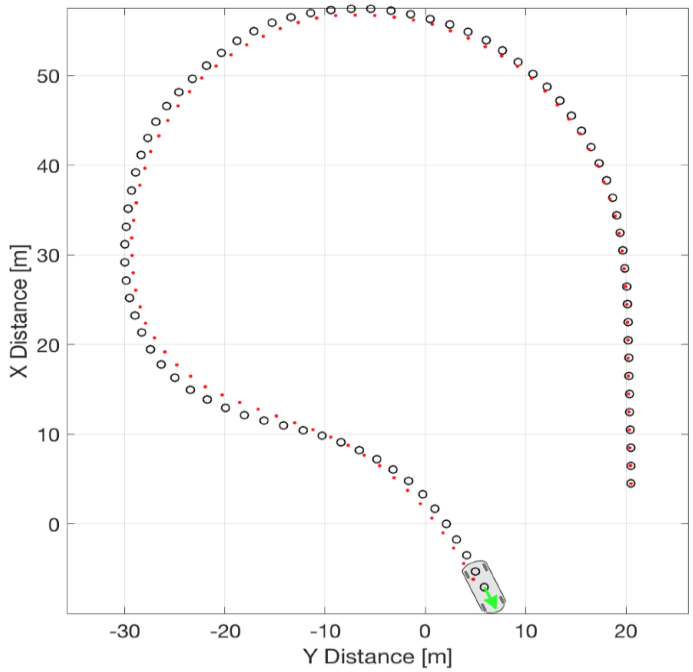

Figure 7. 11 Autonomous vehicle path tracking3 at 36km/h.

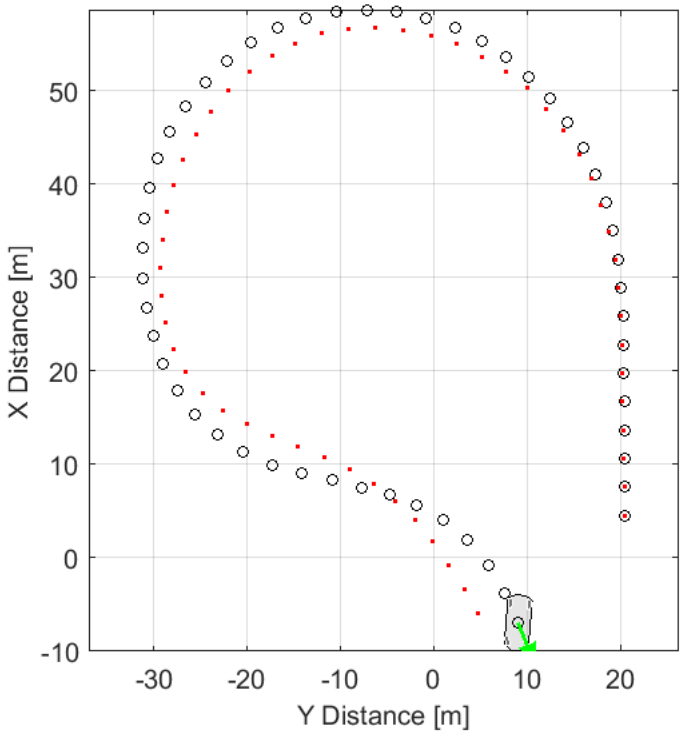

Figure 7. 12 Autonomous vehicle path tracking3 at 55km/h.

At 36 km/h, there is a small deviation between the reference path and the autonomous vehicle path (Figure 7.11). However, at 55 km/h (Figure 7.12), the error is clearly visible and. the autonomous car diverges at that speed.

- **Scenario 4:** In the fourth scenario, four separate figures will be displayed at four different speeds, beginning with the best case at 10 km/h (Figure 7.13) or under this longitudinal velocity which is practically the same as (Figure 7.13) and concluding with the worst case at 45 km/h (Figure 7.16).

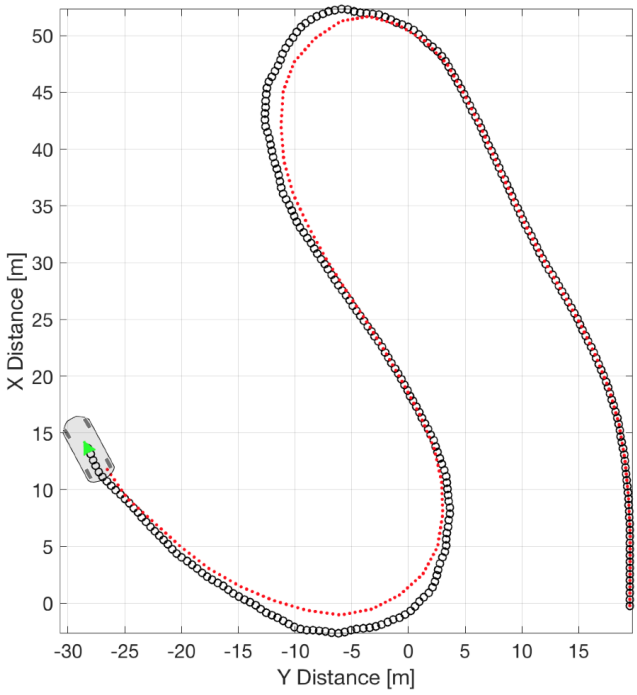

Figure 7. 13 Autonomous vehicle path tracking4 at 10km/h.

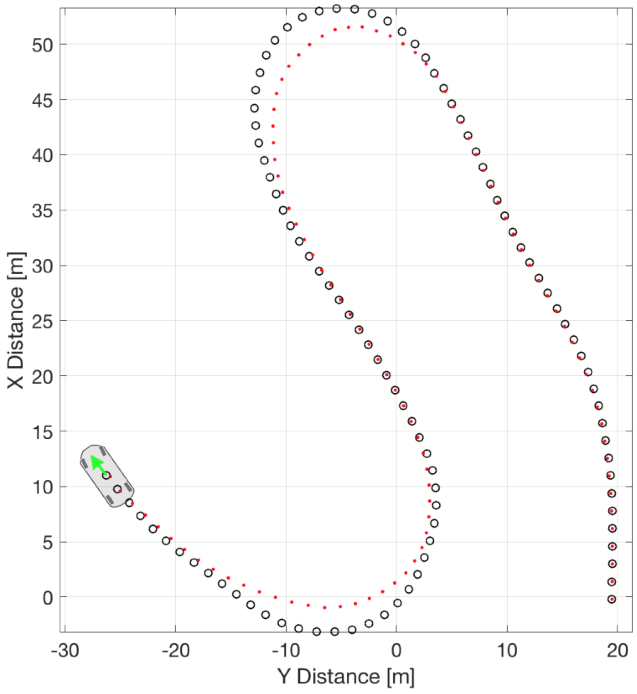

Figure 7. 14 Autonomous vehicle path tracking4 at 28km/h.

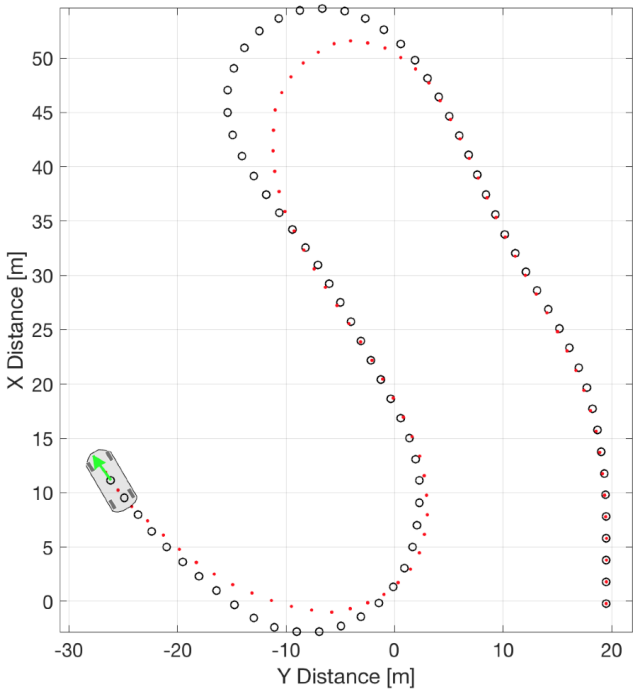

Figure 7. 15 Autonomous vehicle path tracking4 at 36km/h.

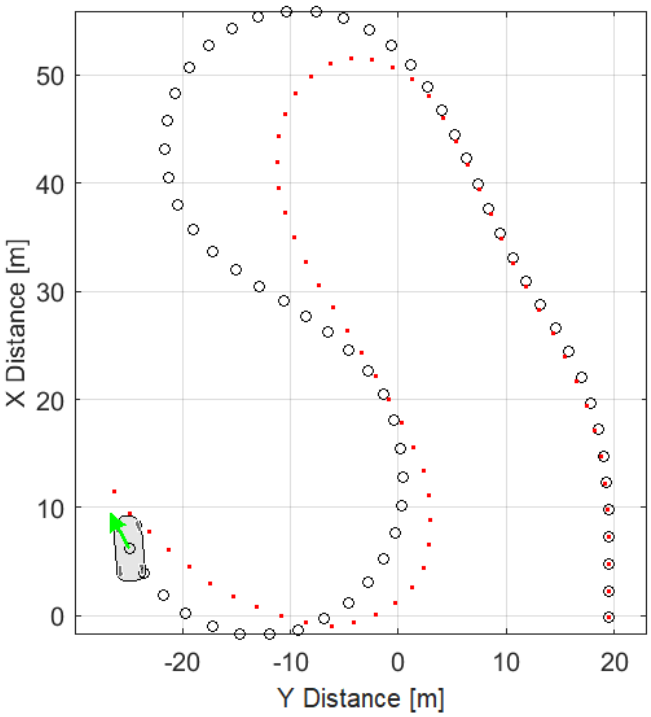

Figure 7. 16 Autonomous vehicle path tracking4 at 45km/h.

The road in this scenario is far more difficult than the roads in scenarios 1, 2 and 3.This road is in the shape of an S, with abrupt turns. Figure 7.14 indicates that the inaccuracy between the reference path and the autonomous vehicle path rose at 28 km/h, increased further at 36 km/h (Figure 7.15), and completely diverged from the planned path at 45 km/h (Figure 7.16).

- **Scenario 5:** In first scenario, we display four distinct figures at four different speeds, beginning with the best case at 10 km/h and ending with the worst situation at 100 km/h.

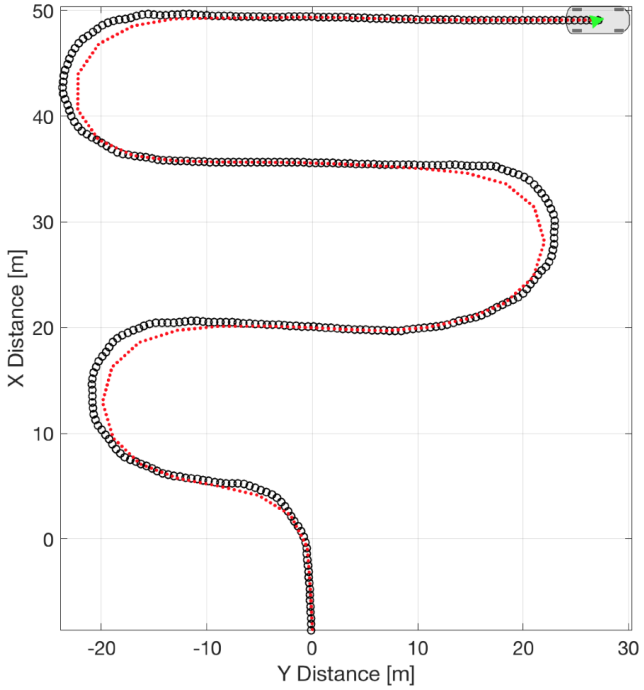

Figure 7. 17 Autonomous vehicle path tracking5 at 10km/h.

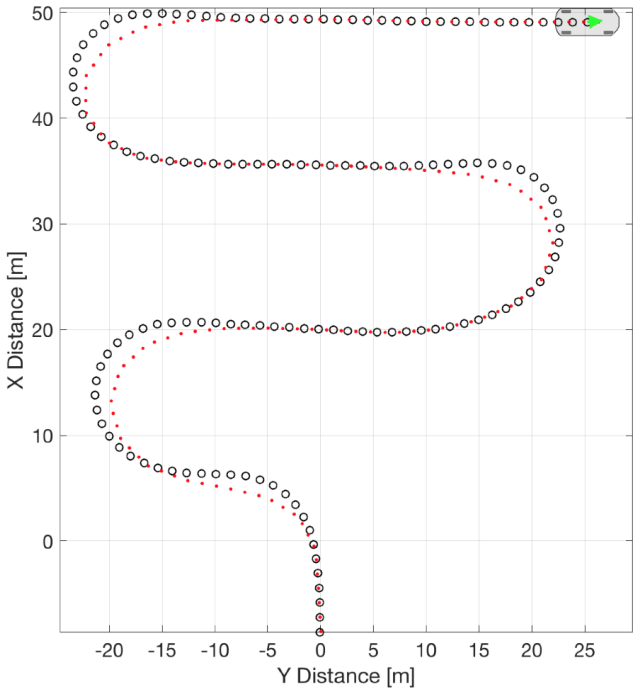

Figure 7. 18 Autonomous vehicle path tracking4 at 25km/h.

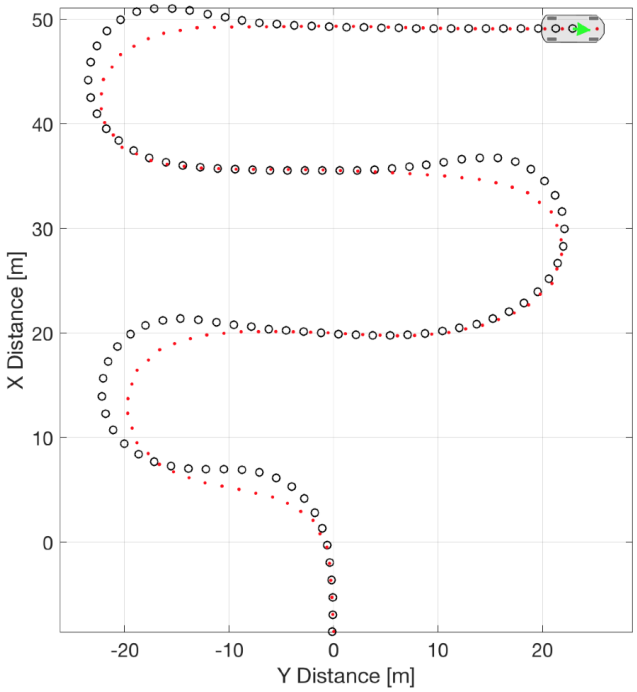

Figure 7. 19 Autonomous vehicle path tracking4 at 30km/h.

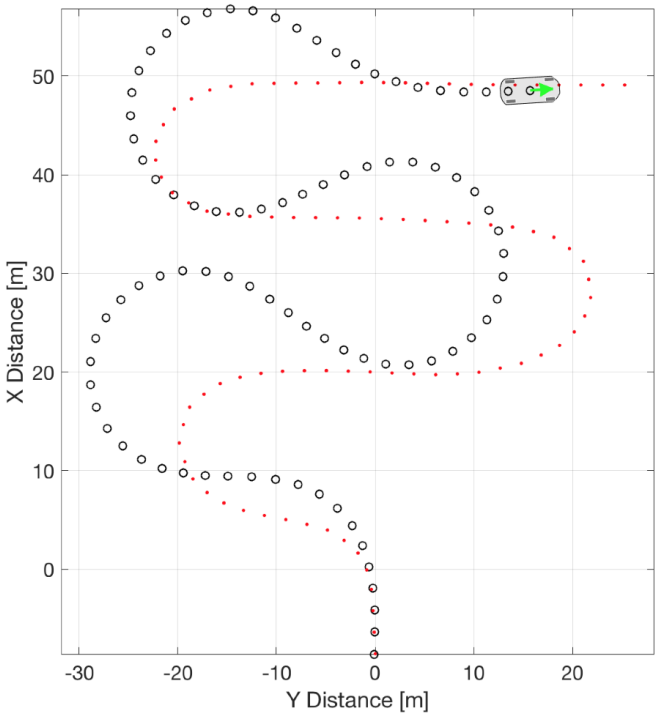

Figure 7. 20 Autonomous vehicle path tracking4 at 40km/h.

Figure 7. 17, Figure 7.18 and Figure 7.19 clearly show that the suggested controller is capable of ensuring effective performance tracking for the investigated autonomous vehicle on a tough challenging road with more than three sharp curves. However, at a constant speed of 40 km/h the controller lost control at the corners when turning left and right .The tracking errors are quite remarkable and visible (Figure 7.20).

7.6 Conclusion

In this chapter, we discussed the simulation design. We mentioned that the system design is composed by three main subsystems which are: The path planner, the controller and the vehicle. We explained the goals and the roles of the simulation subsystems and the relation between all the blocks in terms of inputs, outputs signals and parameters.

In this chapter, we confirm all of the previous chapters' theory and mathematics, and we illustrate our controller's strongest and weakest points through simulation on various road shapes and velocities.

Chapter 8

Conclusions and Future Researches

This chapter, outlines the thesis's key contributions. We present the concluding remarks and we propose the future work.

8.1 Concluding remarks

The autonomous car is critical because it is one of the first much-needed human services, particularly in terms of decreasing deadly accidents. Controlling autonomous cars remains a significant scientific problem since we did not reach the full autonomous vehicle control.

The main contribution in this PhD thesis is the design of a new fuzzy automatic lateral controller called also steering controller to ensure lane keeping under various constraints (torque control) as follow:

1) Unknown curvature.

2) Uncertain lateral wind force.

3) Actuator saturation.

And, this is done by improving the PDC control law. This new formulation of the PDC control law was developed first in chapter4and 5 and then applied to the autonomous vehicle kinematic model presented in chapter6.

Finally, in chapter7, we show the robustness of our fuzzy lateral controller by simulations.

8.2 Future Research Directions

Several avenues for further research might be addressed based on the findings and conclusions in this thesis. These are summarised below:

1) Increase the number of limitations to get closer to realistic scenarios.

2) Enhancing the new controller to follow the centerline in case of high speed.
3) Hardware implementation of our lateral controller.
4) In actuality, other causes of disturbance impacting vehicle dynamics, such as road crown (sloping to one side) or superelevation (banking in turns), may be encountered.
5) Further research maybe useful to use carsim for simulation.

References

[1] J. Navarro, F. Mars, and M. Young, “Lateral control assistance in car driving: Classification, review and future prospects” IET Intelligent Transport Systems., vol. 5, no. 3, pp. 207–220, Jun. 2011.

[2] N. Enache et al., “Driver steering assistance for lane departure avoidance,” Control Engineering Practice., vol. 17, no. 6, pp. 642–651, Jun. 2009.

[3] S.E. Shladover, “PATH at 20-History and major milestones,” IEEE Transactions on Intelligent Transportation Systems,” 8(4), 584–592, 2007.

[4] R. Rajamani, “Vehicle Dynamics and Control. Boston, Springer, 2012.

[5] R. Bishop, “Intelligent vehicle applications worldwide,” IEEE Intelligent Systems and Applications, 15(1), 78–81, 2000.

[6] A. Nguyen, C. Sentouh and J-C.Popieul, “Takagi-Sugeno Model-based Steering Control for Autonomous Vehicles with Actuator Saturation,” IFAC-PapersOnLine, vol. 49, no. 5, pp. 206-211, 2016.

[7] A. Nguyen, C. Sentouh and J-C.Popieul, “Fuzzy steering control for autonomous vehicles under actuator saturation: Design and experiments,” Journal of the Franklin Institute, vol. 355, no. 18, pp. 9374-9395, 2018.

[8] C. Sentouh et al., “Driver-Automation Cooperation Oriented Approach for Shared Control of Lane Keeping Assist Systems,” IEEE Transactions on Control Systems Technology, vol. 27, no. 5, pp. 1962-1978, Sept. 2019.

[9] A. Nguyen, C. Sentouh and J. Popieul, “Driver-Automation Cooperative Approach for Shared Steering Control under Multiple System Constraints: Design and Experiments,” IEEE Transactions on Industrial Electronics, 64(5), 3819-3830, 2017.

[10] A. G. C. Junior, J. A. Riul and P. H. M. Montenegro, “Application of the Subspace Identification Method using the N4SID Technique for a Robotic Manipulator,” Latin America Transactions, IEEE (Revista IEEE America Latina), 14(4), pp.1588–1593, 2016.

[11] M. Manzoor et al., “RFCNN: Traffic Accident Severity Prediction Based on Decision Level Fusion of Machine and Deep Learning Model,” IEEE Access, vol. 9, pp. 128359-128371, 2021, doi: 10.1109/ACCESS.2021.3112546.

[12] D. Paret, H. Rebaine and B. A. Engel, “Aspects Relating to Autonomous and Connected Vehicles,” Autonomous and Connected Vehicles: Network Architectures from Legacy Networks to Automotive Ethernet, Wiley, pp.23-80, 2022, doi: 10.1002/9781119816140.ch2.

[13] W. Xiang, X. Shen and K. Zheng, “5G Mobile Communications,” 1st ed. Switzerland: Springer International. 2017.

[14] M. Stanley, “Autonomous Cars: Self-Driving the New Auto Industry Paradigm,” 2013.

[15] D. Srivastava, P. Sahu and G. Geetha, “Autonomous Vehicle for Physically Impaired People,” International Conference on Innovative Computing, Intelligent Communication and Smart Electrical Systems (ICSES), pp. 1-7, 2022, doi: 10.1109/ICSES55317.2022.9914262.

[16] L. M. Cysneiros, M. Raffi and J. C. Sampaio do Prado Leite, “Software Transparency as a Key Requirement for Self-Driving Cars,” IEEE 26th International Requirements Engineering Conference (RE), pp. 382-387, 2018, doi: 10.1109/RE.2018.00-21.

[17] A. Taeihagh and H. Si Min Lim, “Governing autonomous vehicles: emerging responses for safety, liability, privacy, cybersecurity, and industry risks,” Transport Reviews, 39:1, 103-128, 2019, doi: 10.1080/01441647.2018.1494640.

[18] J. Wang, et al., “Towards the Unified Principles for Level 5 Autonomous Vehicles,” Engineering, Volume 7, Issue 9, Pages 1313-1325, ISSN 2095-8099, 2021.

[19] J. Kester, B. K. Sovacool and V. Heida, “Flying Cars to Tesla: Examining the Personal Automobile Preferences of Primary Schoolchildren,” Denmark and the Netherlands, Energy Research & Social Science, Volume 56, 101204, ISSN 2214-6296, 2019.

[20] J.F. Bonnefon, A. Shariff and I. Rahwan, “The social dilemma of Autonomous vehicles,” Science, 1573-1576, 2016.

[21] Q. F. Tan, “Research on path control strategy of four-wheel-steering and four-wheel-drive vehicle,” Ph.D. dissertation, Beijing Jiaotong Univ., Beijing, China, 2019.

[22] C. Y. Sun, H. Dong, and X. Zhang, “Path tracking controller design for autonomous vehicle based on robust tube MPC,” International Journal of Vehicle Design., vol. 82, nos. 1–4, pp. 120–139, 2020.

[23] Y. Tian, Q. Yao, P. Hang and S. Wang, “A Gain-Scheduled Robust Controller for Autonomous Vehicles Path Tracking Based on LPV System With MPC and H∞,” IEEE Transactions on Vehicular Technology, vol. 71, no. 9, pp. 9350-9362, Sept. 2022, doi: 10.1109/TVT.2022.3176384.

[24] Y. Liang et al., “A Novel Combined Decision and Control Scheme for Autonomous Vehicle in Structured Road Based on Adaptive Model Predictive Control,” IEEE Transactions on Intelligent Transportation Systems, vol. 23, no. 9, pp. 16083-16097, Sept. 2022, doi: 10.1109/TITS.2022.3147972.

[25] H. Atoui et al., “LPV-Based Autonomous Vehicle Lateral Controllers: A Comparative Analysis,” IEEE Transactions on Intelligent Transportation Systems, vol. 23, no. 8, pp. 13570-13581, Aug. 2022, doi: 10.1109/TITS.2021.3125771.

[26] Z. Qin et al., “A Lateral and Longitudinal Dynamics Control Framework of Autonomous Vehicles Based on Multi-Parameter Joint Estimation,” IEEE Transactions on Vehicular Technology, vol. 71, no. 6, pp. 5837-5852, June 2022, doi: 10.1109/TVT.2022.3163507.

[27] T. K. C. and T. Lee, “Constrained Imitation Learning for a Flapping Wing Unmanned Aerial Vehicle,” IEEE Robotics and Automation Letters, vol. 7, no. 4, pp. 10534-10541, Oct. 2022, doi: 10.1109/LRA.2022.3194682.

[28] B. W. Abegaz, “A Parallelized Self-Driving Vehicle Controller Using Unsupervised Machine Learning,” IEEE Transactions on Industry Applications, vol. 58, no. 4, pp. 5148-5156, July-Aug. 2022, doi: 10.1109/TIA.2022.3164861.

[29] F. Tian, F. -Y. Wang and L. Li, “Enhancing Feedback Steering Controllers for Autonomous Vehicles With Deep Monte Carlo Tree Search,” IEEE Robotics and Automation Letters, vol. 7, no. 4, pp. 10438-10445, Oct. 2022, doi: 10.1109/LRA.2022.3193452.

[30] D. Silver et al., “Mastering the game of go without human knowledge,” Nature, vol. 550, no. 7676, pp. 354–359, 2017.

[31] W. Wang et al., “A Path Following Lateral Control Scheme for Four-Wheel Independent Drive Autonomous Vehicle Using Sliding Mode Prediction Control,” IEEE Transactions on Transportation Electrification, vol. 8, no. 3, pp. 3192-3207, Sept. 2022, doi: 10.1109/TTE.2022.3170059.

[32] S. Victor et al., “Optimal Trajectory Planning and Robust Tracking Using Vehicle Model Inversion,” IEEE Transactions on Intelligent Transportation Systems, vol. 23, no. 5, pp. 4556-4569, May 2022, doi: 10.1109/TITS.2020.3045917.

[33] Y. Sun et al., “Robust Path Planner for Autonomous Vehicles on Roads With Large Curvature,” IEEE Robotics and Automation Letters, vol. 7, no. 2, pp. 2503-2510, April 2022, doi: 10.1109/LRA.2022.3143294.

[34] J. K. Hedrick, M. Tomizuka and P. Varaiya, “Control issues in automated highway systems,” IEEE Control Systems Magazine, vol. 14, no. 6, pp. 21-32, Dec. 1994, doi: 10.1109/37.334412.

[35] J. M. Snider, “Automatic steering methods for autonomous automobile path tracking,” Robotics Institute., Carnegie Mellon University., Pittsburgh, PA, USA, Tech. Rep. CMU-RI-TR-09-08, Feb. 2009.

[36] L. Li et al., “Cognitive Cars: A New Frontier for ADAS Research,” IEEE Transactions on Intelligent Transportation Systems, vol. 13, no. 1, pp. 395-407, March 2012.

[37] S. Tong, X. Min and Y. Li, “Observer-Based Adaptive Fuzzy Tracking Control for Strict-Feedback Nonlinear Systems With Unknown Control Gain Functions,” IEEE Transactions on Cybernetics, vol. 50, no. 9, pp. 3903-3913, Sept. 2020.

[38] G. Tagne, R. Talj and A. Charara, “Higher-order sliding mode control for lateral dynamics of autonomous vehicles, with experimental validation,” IEEE Intelligent Vehicles Symposium (IV), Gold Coast, QLD, pp. 678-683. 2013.

[39] C. Hatipoglu, U. Ozguner and K. A. Redmill, “Automated lane change controller design,” IEEE Transactions on Intelligent Transportation Systems, vol. 4, no. 1, pp. 13-22, March 2003.

[40] J. Jiang and A. Astolfi, “Lateral Control of an Autonomous Vehicle,” IEEE Transactions on Intelligent Vehicles, vol. 3, no. 2, pp. 228-237, June 2018.

[41] Y. Xia et al., “Lateral Path Tracking Control of Autonomous Land Vehicle Based on ADRC and Differential Flatness,” IEEE Transactions on Industrial Electronics, vol. 63, no. 5, pp. 3091-3099, May 2016, doi: 10.1109/TIE.2016.2531021.

[42] W. Sun, X. Wang and C. Zhang, “A Model-Free Control Strategy for Vehicle Lateral Stability With Adaptive Dynamic Programming,” IEEE Transactions on Industrial Electronics, vol. 67, no. 12, pp. 10693-10701, Dec. 2020, doi: 10.1109/TIE.2019.2958308.

[43] D. Li, D. Zhao, Q. Zhang and Y. Chen, “Reinforcement Learning and Deep Learning Based Lateral Control for Autonomous Driving [Application Notes],” IEEE Computational Intelligence Magazine, vol. 14, no. 2, pp. 83-98, May 2019, doi: 10.1109/MCI.2019.2901089.

[44] H. Zhang and J. Wang, “Vehicle Lateral Dynamics Control Through AFS/DYC and Robust Gain-Scheduling Approach,” IEEE Transactions on Vehicular Technology, vol. 65, no. 1, pp. 489-494, Jan. 2016, doi: 10.1109/TVT.2015.2391184.

[45] M.A. Jemmali et al., “Robust stabilization for discrete-time Takagi-Sugeno fuzzy system based on N4SID models,” Engineering Computations, Vol. 36 No. 4, pp. 1400-1427, 2019, https://doi.org/10.1108/EC-06-2018-0285.

[46] L. Wei et al., “T-S Fuzzy Model Predictive Control for Vehicle Yaw Stability in Nonlinear Region,” IEEE Transactions on Vehicular Technology, vol. 70, no. 8, pp. 7536-7546, Aug. 2021, doi: 10.1109/TVT.2021.3091809.

[47] J.Wang et al., “Coordination control of differential drive assist steering and vehicle stability control for fourwheel- independent-drive EV,” IEEE Transactions on Vehicular Technology., vol. 67, no. 12, pp. 11 453–11 467, Dec. 2018.

[48] X. Ji et al., “A vehicle stability control strategy with adaptive neural network sliding mode theory based on system uncertainty approximation,” Vehicle System Dynamics., vol. 56, no. 6, pp. 923–946, 2018.

[49] S. Cheng et al., “Robust LMI-Based H-Infinite Controller Integrating AFS and DYC of Autonomous Vehicles With Parametric Uncertainties,” IEEE Transactions on Systems, Man, and Cybernetics: Systems, vol. 51, no. 11, pp. 6901-6910, Nov. 2021.

[50] A. -T. Nguyen et al., “Robust Set-Invariance Based Fuzzy Output Tracking Control for Vehicle Autonomous Driving Under Uncertain Lateral Forces and Steering Constraints,” IEEE Transactions on Intelligent Transportation Systems, vol. 22, no. 9, pp. 5849-5860, Sept. 2021, doi: 10.1109/TITS.2020.3021292.

[51] S. Xu and H. Peng, “Design, analysis, and experiments of preview path tracking control for autonomous vehicles,” IEEE Transactions on Intelligent Transportation Systems., vol. 21, no. 1, pp. 48–58, Jan. 2020.

[52] P. Zhao et al., “Design of a control system for an autonomous vehicle based on adaptive-PID,” International Journal of Advanced Robotic Systems., vol. 9, no. 2, p. 44, Jan. 2012.

[53] J. E. Naranjo et al., “Power-steering control architecture for automatic driving,” IEEE Transactions on Intelligent Transportation Systems., vol. 6, no. 4, pp. 406–415, Dec. 2005.

[54] H. Taghavifar and S. Rakheja, “Path-tracking of autonomous vehicles using a novel adaptive robust exponential-like-sliding-mode fuzzy type-2 neural network controller,” Mechanical Systems and Signal Processing. vol. 130, pp. 41–55, Sep. 2019.

[55] N. H. Amer et al., “Modelling and control strategies in path tracking control for autonomous ground vehicles: A review of state of the art and challenges,” Journal of Intelligent and Robotic Systems., vol. 86, no. 2, pp. 225–254, May 2017.

[56] E. Alcala et al.,“Autonomous vehicle control using a kinematic Lyapunov-based technique with LQR-LMI tuning,” Control Engineering Practice., vol. 73, pp. 1–12, Apr. 2018.

[57] B. Paden et al., “A survey of motion planning and control techniques for self-driving urban vehicles,” IEEE Transactions on Intelligent Vehicles, vol. 1, no. 1, pp. 33–55, Mar. 2016.

[58] K. Lee, S. E. Li, and D. Kum, “Synthesis of robust lane keeping systems: Impact of controller and design parameters on system performance,” IEEE Transactions on Intelligent Transportation Systems., vol. 20, no. 8, pp. 3129–3141, Aug. 2019.

[59] S. Dixit et al., “Trajectory planning for autonomous high-speed overtaking in structured environments using robust MPC,” IEEE Transactions on Intelligent Transportation Systems., vol. 21, no. 6, pp. 2310–2323, Jun. 2020.

[60] J. Suh, H. Chae, and K. Yi, “Stochastic model-predictive control for lane change decision of automated driving vehicles,” IEEE Transactions on Vehicular Technology., vol. 67, no. 6, pp. 4771–4782, Jun. 2018.

[61] H. Wang et al., “Crash mitigation in motion planning for autonomous vehicles,” IEEE Transactions on Intelligent Transportation Systems., vol. 20, no. 9, pp. 3313–3323, Sep. 2019.

[62] L. Yang, M. Yue, and T. Ma, “Path following predictive control for autonomous vehicles subject to uncertain tire-ground adhesion and varied road curvature,” International Journal of Control, Automation and Systems., vol. 17, no. 1, pp. 193–202, Jan. 2019.

[63] J. Funke et al., “Collision avoidance and stabilization for autonomous vehicles in emergency scenarios,” IEEE Transactions on Control Systems Technology., vol. 25, no. 4, pp. 1204–1216, Jul. 2017.

[64] H. Guo et al., “Simultaneous trajectory planning and tracking using an MPC method for cyber physical systems: A case study of obstacle avoidance for an intelligent vehicle,” IEEE Transactions on Industrial Informatics., vol. 14, no. 9, pp. 4273–4283, Sep. 2018.

[65] C. Zhang et al., “A novel fuzzy observer-based steering control approach for path tracking in autonomous vehicles,” IEEE Transactions on Fuzzy Systems., vol. 27, no. 2, pp. 278–290, Feb. 2019.

[66] H. Dahmani, O. Pagès, and A. El Hajjaji, “Observer-based state feedback control for vehicle chassis stability in critical situations,” IEEE Transactions on Control Systems Technology., vol. 24, no. 2, pp. 636–643, Mar. 2016.

[67] A.-T. Nguyen et al., “Fuzzy static output feedback control for path following of autonomous vehicles with transient performance improvements,” IEEE Transactions on Intelligent Transportation Systems., vol. 21, no. 7, pp. 3069–3079, Jul. 2020.

[68] B. L. Boada, M. J. L. Boada, and V. Díaz, “Fuzzy-logic applied to yaw moment control for vehicle stability,” Vehicle System Dynamics., vol. 43, no. 10, pp. 753–770, Oct. 2005.

[69] S.-J. Wu et al., “The heterogeneous systems integration design and implementation for lane keeping on a vehicle,” IEEE Transactions on Intelligent Transportation Systems., vol. 9, no. 2, pp. 246–263, Jun. 2008.

[70] A.-T. Nguyen et al., “Fuzzy control systems: Past, present and future,” IEEE Computational Intelligent Magazine., vol. 14, no. 1, pp. 56-68, Feb. 2019.

[71] A.-T. Nguyen et al., “Constrained output-feedback control for discrete-time fuzzy systems with local nonlinear models subject to state and input constraints,” IEEE Transactions on Cybernetics, early access, Aug. 4, 2020, doi: 10.1109/TCYB.2020.3009128.

[72] B. Zhang et al., “A novel observer design for simultaneous estimation of vehicle steering angle and sideslip angle,” IEEE Transactions on Industrial Electronics., vol. 63, no. 7, pp. 4357–4366, Jul. 2016.

[73] C. Hu et al., “MME-EKF-Based path-tracking control of autonomous vehicles considering input saturation,” IEEE Transactions on Vehicular Technology., vol. 68, no. 6, pp. 5246–5259, Jun. 2019.

[74] A.-T. Nguyen, C. Sentouh, and J.-C. Popieul, “Sensor reduction for driver-automation shared steering control via an adaptive authority allocation strategy,” IEEE/ASME Transactions on Mechatronics, vol. 23, no. 1, pp. 5–16, Feb. 2018.

[75] C.-S. Ting, “An output-feedback fuzzy approach to guaranteed cost control of vehicle lateral motion,” Mechatronics, vol. 19, no. 3, pp. 304–312, Apr. 2009.

[76] K. Nam, S. Oh, H. Fujimoto, and Y. Hori, “Estimation of sideslip and roll angles of electric vehicles using lateral tire force sensors through RLS and Kalman filter approaches,” IEEE Transactions on Industrial Electronics., vol. 60, no. 3, pp. 988–1000, Mar. 2013.

[77] A.-T. Nguyen et al., “Unknown input observers for simultaneous estimation of vehicle dynamics and driver torque: Theoretical design and hardware experiments,” IEEE/ASME Transactions on Mechatronics, vol. 24, no. 6, pp. 2508–2518, Dec. 2019.

[78] L. Li, F. Y. Wang, and Q. Zhou, “Integrated longitudinal and lateral Tire/Road friction modeling and monitoring for vehicle motion control,” IEEE Transactions on Intelligent Transportation Systems., vol. 7, no. 1, pp. 1–19, Mar. 2006.

[79] H. Du, N. Zhang, and G. Dong, “Stabilizing vehicle lateral dynamics with considerations of parameter uncertainties and control saturation through robust yaw control,” IEEE Transactions on Vehicular Technology., vol. 59, no. 5, pp. 2593–2597, Jun. 2010.

[80] H. Yang, V. Cocquempot, and B. Jiang, “Optimal fault-tolerant path tracking control for 4WS4WD electric vehicles,” IEEE Transactions on Intelligent Transportation Systems., vol. 11, no. 1, pp. 237–243, Mar. 2010.

[81] A. -T. Nguyen et al., “Takagi–Sugeno Fuzzy Unknown Input Observers to Estimate Nonlinear Dynamics of Autonomous Ground Vehicles: Theory and Real-Time Verification,” IEEE/ASME Transactions on Mechatronics, vol. 26, no. 3, pp. 1328-1338, June 2021.

[82] Q. Shi and H. Zhang, “Fault diagnosis of an autonomous vehicle with an improved SVM algorithm subject to unbalanced datasets,” IEEE Transactions on Industrial Electronics, early access, May 20, 2020, doi: 10.1109/TIE.2020.2994868.

[83] H. Zhang et al., “Robust energy-to-peak sideslip angle estimation with applications to ground vehicles,” Mechatronics, vol. 30, pp. 338–347, Sep. 2015.

[84] A.-T. Nguyen, C. Sentouh, and J.-C. Popieul, “Sensor reduction for driver automation shared steering control via an adaptive authority allocation strategy,” IEEE/ASME Transactions on Mechatronics, vol. 23, no. 1, pp. 5–16, Feb. 2018.

[85] X.Wang, L. Guo, and Y. Jia, “Online sensing of human steering intervention torque for autonomous driving actuation systems,” IEEE Sensors Journal., vol. 18, no. 8, pp. 3444–3453, Apr. 2018.

[86] E. Hashemi et al., “Opinion dynamics-based vehicle velocity estimation and diagnosis,” IEEE Transactions on Intelligent Transportation Systems., vol. 19, no. 7, pp. 2142–2148, Jul. 2018.

[87] D. Piyabongkarn et al., “Development and experimental evaluation of a slip angle estimator for vehicle stability control,” IEEE Transactions on Control Systems Technology., vol. 17, no. 1, pp. 78–88, Jan. 2009.

[88] W. Chen, D. Tan, and L. Zhao, “Vehicle sideslip angle and road friction estimation using online gradient descent algorithm,” IEEE Transactions on Vehicular Technology., vol. 67, no. 12, pp. 11475–11485, Dec. 2018.

[89] D. Selmanaj et al., “Vehicle sideslip estimation: A kinematic based approach,” Control Engineering Practice., vol. 67, pp. 1–12, Oct. 2017.

[90] M. Doumiati et al., “Onboard real-time estimation of vehicle lateral tire-road forces and sideslip angle,” IEEE/ASME Transactions on Mechatronics, vol. 16, no. 4, pp. 601–614, Aug. 2011.

[91] M. Viehweger et al., “Vehicle state and tyre force estimation: Demonstrations and guidelines,” Vehicle System Dynamics., pp. 1–28, 2020.

[92] H. Du et al., “Sideslip angle estimation and stability control for a vehicle with a non-linear tyre model and a varying speed,” Proceedings of Institution of Mechanical Engineers, Part D, vol. 229, no. 4, pp. 486–505, Feb. 2015.

[93] A.-T. Nguyen et al., “Unknown input observers for simultaneous estimation of vehicle dynamics and driver torque: Theoretical design and hardware experiments,” IEEE/ASME Transactions on Mechatronics, vol. 24, no. 6, pp. 2508–2518, Dec. 2019.

[94] B. Boada, M. Boada, and V. Diaz, “Vehicle sideslip angle measurement based on sensor data fusion using an integrated ANFIS and an unscented Kalman filter algorithm,” Mechanical Systems and Signal Processing., vol. 72, pp. 832–845, May 2016.

[95] S. Cheng, L. Li, and J. Chen, “Fusion algorithm design based on adaptive SCKF and integral correction for side-slip angle observation,” IEEE Transactions on Industrial Electronics., vol. 65, no. 7, pp. 5754–5763, Jul. 2018.

[96] A. Benloucif et al., “Cooperative trajectory planning for haptic shared control between driver and automation in highway driving,” IEEE Transactions on Industrial Electronics., vol. 66, no. 12, pp. 9846–9857, Dec. 2019.

[97] J. Si et al., “High-precision estimation of steering angle of agricultural tractors using GPS and low-accuracy MEMS,” IEEE Transactions on Vehicular Technology., vol. 68, no. 12, pp. 11738–11745, Dec. 2019.

[98] J.Yang, E. Hou, and M. Zhou, “Front sensor and GPS-based lateral control of automated vehicles,” IEEE Transactions on Intelligent Transportation Systems., vol. 14, no. 1, pp. 146–154, Mar. 2013.

[99] S. Moon, I. Moon, and K. Yi, “Design, tuning, and evaluation of a full range adaptive cruise control system with collision avoidance,” Control Engineering Practice., vol. 17, no. 4, pp. 442–455, Apr. 2009.

[100] J. Franco, M. Franchek, and K. Grigoriadis, “Real-time brake torque estimation for internal combustion engines,” Mechanical Systems Signal Processing., vol. 22, no. 2, pp. 338–361, 2008.

[101] K. Hedrick et al., “Longitudinal vehicle controller design for IVHS systems,” American Control Conference., Boston, pp. 3107–3112, Jun. 1991.

[102] Q. Ahmed and A. Bhatti, “Estimating SI engine efficiencies and parameters in second-order slidingmodes,” IEEE Transactions on Industrial Electronics., vol. 58, no. 10, pp. 4837–4846, Oct. 2011.

[103] S. Helm, M. Kozek, and S. Jakubek, “Combustion torque estimation and misfire detection for calibration of combustion engines by parametric Kalman filtering,” IEEE Transaction on Industrial Electronics., vol. 59, no. 11, pp. 4326–4337, Nov. 2012.

[104] M. Hong et al., “Torque observers design for SI engines with different intake air measurement sensors,” IEEE Transactions on Control Systems Technology., vol. 19, no. 1, pp. 229–237, Jan. 2011.

[105] J. Na et al., “Vehicle engine torque estimation via UI observer and adaptive parameter estimation,” IEEE Transactions on Vehicular Technology., vol. 67, no. 1, pp. 409–422, Jan. 2018.

[106] K. Tanaka and H. Wang, “Fuzzy Control Systems Design and Analysis: A Linear Matrix Inequality Approach,” New York, NY, USA: Wiley- Interscience, 2004.

[107] Q. Jia et al., “Fault reconstruction and fault tolerant control via learning observers in Takagi-Sugeno fuzzy descriptor systems with time delays,” IEEE Transactions on Industrial Electronics., vol. 62, no. 6, pp. 3885–3895, Jun. 2015.

[108] J. Pan et al., “A unified framework for asymptotic observer design of fuzzy systems with unmeasurable premise variables,” IEEE Transactions on Fuzzy Systems., early access, Jul. 16, 2020, doi: 10.1109/TFUZZ.2020.3009737.

[109] M. A. Jammali and H. T. Mouftah, “Takagi-Sugeno fuzzy control for Multi-input Multi-output systems based on subspace state space identification,” 20th International Conference on Sciences and Techniques of Automatic Control and Computer Engineering (STA), pp. 18-23, 2020, doi: 10.1109/STA50679.2020.9329299.

[110] M.A. Jemmali, H.T. Mouftah, “Discrete-Time Takagi-Sugeno Stabilization Approach Applied in Autonomous Vehicles,” Journal of Sensor and Actuator Networks, 11(1):12, 2022, https://doi.org/10.3390/jsan11010012.

[111] M. W. Choi, et al, “Robust lateral controller design for an unmanned vehicle using a system identification method,” IEEE International Symposium on Industrial Electronics, Cambridge, pp. 1177-1182, 2008, doi: 10.1109/ISIE.2008.4677228.

[112] H. Abdellatif, B. Heimann, “Accurate Modeling and Identification of Vehicle’s Nonlinear Lateral Dynamics,” IFAC Proceedings Volumes, Vol. 38, Issue 1, 2005.

[113] E. Mamdani and S. Assilian, “An experiment in linguistic synthesis with a fuzzy logic controller,” International Journal of Man- Machine Studies., vol. 7, no. 1, pp. 1–13, 1975.

[114] M. Sugeno, “On stability of fuzzy systems expressed by fuzzy rules with singleton consequents,” IEEE Transactions on Fuzzy Systems., vol. 7, no. 2, pp. 201–224, 1999.

[115] T. Takagi and M. Sugeno, “Fuzzy identification of systems and its applications to modeling and control,” IEEE Transactions on Systems, Man, and Cybernetics, Part B, (Cybernetics). Vol. SMC-15, no. 1, pp. 116–132, 1985.

[116] A.-T. Nguyen et al., “LMI-based stability analysis for piecewise multi-affine systems,” IEEE Transactions on Fuzzy Systems., vol. 25, no. 3, pp. 707–714, 2017.

[117] E. Kim, “A new computational approach to stability analysis and synthesis of linguistic fuzzy control system,” IEEE Transactions on Fuzzy Systems., vol. 12, no. 3, pp. 379–388, 2004.

[118] B. Kosko, “Fuzzy systems as universal approximators,” IEEE Transactions on Computers, vol. 43, no. 11, pp. 1329–1333, 1994

[119] A. Sala, T.-M. Guerra, and R. Babuška, “Perspectives of fuzzy systems and control,” Fuzzy Sets and Systems, vol. 156, no. 3, pp. 432–444, 2005.

[120] T.-M. Guerra, A. Sala, and K. Tanaka, “Fuzzy control turns 50: 10 years later,” Fuzzy Sets and Systems., vol. 281, pp. 168–182, 2015.

[121] M. Sugeno, “An introductory survey of fuzzy control,” Information Sciences., vol. 36, no. 1-2, pp. 59–83, 1985.

[122] K. Tanaka and M. Sugeno, “Stability analysis and design of fuzzy control systems,” Fuzzy Sets and Systems, vol. 45, no. 2, pp. 135–156, 1992.

[123] M. Sugeno and T. Taniguchi, “On improvement of stability conditions for continuous Mamdani-like fuzzy systems.” IEEE Transactions on Systems, Man and Cybernetics, Part B, (Cybernetics), vol. 34, no. 1, pp. 120–131, 2004.

[124] W. Pedrycz, “Fuzzy Control and Fuzzy Systems,” Research Studies Press Ltd., 1993.

[125] R. Babuška, “Fuzzy Modeling for Control,” Springer Science, 2012.

[126] J. M. Mendel, “Fuzzy logic systems for engineering: A tutorial,” Proceedings of the IEEE, vol. 83, no. 3, pp. 345–377, 1995.

[127] R.-E. Precup and H. Hellendoorn, “A survey on industrial applications of fuzzy control,” Computers in Industry, vol. 62, no. 3, pp. 213–226, 2011.

[128] G. Feng, “A survey on analysis and design of model-based fuzzy control systems,” IEEE Transactions on Fuzzy Systems., vol. 14, no. 5, pp. 676–697, 2006.

[129] K. Tanaka and M. Sugeno, “Stability analysis of fuzzy systems using Lyapunov’s direct method,” Proc. NAFIPS’90, vol. 1, Toronto, Canada, pp. 133–136, 1990.

[130] S. Boyd, E. Feron, L. El Ghaoui and V. Balakrishnan, "Linear matrix inequalities in system and control theory" SIAM studies in applied and numerical mathematics; vol. 15. Philadelphia, PA: Society for Industrial and Applied Mathematics, 1994.

[131] P. P. Bonissone et al., “Industrial applications of fuzzy logic at General Electric,” Proceedings in the IEEE, vol. 83, no. 3, pp. 450–465, 1995.

[132] H.-K. Lam, “A review on stability analysis of continuous-time fuzzy-model-based control systems: From membership-function-independent to membership-function-dependent analysis,” Engineering Applications of Artificial Intelligence., vol. 67, pp. 390–408, 2018.

[133] A. Van der Wal, “Application of fuzzy logic control in industry,” Fuzzy Sets and Systems, vol. 74, no. 1, pp. 33–41, 1995.

[134] L. Mozelli, R. Palhares, and G. Avellar, “A systematic approach to improve multiple Lyapunov function stability and stabilization conditions for fuzzy systems,” Information Sciences., vol. 179, no. 8, pp. 1149–1162, 2009.

[135] T.-M. Guerra et al., “Non-quadratic local stabilization for continuous-time Takagi-Sugeno models,” Fuzzy Sets and Systems, vol. 201, pp. 40–54, 2012.

[136] B.-J. Rhee and S. Won, “A new fuzzy Lyapunov function approach for a Takagi-Sugeno fuzzy control system design,” Fuzzy Sets and Systems., vol. 157, no. 9, pp. 1211–1228, 2006.

[137] K. Tanaka, T. Hori, and H. O. Wang, “A multiple Lyapunov function approach to stabilization of fuzzy control systems,” IEEE Transactions on Fuzzy Systems., vol. 11, no. 4, pp. 582–589, 2003.

[138] T. González, A. Sala, and M. Bernal, “A generalised integral polynomial Lyapunov function for nonlinear systems,” Fuzzy Sets and Systems, 2018.

[139] E. Tognetti, R. Oliveira, and P. Peres, “Selective H2 and H∞ stabilization of Takagi-Sugeno fuzzy systems,” IEEE Transactions on Fuzzy Systems., vol. 19, no. 5, pp. 890–900, 2011.

[140] D.-H. Lee, Y.-H. Joo, and M.-H. Tak, “Local stability analysis of continuous-time Takagi-Sugeno fuzzy systems: a fuzzy Lyapunov function approach,” Information Sciences., vol. 257, pp. 163–175, 2014.

[141] L. Mozelli et al., “Reducing conservativeness in recent stability conditions of T-S fuzzy systems,” Automatica, vol. 45, no. 6, pp. 1580–1583, 2009.

[142] V. Campos, A.-T. Nguyen, and R. Palhares, “A comparison of different upper-bound inequalities for the membership functions derivative,” IFACPapersOnLine, vol. 50, no. 1, pp. 3001–3006, 2017.

[143] M. Johansson, A. Rantzer, and K.-E. Årzén, “Piecewise quadratic stability of fuzzy systems,” IEEE Transactions on Fuzzy Systems., vol. 7, no. 6, pp. 713–722, 1999.

[144] G. Feng, “Stability analysis of discrete-time fuzzy dynamic systems based on piecewise Lyapunov functions,” IEEE Transactions on Fuzzy Systems., vol. 12, no. 1, pp. 22–28, 2004.

[145] A.-T. Nguyen, R. Márquez, and A. Dequidt, “An augmented system approach for LMI-based control design of constrained Takagi-Sugeno fuzzy systems,” Engineering Applications of Artificial Intelligence, vol. 61, pp. 96–102, 2017.

[146] T.-M. Guerra and L. Vermeiren, “LMI-based relaxed non-quadratic stabilization conditions for nonlinear systems in the Takagi-Sugeno’s form,” Automatica, vol. 40, no. 5, pp. 823–829, 2004.

[147] A. Sala and C. Ariño, “Relaxed stability and performance conditions for Takagi-Sugeno fuzzy systems with knowledge on membership function overlap,” IEEE Transactions on Systems, Man, and Cybernetics. Part B, vol. 37, no. 3, pp. 727–732, 2007.

[148] M. Narimani and H.-K. Lam, “Relaxed LMI-based stability conditions for Takagi-Sugeno fuzzy control systems using regional-membership- function shape-dependent analysis approach,” IEEE Transactions on Fuzzy Systems., vol. 17, no. 5, pp. 1221–1228, 2009.

[149] X. Yang, H.-K. Lam, and L. Wu, “Membership-dependent stability conditions for type-1 and interval type-2 T-S fuzzy systems,” Fuzzy Sets and Systems, 2018, doi: 10.1016/j.fss.2018.01.018.

[150] H.-K. Lam and M. Narimani, “Quadratic-stability analysis of fuzzy-model-based control systems using staircase membership functions,” IEEE Transactions on Fuzzy Systems., vol. 18, no. 1, pp. 125–137, Feb 2010.

[151] H.-K. Lam, “Polynomial fuzzy-model-based control systems: stability analysis via piecewise-linear membership functions,” IEEE Transactions on Fuzzy Systems., vol. 19, no. 3, pp. 588–593, 2011.

[152] A. Sala and C. AriÑo, “Relaxed Stability and Performance LMI Conditions for Takagi--Sugeno Fuzzy Systems With Polynomial Constraints on Membership Function Shapes,” IEEE Transactions on Fuzzy Systems, vol. 16, no. 5, pp. 1328-1336, Oct. 2008, doi: 10.1109/TFUZZ.2008.926585.

[153] M. Bernal, T.-M. Guerra, and A. Kruszewski, “A membership-function-dependent approach for stability analysis and controller synthesis of Takagi-Sugeno models,” Fuzzy Sets and Systems, vol. 160, no. 19, pp. 2776–2795, 2009.

[154] V. Campos, L. Torres, and R. Palhares, “Using information on membership function shapes in asymptotically exact triangulation approaches,” 51st IEEE Conference on Decision and Control (CDC), 2012, pp. 6205–6210. 2012.

[155] R. Márquez, T.-M. Guerra, M. Bernal, and A. Kruszewski, “Asymptotically necessary and sufficient conditions for Takagi-Sugeno models using generalized non-quadratic parameter-dependent controller design,” Fuzzy Sets and Systems., vol. 306, pp. 48–62, 2017.

[156] A. Sala and C. Ariño, “Asymptotically necessary and sufficient conditions for stability and performance in fuzzy control: Applications of Polya’s theorem,” Fuzzy Sets and Systems., vol. 158, no. 24, pp. 2671–2686, 2007.

[157] G. Goodwin, “Dynamic System Identification: Experiment Design and Data Analysis,” Academic Press, 1977.

[158] S. A. Billings, “Nonlinear System Identification: NARMAX Methods in the Time, Frequency, and Spatio-Temporal Domains,” Wiley, 2013.

[159] R. Haber and L. Keviczky, “Nonlinear system identification – input-output modeling approach, volume 2: Nonlinear system structure identification,” Kluwer Academic Publishers, London. 1999.

[160] R. Nowak, “Nonlinear system identification.” Circuits, Systems, and Signal Processing, 21(1):109–122. 2002.

[161] L. Ljung, “System Identification: Theory for the User (Prentice-Hall Information and System Sciences Series),” Prentice Hall, 530, 1987.

[162] B. Larroque**,** “Observateurs de systèmes linéaires Application à la détection et localisation de fautes, ” Thèse de doctorat de l’université de Toulouse, 2008.

[163] P. Borne et al., “Zambettakis I.“Modélisation et identification des processus, ” Tome 1, éditions Technip, 1991.

[164] D. P. Atherton and P. Borne, “Concise encyclopedia of modeling and simulation,” Pergamon press, 1992.

[165] Y. C. Hammami, “Commande de suivi de trajectoire pour les systèmes complexe et /ou incertains, ” Thèse de doctorat de l’Ecole Centrale de Lille, 2012.

[166] V. Bompart, “Optimisation non lisse pour la commande des systèmes de l'Aéronautique, ” Thèse de doctorat de l’université Paul Sabatier-Toulouse III, 2007.

[167] S. James and S. R. Anderson, “Linear System Identification of Longitudinal Vehicle Dynamics Versus Nonlinear Physical Modelling,” UKACC 12th International Conference on Control (CONTROL), Sheffield, 2018.

[168] K. Gasso, “Identification des systèmes dynamiques non- linéaire: approche multimodèle,” Doctorat de l’InstitueNational de Lorraine, Nancy, 2000.

[169] S. D. M. Borjas and C. Garcia, “Subspace Identification for Industrial Processes,” TEMA (São Carlos), 12, 183-194, 2011.

[170] Y. Ma et al., “Active-Reactive Additional Damping Control of a Doubly-Fed Induction Generator Based on Active Disturbance Rejection Control,” Energies, 11, 1314, 2018.

[171] M.C. De Simone and D. Guida, “Identification and control of a Unmanned Ground Vehicle by using Arduino,” UPB Scientific Bulletin, Series D: Mechanical Engineering, 80(1), 141-154, 2018.

[172] D. Kishore et al., “An improved identification and control of 3×3 multi-input multi-output system using relay and subspace method,” Indian Chemical Engineer, 1-15, 2018.

[173] S. Borjas and C. Garcia, “Subspace identification using the integration of MOESP and

N4SID methods applied to the Shell benchmark of a distillation column,” Computer Science, 2010.

[174] S. Hachicha, M. Kharrat and A. Chaari, “N4sid and Moesp Algorithms to Highlight the Ill-Conditioning into Subspace Identification,” International Journal of Automation and Computing, 11(1), 30-38, 2014.

[175] S. Privara et al., “Subspace identification of poorly excited industrial systems,” Paper presented at the 49th IEEE Conference on Decision and Control (CDC), 2010.

[176] M. Verhaegen, “Identification of the deterministic part of MIMO state space models given in innovations form from input-output data,” Elsevier Automatica, 30, 61-74, 1994.

[177] W.E. Larimore, “Canonical variate analysis in identification, filtering, and adaptive control,” Paper presented at Proceedings of the 29th IEEE Conference on the Decision and Control, 1990.

[178] P. v. Overschee and B. L. R. Moor, “Subspace identification for linear systems: theory, implementation, applications,” Boston: Kluwer Academic Publishers, 1996.

[179] M. Verhaegen and P. Dewilde, “Subspace model identification Part 1. The output-error state-space model identification class of algorithms,” International Journal of Control, 56:5, 1187-1210, 1992.

[180] P. Van Overschee and B. De Moor, “N4SID: Subspace algorithms for the identification of combined deterministic-stochastic systems,” Elsevier Automatica, 30, 75-93, 1994.

[181] D. Ichalal et al., “Fault detection, isolation and estimation for Takagi-Sugeno nonlinear systems,” Elsevier Journal of the Franklin Institute, 351, 3651-3676, 2014.

[182] K. Cao et al., “A New Relaxed Stability Condition for Takagi-Sugeno Fuzzy Control Systems Using Quadratic Fuzzy Lyapunov Functions and Staircase Membership Functions.,” International Journal of Fuzzy Systems, 16(3), 2014.

[183] M. Muhammad et al., “Takagi-Sugeno fuzzy modeling of a two-wheeled inverted pendulum robot,” Journal of Intelligent and Fuzzy Systems, 25(3), 535-546, 2013, doi: 10.3233/IFS-120658.

[184] M. Muhammad et al., “A new approach to stabilization of continuous-time T-S fuzzy control systems via fuzzy lyapunov function,” International Journal of Mechanical and Mechatronics Engineering, 13(6), 1-6, 2013.

[185] B. Bhushan, S. K. Valluru and M. Singh. “Takagi-Sugeno Fuzzy System based Stable Direct Adaptive Control of Nonlinear Systems.” International Journal of Computer Applications 68: 30-36, 2013.

[186] K. Zhang et al., “Analysis and Design of Robust H_\infty H_\infty Fault Estimation Observer With Finite-Frequency Specifications for Discrete-Time Fuzzy Systems,” IEEE Transactions on Cybernetics, vol. 45, no. 7, pp. 1225-1235, July 2015, doi: 10.1109/TCYB.2014.2347697.

[187] A.T. Nguyen et al., “Takagi–Sugeno fuzzy observer design for nonlinear descriptor systems with unmeasured premise variables and unknown inputs,” International Journal of Robust and Nonlinear Control, 31: 8353– 8372, 2021.

[188] Z. Zhang et al., "New Results on Sliding-Mode Control for Takagi–Sugeno Fuzzy Multiagent Systems," IEEE Transactions on Cybernetics, vol. 49, no. 5, pp. 1592-1604, May 2019, doi: 10.1109/TCYB.2018.2804759.

[189] M. Zhang et al., "Quantized Feedback Control of Fuzzy Markov Jump Systems," IEEE Transactions on Cybernetics, vol. 49, no. 9, pp. 3375-3384, Sept. 2019, doi: 10.1109/TCYB.2018.2842434.

[190] X. Xie et al., "Enhanced Stabilization of Discrete-Time Takagi–Sugeno Fuzzy Systems Based on a Comprehensive Real-Time Scheduling Model," IEEE Transactions on Systems, Man, and Cybernetics: Systems, vol. 52, no. 2, pp. 881-892, Feb. 2022, doi: 10.1109/TSMC.2020.3009728.

[191] K. Tanaka, M. Nishimura and H. O. Wang, "Multi-objective fuzzy control of high rise/high speed elevators using LMIs," Proceedings of the 1998 American Control Conference. ACC (IEEE Cat. No.98CH36207), Philadelphia, PA, USA, pp. 3450-3454 vol.6, 1998, doi: 10.1109/ACC.1998.703237.

[192] Z. Zhang et al., “New Results on Sliding-Mode Control for Takagi-Sugeno Fuzzy Multiagent Systems,” IEEE Transactions on Cybernetics, PP (99), 1-13, 2018.

[193] M. Zhang et al., "Quantized Feedback Control of Fuzzy Markov Jump Systems," IEEE Transactions on Cybernetics, vol. 49, no. 9, pp. 3375-3384, Sept. 2019, doi: 10.1109/TCYB.2018.2842434.

[194] E. Kim and H. Lee, "New approaches to relaxed quadratic stability condition of fuzzy control systems," IEEE Transactions on Fuzzy Systems, vol. 8, no. 5, pp. 523-534, Oct. 2000.

[195] M. Chadli, D. Maquin and J. Ragot, "An LMI formulation for output feedback stabilization in multiple model approach," Proceedings of the 41st IEEE Conference on Decision and Control, Las Vegas, NV, USA, pp. 311-316 vol.1, 2002.

[196] S. Kung, “A new identification and model reduction algorithm via singular value decomposition,” Computer Sciences, 1978.

[197] M. Moonen et al., “On- and off-line identification of linear state-space models,” International Journal of Control, 49:1, 219-232, 1989, doi: 10.1080/00207178908559631

[198] M. Moonen and J. Ramos, "A subspace algorithm for balanced state space system identification," IEEE Transactions on Automatic Control, vol. 38, no. 11, pp. 1727-1729, Nov. 1993, doi: 10.1109/9.262050.

[199] K. S. Arun and S. Y. Kung, “Balanced Approximation of Stochastic Systems,” SIAM Journal on Matrix Analysis and Applications, 11:1, 42-68, 1990.

[200] P. Van Overschee and B. De Moor, "Subspace algorithms for the stochastic identification problem," Proceedings of the 30th IEEE Conference on Decision and Control, Brighton, UK, pp. 1321-1326 vol.2, 1991, doi: 10.1109/CDC.1991.261604.

[201] T. Söderström and P. Stoica, “System Identification,” Prentice Hall International, London, UK, 1989.

[202] H. Akaike, “Markovian Representation of Stochastic Processes by Canonical Variables,” SIAM Journal on Control, 13:1, 162-173, 1975.

[203] M. Mansouri, D. Westwick and A. M. Knight, "A N4SID-Based Strategy to Estimate the Parameters of Disturbances in Power Systems," IEEE PES Innovative Smart Grid Technologies Conference Europe (ISGT-Europe), Sarajevo, pp. 1-6, 2018, doi: 10.1109/ISGTEurope.2018.8571689.

[204] R. S. B. Benyamin et al., "Dynamic modeling using system identification and attitude control design of GaneFly flapping wings micro aerial vehicle (FWMAV)," 7th IEEE International Conference on System Engineering and Technology (ICSET), Shah Alam, pp. 200-205, 2017, doi: 10.1109/ICSEngT.2017.8123446.

[206] H. Shi et al., "Robust Fuzzy Predictive Control for Discrete-Time Systems With Interval Time-Varying Delays and Unknown Disturbances," IEEE Transactions on Fuzzy Systems, vol. 28, no. 7, pp. 1504-1516, July 2020, doi: 10.1109/TFUZZ.2019.2959539.

[205] J. E. Naranjo et al., “Power-steering control architecture for automatic driving,” IEEE Transactions on Intelligent Transportation Systems, vol. 6, no. 4, pp. 406-415, Dec. 2005, doi: 10.1109/TITS.2005.858622.

[207] H.T. Nguyen and M. Sugeno, “Fuzzy systems, modelling and control,” Kluwer academic publisher, USA, 1988.

[208] K. Tanaka, T. Ikeda and H. O. Wang, “Fuzzy regulators and fuzzy observers: relaxed stability conditions and LMI-based designs,” IEEE Transactions on Fuzzy Systems, vol. 6, no. 2, pp. 250-265, May 1998.

[209] W. Li et al., "Adaptive-Event-Trigger-Based Fuzzy Nonlinear Lateral Dynamic Control for Autonomous Electric Vehicles Under Insecure Communication Networks," IEEE Transactions on Industrial Electronics, vol. 68, no. 3, pp. 2447-2459, March.

[210] M. Liu et al., “Lateral Control of an Autonomous and Connected Vehicle with Limited Preview Information," IEEE Transactions on Intelligent Vehicles, October 2020, doi: 10.1109/TIV.2020.3033773.

[211] Y. Hwang, C. M. Kang and W. Kim, “Robust Nonlinear Control Using Barrier Lyapunov Function Under Lateral Offset Error Constraint for Lateral Control of Autonomous Vehicles,” IEEE Transactions on Intelligent Transportation Systems, doi:10.1109/TITS.2020.3023617.

[212] Y. Huang, S. Z. Yong and Y. Chen, “Stability Control of Autonomous Ground Vehicles Using Control-Dependent Barrier Functions,” IEEE Transactions on Intelligent Vehicles, Feb. 2021.

[213] C. Hu et al., “Robust H∞ output-feedback control for path following of autonomous ground vehicles,” Mechanical Systems and Signal Processing, Volumes 70–71, Pages 414-427, 2016.

[214] B. Paden et al., “A Survey of Motion Planning and Control Techniques for Self-Driving Urban Vehicles,” IEEE Transactions on Intelligent Vehicles, vol. 1, no. 1, pp. 33-55, March 2016, doi: 10.1109/TIV.2016.2578706.

[215] L. Menhour et al., “An Efficient Model-Free Setting for Longitudinal and Lateral Vehicle Control: Validation Through the Interconnected Pro-SiVIC/RTMaps Prototyping Platform,” IEEE Transactions on Intelligent Transportation Systems, vol. 19, no. 2, pp. 461-475, Feb. 2018.

[216] R. Marino, S. Scalzi and M. Netto, “Nested PID steering control for lane keeping in autonomous vehicles,” Control Engineering Practice, Volume 19, Issue 12,Pages 1459-1467, 2011.

[217] G. Tagne, R. Talj and A. Charara, “Design and Comparison of Robust Nonlinear Controllers for the Lateral Dynamics of Intelligent Vehicles,” IEEE Transactions on Intelligent Transportation Systems, vol. 17, no. 3, pp. 796-809, March 2016.

[218] K. Lee, S. E. Li and D. Kum, “Synthesis of Robust Lane Keeping Systems: Impact of Controller and Design Parameters on System Performance,” IEEE Transactions on Intelligent Transportation Systems, vol. 20, no. 8, pp. 3129-3141, Aug. 2019.

[219] U. Rosolia, S. De Bruyne and A. G. Alleyne, “Autonomous Vehicle Control: A Nonconvex Approach for Obstacle Avoidance,” IEEE Transactions on Control Systems Technology, vol. 25, no. 2, pp. 469-484, March 2017.

[220] R. Attia, R. Orjuela and M. “Basset Combined longitudinal and lateral control for automated vehicle guidance,” Vehicle System Dynamics, 52:2, 261-279, 2014.

[221] E. Kayacan, H. Ramon and W. Saeys, “Robust Trajectory Tracking Error Model-Based Predictive Control for Unmanned Ground Vehicles,” IEEE/ASME Transactions on Mechatronics, vol. 21, no. 2, pp. 806-814, April 2016.

[222] J. Suh, H. Chae and K. Yi, “Stochastic Model-Predictive Control for Lane Change Decision of Automated Driving Vehicles,” IEEE Transactions on Vehicular Technology, vol. 67, no. 6, pp. 4771-4782, June 2018, doi: 10.1109/TVT.2018.2804891.

[223] K. Nam, S. Oh, H. Fujimoto and Y. Hori, “Estimation of Sideslip and Roll Angles of Electric Vehicles Using Lateral Tire Force Sensors Through RLS and Kalman Filter Approaches,” IEEE Transactions on Industrial Electronics, vol. 60, no. 3, pp. 988-1000, March 2013.

[224] A.T. Nguyen, A. Dequidt and M. Dambrine, “Anti-windup based dynamic output feedback controller design with performance consideration for constrained Takagi–Sugeno systems,” Engineering Applications of Artificial Intelligence, Volume 40, Pages 76-83, 2015.

[225] D. Q. Mayne, “Model predictive control: Recent developments and future promise,”

Automatica, Volume 50, Issue 12, Pages 2967-2986, 2014.

[226] H.B. Pacejka, “Tire and vehicle dynamics,” Elsevier, 2004.

[227] Z. Wendt and S. Jeremy Cook, “Saved by the Sensor: Vehicle Awareness in the Self-Driving Age,” (Accessed on 26 April 2022). https://www.machinedesign.com/mechanical-motion-systems/article/21836344/saved-by-the-sensor-vehicle-awareness-in-the-selfdriving-age.

Appendix A: Mathematical tools

In this appendix, we present the mathematical tools of linear algebra used in subspace method. We define first the extended observability matrix (we extend the observability to an order that is superior to the one of the system) [180]:

$$\Gamma_i = \begin{pmatrix} C \\ CA \\ \dots \\ CA^{i-1} \end{pmatrix}. \tag{A.1}$$

Then, the reversed extended controllability matrix is:

$$\Delta_i = \begin{pmatrix} A^{i-1}B & A^{i-2}B & \dots & B \end{pmatrix}. \tag{A.2}$$

The input block Hankel matrix is defined as:

$$U_{0|i-1} = \begin{pmatrix} u_0 & u_1 & u_2 & \dots & u_{j-i} \\ u_1 & u_2 & u_3 & \dots & u_j \\ \dots & \dots & \dots & \dots & \dots \\ u_{i-1} & u_i & u_{i+1} & \dots & u_{i+j-2} \end{pmatrix}. \tag{A.3}$$

and the output block Hankel matrix is:

$$Y_{0|i-1} = \begin{pmatrix} y_0 & y_1 & y_2 & \dots & y_{j-i} \\ y_1 & y_2 & y_3 & \dots & y_j \\ \dots & \dots & \dots & \dots & \dots \\ y_{i-1} & y_i & y_{i+1} & \dots & y_{i+j-2} \end{pmatrix}. \tag{A.4}$$

The following matrices are used: $U_p = U_{0|i-1}$, $U_f = U_{i|2i-1}$, $U_p^+ = U_{0|i}$ and $U_f^- = U_{i+1|2i-1}$. A similar definitions is presented for Hankel block output matrices: Y_p , Y_p^+ , Y_f and, Y_f^+ where subscript stands ‘f’ for the “future” and ‘P’ for the “past”.

For the stochastic sub- model, we define:

$$\begin{cases} P^s = E\left[x_k^s \left(x_k^s\right)^T \right] = AP^s A^T + Q^s. \\ \nabla = E\left[x_{k+1}^s \left(y_k^s\right)^T \right] = AP^s C^T + S^s. \\ \Lambda_0 = E\left[x_{k+1}^s \left(y_k^s\right)^T \right] = CP^s C^T + R^s. \end{cases} \tag{A.5}$$

The matrix Δ_i^s associated with the stochastic sub-model is:

$$\Delta_i^s = \left(A^{i-1}\nabla \quad ... \quad A\nabla \quad \nabla \right). \tag{A.6}$$

The Block lower triangular Toeplitz matrix and the block Toeplitz cross covariance matrix are:

$$H_i^d = \begin{pmatrix} D & 0 & 0 & \dots & 0 \\ CB & D & 0 & \dots & 0 \\ CAB & CB & D & \cdots & 0 \\ \dots & \dots & \dots & \dots & \dots \\ CA^{i-2}B & CA^{i-3}B & CA^{i-4}B & \dots & D \end{pmatrix}. \text{ and}$$

$$H_i^s = \begin{pmatrix} I & 0 & 0 & \dots & 0 \\ CK & I & 0 & \dots & 0 \\ CAK & CK & I & \cdots & 0 \\ \dots & \dots & \dots & \dots & \dots \\ CA^{i-2}K & CA^{i-3}K & CA^{i-4}K & \dots & K \end{pmatrix}. \tag{A.7}$$

Appendix B: Kalman states

From the matrices of block Hankel, the matrices system are determined directly through the determination of projections from which to estimate the two states sequences which are the outputs of the extended Kalman filter [180]:

$$\begin{aligned} X_i^d &= [x_i^d \cdots x_{i+j-1}^d]. \\ X_i^s &= [x_i^s \cdots x_{i+j-1}^s]. \end{aligned} \tag{B.1}$$

If both noises are jointly Gaussian, we have the best estimates of the Kalman states in the quadratic mean sense. If we knew the initial states $\hat{X}_0$ and its covariance P_0 , inputs and outputs $u = [u_1\ u_2 \cdots u_n]$, $y = [y_1\ y_2 \cdots y_n]$ and all system matrices A, B, C, D, Q, S, R, the states can be easily computed using the following recursive formulas:

$$\begin{cases} \hat{x}_k = A\hat{x}_{k-1} + Bu_{k-1} + K_{k-1}\left(y_{k-1} - C\hat{x}_{k-1} - Du_{k-1}\right). \\ K_{k-1} = \left(AP_{k-1}C^T + \nabla\right)\left(\Lambda_0 + CP_{k-1}C^T\right)^{-1}\left(AP_{k-1}C^T + \nabla\right)^T. \\ P_k = AP_{k-1}A^T - \left(AP_{k-1}C^T + \nabla\right)\left(\Lambda_0 + CP_{k-1}C^T\right)^{-1}\left(AP_{k-1}C^T + \nabla\right)^T. \end{cases} \tag{B.2}$$

Based on last equation, we computed the Kalman gain and recursively defined the error covariance matrix $E\left[\left(x_k - \hat{x}_k\right)\left(x_k - \hat{x}_k\right)^T\right]$ which estimates P^s.

From previous equations, it was possible to establish the following formulas:

$$\hat{X}_{i+1} = A\hat{X}_i + BU_{i|i} + K_i\left(Y_{i|i} - C\hat{X}_i - DU_{i|i}\right).$$

$$Y_{i|i} = C\hat{X}_i + BU_{i|i} + \left(Y_{i|i} - C\hat{X}_i - DU_{i|i}\right). \tag{B.3}$$

If it was possible to obtain Kalman states directly from input- output data, the equations above would satisfy the assumption on consistent applications of least squares to estimate system matrices A, B, C, D . We determine from the residuals matrices the covariance matrices (Q^s, S^s, R^s) .

Appendix C: Orthogonal projection

In this appendix, we present the geometric tools of linear algebra used in subspace method. We assume that the matrices A, B, C are given.

The orthogonal projection of the row space of *A* into the row space of *B* is defined as [180]:

$$A \ / B \quad = A \ \Pi_B = A \ B(B \ B^t)^+ B. \tag{C.1}$$

Where $(.)^+$ denotes the Moore-Penrose of the matrix $(.)$ and $\Pi_B = B^{\ T}\left(B.B^T\right)^+.B$. It is important to note that Π_B defined the operator of orthogonal projection that projects the row space of matrix onto the row space of the matrix B.

The projection of the row space of *A* into the orthogonal complement of the row space of *B* is:

$$A \ / B^{\perp} \quad = A\Pi_{B^{\perp}} = A \ - A \ / B \ = A\left(I_j - \Pi_B\right). \tag{C.2}$$

Where $B^{\perp}$ denotes a base of the orthogonal space to the row space of *B*, and $\Pi_{B^{\perp}}$ defines the geometric operator that projects the row space of a matrix onto the orthogonal complement to the row space of the matrix B. From the expression of Π_B and $\Pi_{B^{\perp}}$, one can easily show that matrix *A* can be decomposed into two matrices where their row spaces are orthogonal such as:

$$A = A\Pi_B + A\Pi_{B^{\perp}} \ . \tag{C.3}$$

Therefore, one defines the oblique projection of a matrix *A* along the row space of the matrix *B* onto the row space of the matrix:

$$A /_B C \quad = \left[A / B^{\perp}\right]\left[C / B^{\perp}\right]^+.C = A\Pi_{B^{\perp}} + \left(C\Pi_{B^{\perp}}\right)^+.C \tag{C.4}$$

Then, another one defines the properties of the orthogonal and oblique projections as follow:

$$A_x / A_x^{\perp} = \ 0.$$

$$A_x / A_x C_x = \ 0. \tag{C.5}$$

N4sid method 1:

The identification algorithm N4SID is determined by four steps which include:

Determine the projection

$$Z_i = Y_{i|2i-1} / \begin{pmatrix} u_{0|i-1} \\ u_{i|2i-1} \\ Y_{0|i-1} \end{pmatrix} = (\underbrace{L_i^1}_{li\times mi} \mid \underbrace{L_i^2}_{li\times mi} \mid \underbrace{L_i^3}_{li\times li}) \begin{pmatrix} u_p \\ u_f \\ Y_p \end{pmatrix}.$$

$$Z_{i+1} = Y_{i+1|2i-1} \begin{pmatrix} u_p^+ \\ u_f^- \\ Y_p^+ \end{pmatrix}. \tag{C.6}$$

Computing singular value decomposition (SVD)

Let the matrix M be the rank deficient space which coincides with that of columns Γ_i . Therefore, we compute the singular value decomposition SVD passing through the following mathematical steps:

$$M = \begin{pmatrix} U_1 & U_2 \end{pmatrix} \begin{pmatrix} \Sigma_1 & 0 \\ 0 & 0 \end{pmatrix} V^t. \tag{C.7}$$

$$\begin{aligned} L_i^1 &= \Gamma_i \left(\left[A^i - Q_i \Gamma_i \right] S \left(R^{-1} \right)_{1|mi} + \Delta_i^d - Q_i H_i^d \right). \\ L_i^2 &= H_i^d + \Gamma_i \left(\left[A^i - Q_i \Gamma_i \right] S \left(R^{-1} \right)_{mi+1|2mi} \right). \\ L_i^3 &= \Gamma_i Q_i. \end{aligned} \tag{C.8}$$

Where $(R^{-1})_{1|mi}$ is the sub-matrix of the column 1 to the column mi.

$$(\underbrace{L_i^1}_{li\times mi} \mid \underbrace{L_i^3}_{li\times li}) \begin{pmatrix} u_{0|i-1} \\ \\ Y_{0|i-1} \end{pmatrix} = \begin{pmatrix} U_1 & U_2 \end{pmatrix} \begin{pmatrix} \Sigma_1 & 0 \\ 0 & 0 \end{pmatrix} V^t. \tag{C.9}$$

$\Gamma_{i-1} = \underline{U_1} \Sigma_1^{1/2}$ where $\underline{U_1}$ denote respectively the last $l_{(i-1)}$ rows of U_1.

Determine the system matrices:

We assume that Γ_i , Γ_{i-1} and n the order of system are determined.

$$\begin{cases} Z_i = \Gamma_i \hat{X}_i + H_i^d U_{i|2i-1.} \\ Z_{i+1} = \Gamma_{i-1} \hat{X}_{i+1} + H_{i-1}^d U_{i+1|2i-1.} \end{cases} \tag{C.10}$$

We can extract:

$$\begin{cases} \hat{X}_i = \Gamma_i^{+}(Z_i - H_i^d U_{i|2i-1}). \\ \hat{X}_{i+1} = \Gamma_{i-1}^{+}(Z_{i+1} - H_{i-1}^d U_{i+1|2i-1.} \end{cases} \tag{C.11}$$

In our case, we need to know H_i^d and H_{i-1}^d from:

$$\hat{X}_{i+1} = A\hat{X}_i + BU_{i|i} + \begin{pmatrix} u_{0|2i-1} \\ u_{0|i-1} \\ \hat{X}_i \end{pmatrix}^{-} \text{ and}$$

$$Y_{i|i} = C\hat{X}_i + DU_{i|i} + \begin{pmatrix} u_{0|2i-1} \\ u_{0|i-1} \\ \hat{X}_i \end{pmatrix}^{-}, \tag{C.12}$$

Where $(.)^{-}$ indicates a matrix whose row space is perpendicular to the row space of $(.)$. Also, we know that:

$$\begin{pmatrix} \hat{X}_{i+1} \\ Y_{i|i} \end{pmatrix} = \begin{pmatrix} A \\ C \end{pmatrix} \hat{X}_i + \begin{pmatrix} B \\ D \end{pmatrix} U_{i|i} + \begin{pmatrix} u_{0|2i-1} \\ Z_i \\ \hat{X}_i \end{pmatrix}^{-}, \tag{C.13}$$

Then, if we subtitle the expression for $\hat{X}_i$ and $\hat{X}_{i+1}$, we get:

$$\begin{pmatrix} \Gamma_{i-1}^{+} Z_{i+1} \\ Y_{i|i} \end{pmatrix} = \begin{pmatrix} A \\ C \end{pmatrix} \Gamma_i^{+} Z_i + \begin{pmatrix} K_{12} \\ K_{22} \end{pmatrix} U_{i|2i-1} + \begin{pmatrix} U_{0|2i-1} \\ Z_i \\ \hat{X}_i \end{pmatrix}^{-}, \tag{C.14}$$

where we define:

$$\begin{pmatrix} K_{12} \\ K_{22} \end{pmatrix} = \begin{bmatrix} B - A\Gamma_i^+ \begin{pmatrix} D \\ \Gamma_{i-1} B \end{pmatrix} \Gamma_{i-1}^+ H_{i-1}^d - A\Gamma_i^+ \begin{pmatrix} 0 \\ H_i^d \end{pmatrix} \\ D - C\Gamma_i^+ \begin{pmatrix} D \\ \Gamma_{i-1} B \end{pmatrix} - A\Gamma_i^+ \begin{pmatrix} 0 \\ H_i^d \end{pmatrix} \end{bmatrix}. \quad \text{(C.15)}$$

We observe that the matrices B and D appear linearly in the matrices K_{12} , K_{22}. From the last equation, we obtain:

$$\begin{pmatrix} \Gamma_{i-1}^+ Z_{i+1} \\ Y_{i|i} \end{pmatrix} / \Pi = \begin{pmatrix} A & K_{12} \\ C & K_{22} \end{pmatrix} \begin{pmatrix} \Gamma_i^+ Z_i \\ U_{i|2i-1} \end{pmatrix} / \Pi. \quad \text{(C.16)}$$

The unknown in this set of linear equations are , C, K_{12} , K_{22} . The solution is to compute the least mean square:

$$\min_{A,C,K_{12},K_{22}} \left\| \begin{pmatrix} \Gamma_{i-1}^+ Z_{i+1} \\ Y_{i|i} \end{pmatrix} - \begin{pmatrix} A & K_{12} \\ C & K_{22} \end{pmatrix} \begin{pmatrix} \Gamma_i^+ Z_i \\ U_{i|2i-1} \end{pmatrix} \right\|_F^2 \text{ with}$$

$$\begin{pmatrix} \Gamma^+{}_{i-1} Z_{i+1} \\ Y_{i|i} \end{pmatrix} = \begin{pmatrix} K_{11} & K_{12} \\ K_{21} & K_{22} \end{pmatrix} \times \begin{pmatrix} \Gamma_i^+ Z_i \\ U_{i|2i-1} \end{pmatrix} + \begin{pmatrix} p_v \\ p_w \end{pmatrix}, \quad \text{(C.17)}$$

where p_v, p_w are residues.

The system matrix A is equal to K_{11} and C is equal to K_{21} . Then we compute the matrices B and D from K_{12} , K_{22} , A and C by solving a set of linear equations. Finally, we compute the covariance's matrices as follows:

$$\begin{pmatrix} Q^s & S^s \\ (S^s)^t & R^s \end{pmatrix} \leftarrow \frac{1}{j} \begin{pmatrix} p_v p_v^t & p_v p_w^t \\ p_w p_v^t & p_w p_w^t \end{pmatrix}. \quad \text{(C.18)}$$

N4sid method 2:

The N4SID2 identification algorithm could also be determined by the next four steps which are:

1-Determine the projections:

$$Z_{i+1} = Y_{i+1|2i-1} / \begin{pmatrix} u_{0|i-1} \\ u_{i+1|2i-1} \\ Y_{0|i} \end{pmatrix}. \tag{C.19}$$

$$Z_{i+1} = Y_{i+1|2i-1} \begin{pmatrix} u_{0|i-1} \\ u_{i+1|2i-1} \\ Y_{0|i} \end{pmatrix}. \tag{C.20}$$

$$\begin{aligned} Z_{i+1} &= Y_{i+1|2i-1} / \begin{pmatrix} u_{0|i-1} \\ u_{i+1|2i-1} \\ Y_{0|i} \end{pmatrix}. \\ &= \underset{l(i-1)\times m(i+1)}{L_{i+1}^{1}} \Big| \underset{l(i-1)\times m(i-1)}{L_{i+1}^{2}} \Big| \underset{l(i-1)\times l(i+1)}{L_{i+1}^{3}} \begin{pmatrix} u_p^+ \\ u_f^- \\ Y_p^+ \end{pmatrix}. \end{aligned} \tag{C.21}$$

2-Compute singular value decomposition (SVD)

$$\underset{li\times mi}{(L_i^1} \Big| \underset{li\times li}{L_i^3)} \begin{pmatrix} u_{0|i-1} \\ \\ Y_{0|i-1} \end{pmatrix} = \begin{pmatrix} U_1 & U_2 \end{pmatrix} \begin{pmatrix} \Sigma_1 & 0 \\ 0 & 0 \end{pmatrix} V^t. \tag{C.22}$$

The order of the system is equal to the number of non-zero singular values.

$$\Gamma_i = U_1 \Sigma_1^{1/2} \text{ and } \Gamma_{i-1} = \underline{U_1} \Sigma_1^{1/2}. \tag{C.23}$$

3-Estimate the states $\tilde{X}_i$ and $\tilde{X}_{i+1}$

$$\tilde{X}_i = \Gamma_i^+ \underset{li\times mi}{(L_i^1} \Big| \underset{li\times li}{L_i^3)} \begin{pmatrix} u_{0|i-1} \\ \\ Y_{0|i-1} \end{pmatrix}. \tag{C.24}$$

$$\tilde{X}_{i+1} = \Gamma_i^+ \underset{l(i-1)\times m(i+1)}{(L_{i+1}^1} \Big| \underset{i(i-1)\times l(i+1)}{L_{i+1}^3)} \begin{pmatrix} u_{0|i} \\ \\ Y_{0|i} \end{pmatrix}. \tag{C.25}$$

4-Extract system matrices from least square solution

$$\begin{pmatrix} \tilde{X}_{i+1} \\ \overline{Y_{i|i}} \end{pmatrix} = \begin{pmatrix} \tau_{11} & \tau_{12} \\ \tau_{21} & \tau_{22} \end{pmatrix} \times \begin{pmatrix} \tilde{X}_i \\ \overline{U_{i|i}} \end{pmatrix} + \begin{pmatrix} p_v \\ p_w \end{pmatrix}. \tag{C.26}$$

$$\begin{pmatrix} A & B \\ C & D \end{pmatrix} \leftarrow \begin{pmatrix} \overline{\tau_{11}} & \overline{\tau_{12}} \\ \overline{\tau_{21}} & \overline{\tau_{22}} \end{pmatrix}. \tag{C.27}$$

$$\begin{pmatrix} Q^s & S^s \\ (S^s)^t & R^s \end{pmatrix} \leftarrow \frac{1}{j} \begin{pmatrix} p_v p_v^t & p_v p_w^t \\ p_w p_v^t & p_w p_w^t \end{pmatrix}. \tag{C.28}$$